

---

# **Reactive electron scattering from biomolecules and technologically relevant molecules**

Carolina Raquel Guedes Matias, MSc.

A thesis submitted to the University of  
Innsbruck and Universidade Nova de  
Lisboa for the degree of Philosophy  
Doctor (PhD) in Physics

*Supervisor: Assoz. Prof. Dr. Stephan Denifl*  
*Co-supervisor: Prof. Dr. Paulo Limão-Vieira*

Innsbruck

2015



# Acknowledgments

---

I would like to thank my supervisors, Professor Stephan Denifl and Professor Paulo Limão-Vieira for not only giving me the opportunity to perform my PhD thesis under their supervision, but also for their support, dedication and orientation. They were always available to help me in anything I needed.

To Professor Paul Scheier for accepting me in his working group and for all advises, which certainly made a difference in my training.

To all my colleagues at the Institute for Ion Physics and Applied Physics, University of Innsbruck, for making my stay as comfortable as possible, for the welcoming atmosphere and all support over these years. Especially to David and Josi who always had an answer to my questions. Every day they would provide some minutes of their busy time to help, discuss and advise me. I would also like to make a special thanks to my colleagues and friends, Marcelo and Andi, for the great time we have had together in the research activities as well as for all the support given when I most needed it.

To all my friends who always had a word of support and motivation. They helped me to successfully overcome some difficult times in this past three years.

To my parents for their unconditional support, for their trust and for the opportunities that they provided me over these years. Without their support I would not have been able to come so far.

To my little brother that although I don't say it too loud, I care about him very much.

To my grandmother, who although has no clue of what I am doing about physics, was always calling worried about my diet and my future.



# Abstract

---

The role of a set of gases relevant within the context of biomolecules and technologically relevant molecules under the interaction of low-energy electrons was studied in an effort to contribute to the understanding of the underlying processes yielding negative ion formation. The results are relevant within the context of damage to living material exposed to energetic radiation, to the role of dopants in the ion-molecule chemistry processes, to Electron Beam Induced Deposition (EBID) and Ion Beam Induced Deposition (IBID) techniques. The research described in this thesis addresses dissociative electron attachment (DEA) and electron transfer studies involving experimental setups from the University of Innsbruck, Austria and Universidade Nova de Lisboa, Portugal, respectively.

This thesis presents DEA studies, obtained by a double focusing mass spectrometer, of dimethyl disulphide ( $C_2H_6S_2$ ), two isomers, enflurane and isoflurane ( $C_3F_5Cl_5$ ) and two chlorinated ethanes, pentachloroethane ( $C_2HCl_5$ ) and hexachloroethane ( $C_2Cl_6$ ), along with quantum chemical calculations providing information on the molecular orbitals as well as thermochemical thresholds of anion formation for enflurane, isoflurane, pentachloroethane and hexachloroethane. The experiments represent the most accurate DEA studies to these molecules, with significant differences from previous work reported in the literature. As far as electron transfer studies are concerned, negative ion formation in collisions of neutral potassium atoms with N1 and N3 methylated pyrimidine molecules were obtained by time-of-flight mass spectrometry (TOF). The results obtained allowed to propose concerted mechanisms for site and bond selective excision of bonds.

Keywords: Dissociative electron attachment, electron transfer, biomolecules, technologically relevant molecules, mass spectrometry.



# Symbols and acronyms

---

1-MeT	1-methyl-thymine
1-MeU	1-methyl-uracil
1p	One particle resonance
2p-1h	Two particle-one hole resonance
3-MeT	3-methyl-thymine
3-MeU	3-methyl-uracil
a. m. u.	Atomic mass unit
a.u.	Arbitrary unit
AD	Autodetachment
AE	Appearance energy
B	Magnetic field
BOA	Born-Oppenheimer approximation
D	Bond dissociation energy
DBS	Dipole-bound state
DD	Dipolar dissociation
DEA	Dissociative electron attachment
DMDS	Dimethyl disulphide
DNA	Deoxyribonucleic acid
DSB	Double strand break
e <sup>-</sup>	Electron

## *Symbols and acronyms*

e. g.	for example
EA	Electron affinity
EA <sub>ad</sub>	Adiabatic electron affinity
EA <sub>v</sub>	Vertical electron affinity
EI	Electron ionisation
E <sub>k</sub>	Kinectic energy
ESA	Electrostatic analyser
<i>et al.</i>	and others
eV	electron-volt
FCF	Franck-Condon factor
FWHM	Full width at half maximum
$h$	Plank constant, $6.626 \times 10^{-34} \text{ J.s}^{-1}$
$\hbar$	Reduced Plank constant, $6.6 \times 10^{-16} \text{ eV/s (} h/2\pi \text{)}$
HOMO	Highest occupied molecular orbital
<i>i.e.</i>	in other words (id est)
IE	Ionisation energy
IMS	Ion mobility spectrometry
K	Potassium
K <sub>hyper</sub>	Hyperthermal potassium atom
K <sub>ther</sub>	Thermal potassium atom
kV	kilovolt ( $10^3 \text{ V}$ )
l	Angular momentum



*Symbols and acronyms*

LEE	Low energy electron
LUMO	Lowest unoccupied molecular orbital
M	Molecule
M*	Excited molecule
m*	Apparent mass
m/z	Mass to charge ratio
m <sub>1</sub>	Molecular fragment
MeV	Mega electron-volt (10 <sup>6</sup> eV)
MIKE	Mass analysed ion kinetic energy
MO	Molecular orbitals
MS	Mass spectrometry
NDA	Non dissociative attachment
R	Nuclear coordinates
R <sub>c1</sub>	First crossing radius
R <sub>c2</sub>	Second crossing radius
s	Second
SSB	Single strand break
T	Thymine
Th	Thomson (mass unit)
TNI	Temporary negative ion
TNT	Trinitrotoluene
TOF	Time-of-flight

*Symbols and acronyms*

$U_0$	Initial kinetic energy
$V_a$	Attractive polarization interaction
VDE	Vertical detachment energy
VE	Vertical excitation
VEA	Vertical electron attachment
$V_{\text{eff}}$	Effective potential
VG-ZAB	Double focusing mass spectrometer
$V_l$	Repulsive centrifugal potential
$\Gamma$	Resonance width
$\Delta H_f^\circ$	Heat of formation
$\nu$	Vibrational level
$\sigma^*$	$\sigma$ antibonding orbital
$\tau$	Autodetachment lifetime
$\Psi$	Vibrational wave function

# List of Figures

---

Figure 1.1 – Schematics of the various components present in a mass spectrometer. Represented are: the sample inlet; ion source; m/z analyser (separates the ions according to their individual m/z values); detector (generates a signal whenever an ion reaches the detector); vacuum system (provides binary collision conditions); computer (drives each of the spectrometer’s component, records and stores the data obtained). Adapted from [4]...	2
Figure 2.1 - Schematic representation of direct electron scattering. Adapted from [1].....	6
Figure 2.2 - Schematic representation of resonant electron scattering. Adapted from [1].	6
Figure 2.3 - Born-Oppenheimer potential energy curves for a molecule in the ground state (M) and its electronically excited state (M <sup>-</sup> ). Vertical transitions are shown representatively. Also represented are the vibrational modes (ν) and the Franck-Codon region (shadow). Adapted from [3].	8
Figure 2.4 - Dynamics of Autodetachment (AD) and dissociative attachment (DEA) in electron-molecule scattering through resonances. ν represents a vibrational quantum number. Adapted from [8].	11
Figure 2.5 - Schematics of a potential curve for low energy electron interactions with a molecule ABC. Representation of possible decay processes: DEA (dissociative electron attachment), AD (autodetachment) and NDA (non-dissociative electron attachment). Adapted from [6].....	12
Figure 2.6 – Representation of the collision trajectories between an alkaline atom (A) and a molecule (M). The crossing radius corresponds to the external circle and the repulsive potential region is represented by the dashed area. When the electron is transferred at R <sub>c1</sub> the trajectory is known as ionic, whereas at R <sub>c2</sub> the trajectory is termed covalent. Adapted from [14,17].	15
Figure 2.7 - Schematic diagrams of potential energies. Representation of the electron affinity (EA), vertical detachment energy (VDE) and vertical attachment energy (VAE). Adapt from [6].	16
Figure 2.8 - 1p resonance and 2p-h resonance electronic configuration. The red arrows represent the captured electron. Adapted from [20].	17

## List of Figures

Figure 2.9 - Classification of the different types of resonance according to their energy in comparison to the neutral parent (M). Adapted from [1].....	18
Figure 2.10 - Representation of the effective potential of the electron-molecule interactions depending on their distance (r). Depending on the angular momentum, different potential barriers are formed. For $l = 0$ , no potential barrier is formed, while for $l \neq 0$ a centrifugal barrier is created and the electron can be momentarily trapped inside the effective potential. Adapted from [21].....	19
Figure 2.11 – Representation of a dipole bound state or also called vibrational Feshbach resonance, since its vibrational levels are below the corresponding levels of the neutral. Adapted from [25].....	20
Figure 2.12 – Scheme of a potential energy diagram where the neutral ground state and electronically excited state of molecule AB is visible. Core excited state and Feshbach resonances are also represented. Adapted from [21]. ....	21
Figure 3.1 – Schematics of the double focusing spectrometer used to perform DEA experiments [1]. ....	25
Figure 3.2 – a) Picture of the VG-ZAB ion source chamber and gas and liquid inlets. A heating band and aluminium foil is wrapped around the liquid inlet. b) Detailed view of the ion source and capillary. ....	26
Figure 3.3 - Schematics of the ion block. Adapted from [4]. ....	28
Figure 3.4 - Production of secondary electrons in a channel electron multiplier. The output will be amplified and discriminated by a preamplifier discriminator unit which will trigger a counter. This signal will be processed by a computer. Adapted from [5,6]. ....	32
Figure 3.5 – Negative ion formation of $\text{SF}_6^-$ , $\text{SF}_5^-$ , $\text{F}^-$ and $\text{F}_2^-$ from the collision of electrons with $\text{SF}_6$ . The energies used to calibrate energy spectra are identified in the graph. Adapted from [12]. ....	35
Figure 3.6 - Photograph of the experimental set-up used to perform electron transfer experiments. ....	36
Figure 3.7 - Schematics of the charge transfer set-up. Adapted from [13].....	37
Figure 3.8 – Schematics of the charge exchange beam formation. Adapted from [13]. ...	38
Figure 3.9 - Representation of the ions acceleration in the acceleration region. ....	41

## List of Figures

Figure 3.10 - Generic schematics of a time-of-flight mass spectrometer. ....	42
Figure 4.1 – Time-scale schematic of radiation exposure on biological systems. From [7]. .....	48
Figure 4.2 - Schematics of a single and a double strand break.....	48
Figure 4.3 –a) schematic drawing of a thymine molecule with atom labelling numbers (in red). b) and c) represents the possible N-methylated sites of thymine, 3-methylthymine and 1-methylthymine, respectively.....	49
Figure 4.4 – a) schematic drawing of a uracil molecule with atom labelling numbers (in red). Uracil replaces thymine in the transcription of DNA and is also present in the RNA. b) and c) represents the possible N-methylated sites of uracil, 3-methyluracil and 1-methyluracil, respectively. ....	49
Figure 4.5 - Schematic representation of NCO <sup>-</sup> path formation when a hydrogen atom is removed from position N1. Further reaction steps occur upon the loss of NCO <sup>-</sup> (see publication below). ....	51
Figure 4.6 – Schematic representation of the different NCO <sup>-</sup> path formation when a hydrogen atom is removed from position N3. Further reaction steps occur upon the loss of NCO <sup>-</sup> (see publication below). ....	52
Figure 4.7 - Schematic drawing of a dimethyl disulphide. From [28].....	64
Figure 4.8 - Schematic drawing of an example of IMS. a) Principle of operation and b) the flow of gas inside an IMS apparatus. From [49]. ....	75
Figure 4.9 - Schematic drawing of isoflurane a) and enflurane b). These two molecules are structural isomers. The position of two fluorine atoms are swapped with a chlorine and a hydrogen atoms, as pointed out in the figure. Adapted from [53,54]. ....	77
Figure 4.10 – Schematic drawing of the chlorinated ethanes: hexachloroethane a) and pentachloroethane b) used to perform DEA experiments. From [56,57]. ....	78
Figure 4.11 - Schematic illustration of the EBID and IBID techniques. In EBID an electron beam used, while IBID uses an ion beam. Irradiation by high energy electrons and ions lead to metallic structures from adsorbed organometallic molecules on the surface of a solid substrate. Adapted from [63]. ....	102
Figure 4.12 - Schematic drawing of tungsten hexacarbonyl molecule. From [69].....	104

*List of Figures*

Figure 5.1 – Schematic representation of a) thiothymine and b) thiouracil. These molecules are similar to thymine and uracil, respectively, with the difference that the oxygen in position C2 is replaced by a sulphur. .... 117

# List of Tables

---

Table 3.1 – Specifications of the system. ....	43
Table 4.1– List of representative common nitrogen explosives. Adapted from [47]. ....	74





# Table of contents

---

Acknowledgments.....	i
Abstract.....	iii
Symbols and acronyms .....	v
List of Figures .....	ix
List of Tables .....	xiii
Table of contents.....	xv
1. Motivation .....	1
2. Electron Induced Processes .....	5
2.1. Scattering processes .....	5
2.1.1. Direct elastic scattering.....	5
2.1.2. Direct inelastic scattering.....	6
2.1.3. Resonant scattering .....	6
2.2. Born-Oppenheimer-Approximation .....	7
2.3. The Franck-Condon principle .....	9
2.4. Negative ion formation through electron attachment.....	9
2.4.1. Dissociative electron attachment .....	10
2.4.2. Dipolar dissociation .....	13
2.4.3. Electron transfer.....	13
2.4.4. Electron affinity .....	15
2.4.5. One particle and two particle-one hole resonances.....	17
2.4.6. Metastable ions .....	22
3. Experimental set-up.....	25

## *Table of contents*

3.1.	Apparatus used to perform DEA experiments .....	25
3.1.1.	Introducing a sample in the chamber .....	26
3.1.1.1.	Gas phase sample .....	26
3.1.1.2.	Liquid phase sample .....	27
3.1.1.3.	Solid phase sample.....	27
3.1.2.	Ion source.....	28
3.1.3.	Mass analysis of ions .....	29
3.1.4.	The Electrostatic Analyser and Magnet Combination.....	30
3.1.5.	Detection: Channeltron .....	31
3.1.6.	Mass resolution .....	32
3.1.7.	Measurements .....	32
3.1.8.	Calibration.....	34
3.2.	Apparatus used to study electron transfer .....	36
3.2.1.	Introducing the samples .....	37
3.2.2.	Production of the neutral potassium beam and ions .....	38
3.2.3.	Time of flight spectrometer .....	39
4.	Results and discussion .....	46
4.1.	Biomolecules.....	46
4.1.1.	Comparative studies upon potassium and electron collisions with biomolecules: site selectivity.....	47
4.1.2.	Dissociative electron attachment to dimethyl disulphide .....	64
4.2.	Technologically relevant molecules.....	73

## *Table of contents*

4.2.1. Dissociative electron attachment to enflurane, isoflurane and chlorinated ethanes (pentachloroethane and hexachloroethane) .....	75
4.2.2. Low-energy electron interaction with tungsten hexacarbonyl.....	102
5. Conclusions and further work.....	116
5.1. Biomolecules.....	116
5.1.1. Comparative studies of potassium and electron collisions with biomolecules: site selectivity.....	116
5.1.2. Dissociative electron attachment to dimethyl disulphide .....	118
5.2. Technologically relevant molecules.....	118
5.2.1. Dissociative electron attachment to volatile anaesthetics (enflurane, isoflurane) and chlorinated ethanes (pentachloroethane and hexachloroethane) .....	118
5.2.2. Low-energy electron interaction with tungsten hexacarbonyl.....	120
Appendix I: List of other published papers.....	122
Appendix II: Curriculum vitae.....	123

*Table of contents*

# 1. Motivation

---

The study of the behaviour of charged particle beams with atoms and molecules is among the most significant developments in physics [1] with several applications in science and technology. In the universe, ionised particles are one of the most abundant species, however, in the Earth's environment, and generally speaking, the matter consists mostly of neutral atoms and molecules in different stages of aggregation. Nevertheless under certain conditions ionised atoms and molecules can be created. These conditions are time and space dependent and can vary from a simple lightning striking the Earth to complex devices in science and technology that use techniques with charged particles as a mean of probing a particular target [2].

The question that can be raised now is: Why is then the study of charged particle interactions with atoms and molecules so significant [2]? The answer certainly depends on the particular area of study and the approach needed. The study of charged particles is not only important in physics, but in medicine, chemistry, pharmacy, and many others, so the key issue is to understand and get detailed knowledge on the underlying mechanisms probed by such interactions. However, there is something in common to all fields that use ionised particles: i) ions can be easily controlled by electric and/or magnetic fields and ii) they can be rather easily detected [2]. Using ions as a probing tool, also allows having an insight into the very fundamental aspects of the target behaviour [1,2]. From a fundamental point of view the understanding of the electronic structure of atoms and molecules and their chemical reactivity is of great importance in several scientific and technological areas, as pointed out before. Molecules present in the interstellar medium (e.g.  $C_{60}$ ,  $CH_4$ ), in the Earth's lower atmosphere ( $N_2$ ,  $O_2$ ), those linked with environmental issues as global warming and ozone depletion (e.g.: anthropogenic emissions), explosives and narcotics and molecules of biological interest (e.g.:  $H_2O$ , deoxyribonucleic acid bases and essential amino acids) are some examples of relevant species that play a significant role in our daily lives. Therefore a comprehensive knowledge of how these species behave may result in development of new tools and technologies which may certainly affect our lives.

Mass spectrometry has been largely used as a probing technique for atoms and molecules. This is an important tool in many fields of science and technology and was used in the present work to identify the species formed after the interaction of electrons and

## Motivation

atoms with bare molecules. Briefly, in this technique a neutral gas sample is made to interact with a beam of electrons (either for attachment or ionisation), and the charged particles formed (either positive or negative) are separated according to their mass to charge ratio ( $m/z$ ) and detected [3] (see Figure 1.1). However not all samples are gaseous. Solid and liquid samples can be transferred into the vacuum systems via a proper sample inlet system which in some cases can be heated in order to increase the samples' vapour pressures [3]. In an ion source chamber, for pressures in the range of  $10^{-5} - 10^{-6}$  mbar ( $\sim 10^{-3} - 10^{-4}$  Pa) the mean free path for the ions is long enough, meaning that bimolecular interactions are almost impossible [3].

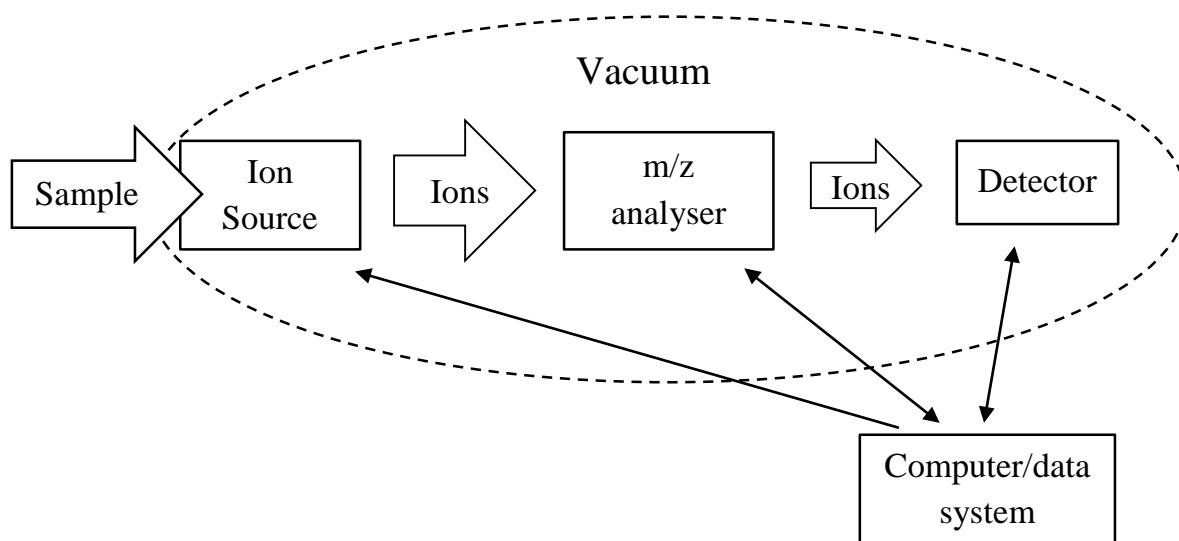


**Figure 1.1 – Schematics of the various components present in a mass spectrometer. Represented are: the sample inlet; ion source;  $m/z$  analyser (separates the ions according to their individual  $m/z$  values); detector (generates a signal whenever an ion reaches the detector); vacuum system (provides binary collision conditions); computer (drives each of the spectrometer's component, records and stores the data obtained). Adapted from [4].**

The interaction of low energy electrons with neutral molecules and/or atoms can produce negatively charged ions, which are dependent on the energy of the incoming electron, whereas positively charged ions can be formed as long as the incoming electron has an energy equal or greater than the ionisation energy (typically for molecules such threshold is  $>10\text{eV}$ ) [2]. The formation of cations or anions by electron interactions with atoms and/or molecules allows to obtain information on their atomic and/or molecular states as it happens in electron scattering processes. Using different experimental methods

## *Motivation*

it is possible to obtain very precise information about energy and angular distribution of the scattered particles, radiation emitted, fragments produced, etc. [1,3]. The studies performed within this thesis made use of mass spectrometry to allow obtaining information about the fragmentation pathways of selected ions. The experimental data obtained in these studies can also help benchmarking theoretical calculations and find out better parameters for complex simulations, which will then help to better understand the whole chemical-physical reaction processes behind the electron/atom interaction with a particular target molecule.

This thesis is divided in 5 chapters. In the second chapter (Electron Induced Processes) a brief description of electron induced processes, the concepts and mechanisms are introduced. Chapter three (Experimental set-up) contains a description of the experimental setups used to perform dissociative electron attachment (Innsbruck laboratory) and electron transfer studies in atom-molecule collision experiments (Lisbon laboratory). In chapter four it is presented the major results from those experiments. Finally, the last chapter deals with the conclusions. This thesis contains studies of several different types of molecules, which were divided into two groups: biomolecules and of technological relevance. As a result of the work performed, several publications have appeared in international peer-review journals.

## **References**

- [1] N.F. Mott, H.S.W. Massey, *The Theory of Atomic Collisions*, Oxford University Press, Great Britain, 1949.
- [2] E. Illenberger, J. Momigny, *Gaseous Molecular Ions. An Introduction to Elementary Processes Induced by Ionization*, Steinkopff/Springer, New York, 1992.
- [3] J.H. Gross, *Mass Spectrometry*, Springer Verlag, Germany, 2004.
- [4] J.T. Watson, O.D. Sparkman, *Introduction to Mass Spectrometry: Instrumentation, Applications and Strategies for Data Interpretation*, Wiley, Chichester, England, 2007.



## 2. Electron Induced Processes

---

The following chapter is an overview of the important processes and mechanisms for the discussion of the results presented in this thesis. The interaction of electrons with molecules is the main focus of the current thesis, however electron transfer experiments have also been performed. Collisions between fast neutral atoms and molecules will be briefly presented. From the interaction of an electron with a molecule, electron attachment is one of the possible processes attained and so studied here. In the case of atom-molecule collisions, an electron donor atom (in the case of this thesis, neutral potassium) transfers an electron to the target molecule in a process well-known as electron transfer. Before going into detail about negative ion formation, some introductory notions are presented in the next sections.

### 2.1. Scattering processes

The interaction of an electron with a molecule is a process that can be divided into two classes: direct (Figure 2.1) and resonant scattering (Figure 2.2). Direct scattering is characterized by the collision of an electron with the target molecule with the electron being scattered after the interaction [1]. If the total kinetic energy of the system (electron + molecule) is conserved, the process is known as elastic scattering, whereas if the total kinetic energy of the system is not conserved is named inelastic scattering. Direct electron scattering is a *non-resonant* process, it means that the incident electron may transfer an amount of its kinetic energy to the molecular target.

#### 2.1.1. Direct elastic scattering

In a first approximation, during an elastic scattering the incident electron energy does not change, *i.e.*, there is a total conservation of the kinetic energy ( $\Delta E_k \sim 0$ ). No energy will be transferred to the target molecule and thus neither excitation nor cleavage of

molecular bonds will occur. However, the electron will be deviated from its original trajectory.

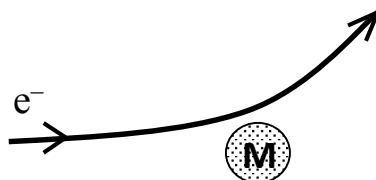
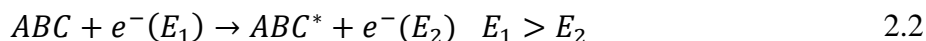


**Figure 2.1 - Schematic representation of direct electron scattering. Adapted from [1].**

### **2.1.2. Direct inelastic scattering**

In contrast with the elastic scattering, in an inelastic scattering there is no conservation of the kinetic energy ( $\Delta E_k \neq 0$ ). The electron loses some kinetic energy that will be transferred to internal excitations of the molecule (electronic, vibrational and rotational). This excess of internal energy, may lead to bond breaking.



### **2.1.3. Resonant scattering**

Resonant scattering means that the incoming electron may stay for a significantly long period of time (longer the direct transit time) [1] in the proximity of a molecule, forming a transient negative ion (TNI or metastable).

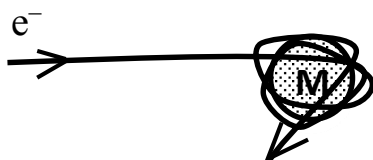


**Figure 2.2 - Schematic representation of resonant electron scattering. Adapted from [1].**

If the electron energy is resonant with the *empty* molecular energy level, the captured extra electron will be trapped and a TNI will be formed. In most of the molecular systems studied the TNI dissociates into fragments, a process known as dissociative electron attachment (DEA). Studying the product anions allows to probe the fragmentation mechanisms of the precursor anion. A TNI's lifetime varies largely, depending on the resonance energy and on the molecule's spatial dimension. This variation goes from some vibrational periods ( $10^{-14}$  s) up to some microseconds (in the case of polyatomic molecules) [1]. According to Heisenberg's uncertainty principle, a TNI's lifetime  $\tau$  is related to the energy's width ( $\Gamma$ ) of the potential energy curve, by [1]:

$$\tau \approx \frac{\hbar}{\Gamma} \quad 2.3$$

with  $\hbar$  the Planck constant ( $\hbar/2\pi = 6.6E^{-16} \text{ eV} \cdot \text{s}$ ).

## **2.2. Born-Oppenheimer-Approximation**

Nuclear motions are classified as *translation*, *rotation* and *vibration*. Taking into account the kinetics of a molecule's centre of mass, translations can be separated from the other motions (or degrees of freedom). Assuming that there is no appreciable change in the internuclear distance, molecular rotations cause the orientations of any dipole moments to change. This allows interactions with radiation to take place. Molecular vibrations disturb the electronic cloud of the molecule due to the motion of the nuclei with respect to each other. The change in the electron cloud distribution brought by transitions between electronic states may also change the electric dipole moment of a molecule.

The way that these three mechanisms can interact may be simplified since they can be treated separately due to the different molecular time scales over which they occur: over the time a molecule takes to complete one rotation it may go through several vibrations, whereas electronic transitions occur so fast, that according to the *Franck-Condon* principle, the nuclear positions do not change appreciably during a transition between two electronic states. The energies involved for each of these mechanisms are also quite different. Rotational energy levels are typically separated by a few meV, vibrational levels have separations of the order of tens to hundreds of meV, and electronic transitions range from

a few to tens of eV. Molecules can experience these different types of motion simultaneously, but due to the fact that the energies of the motions are so different they can be treated separately. In first approximation, the total energy is then the summed contribution of each of type of motion, and generally speaking written as:

$$E_{total} = E_{electronic} + E_{vibrational} + E_{rotational} \quad 2.4$$

with  $E_{electronic} \approx 10^2 E_{vibrational} \approx 10^4 E_{rotational}$  [2]. This is known as the *Born-Oppenheimer* approximation (BOA). This energy is dependent on the internuclear distance of the several components in a molecule. For a diatomic molecule (M) and according to the BOA approximation, its energy potential curve can be plotted as in Figure 2.3. Also represented is the potential curve for the electronically excited molecule ( $M^*$ , which in the case of Figure 2.3, such is represented by the parent anion,  $M^-$ ).

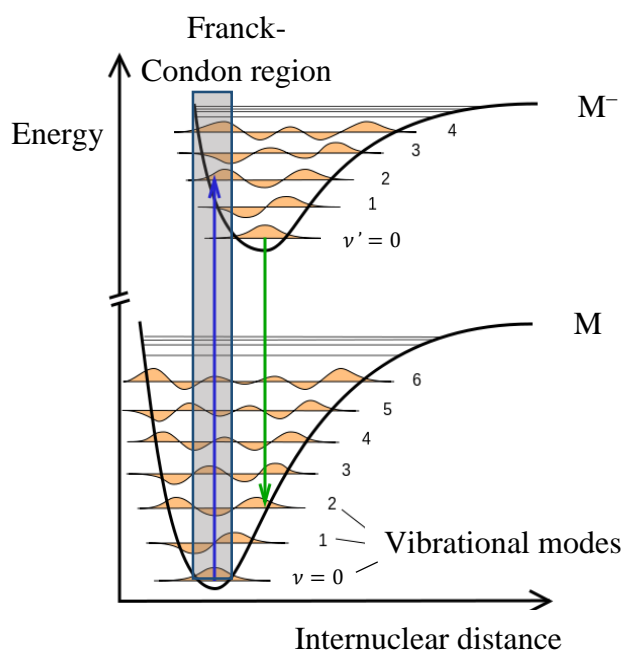


**Figure 2.3 - Born-Oppenheimer potential energy curves for a molecule in the ground state (M) and its electronically excited state ( $M^-$ ). Vertical transitions are shown representatively. Also represented are the vibrational modes ( $v$ ) and the Franck-Codon region (shadow). Adapted from [3].**

### 2.3. The Franck-Condon principle

Transitions between two electronic states can easily be described if one considers that they occur so rapidly that the internuclear distances of the molecule do not have enough time to change appreciably their position of equilibrium. This is known as the *Franck-Condon principle*. Hence an electronic transition between two states may be represented by a vertical line joining the potential energy surfaces, originating from the most probable internuclear separation in the ground state [4]. The electronic transition from the ground-state to an electronically excited state of a molecule occurs within the Franck-Condon region (see Figure 2.3), defined by the superposition of the vibrational wavefunctions of both states [5]. The probability of a transition from a vibrational level  $v$  of the neutral to an excited vibrational level  $v'$  of the upper electronic state is approximately given by the Franck-Condon factor (FCF) [5]:

$$FCF = |\langle \Psi_{v'} | \Psi_v \rangle|^2 \quad 2.5$$

The  $\Psi_v$  represents the vibrational wavefunction of the neutral ground state and  $\Psi_{v'}$  is the vibrational wave function of the upper electronic state.

### 2.4. Negative ion formation through electron attachment

Molecular dissociation can be triggered by the capture of an electron by a neutral molecule. In the context of this thesis two distinct mechanisms are identified: a) electron transfer; and b) dissociative electron attachment. In the electron transfer process, an electron is transfer from a neutral (A) or a negatively charged atom ( $A^-$ ) to a neutral molecule (BC). This process can be exemplified in the following equations [1]:



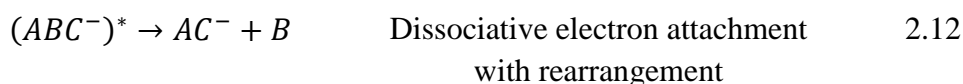
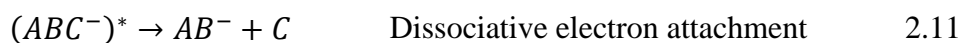
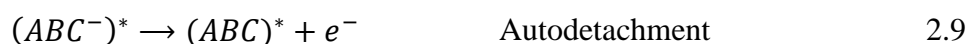
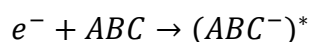
Reaction 2.6 is typically endothermic, which indicates that BC's electron affinity is lower than A's ionisation energy. Namely, reaction 2.6 can only occur if A and/or BC's kinetic energy is above the reaction threshold [1]. On the other hand the dissociative

electron attachment process is characterized by a capture of a free electron, schematically represented as:



### 2.4.1. Dissociative electron attachment

Free electron capture is a resonant process; the electron is trapped by the molecule/atom and produces a temporary negative ion (TNI). After the TNI's formation, it can decay by different processes: autodetachment, radiative stabilisation and dissociative electron attachment. ABC represents a polyatomic molecule and “\*” indicates the anionic transient state.



During the lifetime of the resonance, the presence of the extra electron in the system will incite the movement of the nuclei to larger distances [8]. In reaction (2.9) the TNI does not undergo into dissociation and goes back to the neutral state via spontaneous emission of the electron (see Figure 2.4). However, as briefly pointed out before (see sub-chapter 2.1.3), due to the long-time permanence of the extra electron, the neutral molecule can stay in an excited vibrational state [9]. Within the initial electronic state a reaction with  $\nu' > \nu$  and  $n = n'$  is a vibrational excitation (VE) [8].  $\nu$  represents the ground vibrational state and  $\nu'$  is an excited vibrational state, while  $n$  is the ground electronic quantum number and  $n'$  corresponds to an electronic quantum number in the excited state.

In reaction 2.10, the electron will attach to the molecule, but the excess of internal energy will be released by a photon emission. Because the radiative lifetimes are in the

range of  $10^{-9} - 10^{-8}$  s, this sort of reactions are slower than those in 2.9 and 2.11 . This will make this process non-competitive with the others [1].

Reaction (2.11) describes the dissociative electron attachment channel. The TNI is unstable due to the temporary presence of an extra electron, which will change the intramolecular potential. The TNI decomposition will occur due to the excess of internal energy. In the course of the negative ion formation, the equilibrium internuclear distance of the state that leads to dissociation is overall higher than the equilibrium internuclear distance of the neutral molecule. This is the case, since the bond energy is reduced by the presence of an extra electron. If the DEA channel is available, it will strongly compete with the autodetachment channel [1]. Hence, depending on the autodetachment lifetime, the TNI can decay into the available anionic fragments and corresponding neutral fragments.

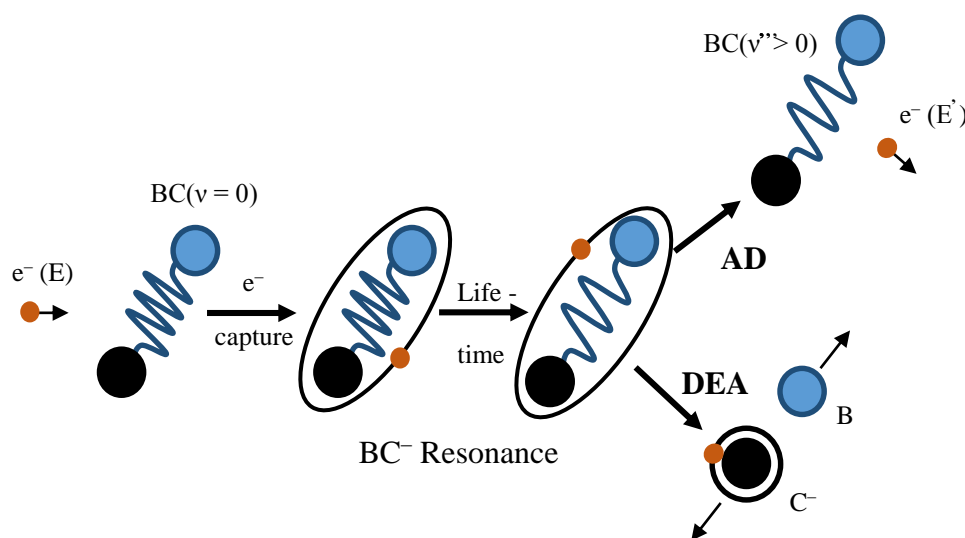


**Figure 2.4 - Dynamics of Autodetachment (AD) and dissociative attachment (DEA) in electron-molecule scattering through resonances.  $\nu$  represents a vibrational quantum number. Adapted from [8].**

Sometimes DEA does not progress directly via a purely repulsive energy surface, instead, it progresses through indirect processes such as electronic, vibrational predissociation or rearrangement of the precursor anion before it dissociates. Such example is shown in reaction 2.12, where internal rearrangement occurs. While reaction 2.11 represents a single cleavage of the B–C bond, reaction 2.12 represents the removal of B from the TNI with a cleavage of the A–B and B–C bonds and rearrangement of the neutral fragments to form AC. In this kind of reaction the energy gained by the formation of the

stable neutral product AC can shift the threshold energy to lower values. The most ordinary rearrangements in a molecule are those containing hydrogen or fluorine [6].

A schematic representation of the dynamics in a potential curve diagram of AD (autodetachment), DEA and NDA (non-dissociative electron attachment) is shown in Figure 2.5. A repulsive anionic potential energy curve in the Franck-Condon region is represented in red. AD is possible until the crossing point  $R_C$ . In contrast with the red potential curve, the blue potential curve has a minimum. If the excess of energy brought by the extra electron is released or redistributed into other vibrational degrees of freedom, the metastable  $ABC^{\#}$  can be formed. On the left-hand side of Figure 2.5 it is represented a sketch where is possible to infer on the ion yields corresponding to the formation of  $BC^-$  (red curve) and  $ABC^-$  (blue curve).

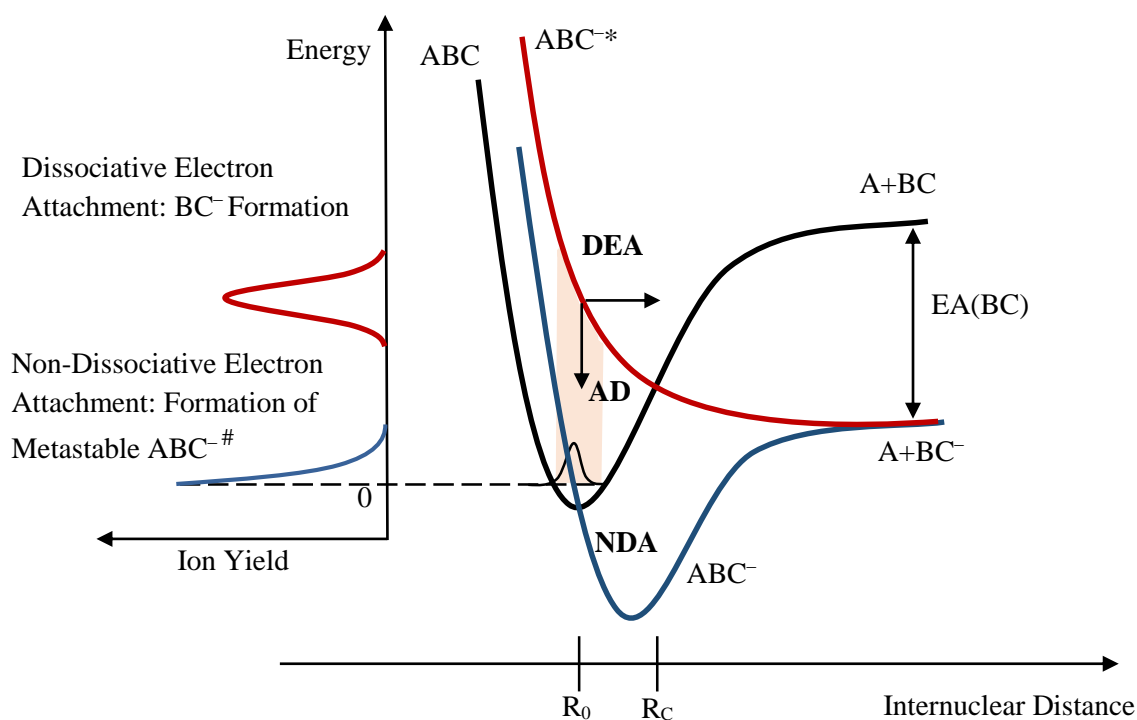


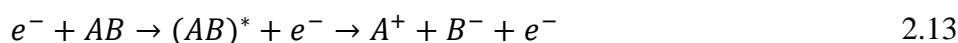
**Figure 2.5 - Schematics of a potential curve for low energy electron interactions with a molecule ABC. Representation of possible decay processes: DEA (dissociative electron attachment), AD (autodetachment) and NDA (non-dissociative electron attachment). Adapted from [6].**



Finally, DEA is also a bond and site selective process, i.e., site (N1-H vs N3-H)- and bond (C-H vs C-N)- selective dissociation in DNA/RNA pyrimidine bases can be achieved by tuning the proper electron energy [10].

### 2.4.2. Dipolar dissociation

While DEA is a resonant process that generally occurs at electron impact energies below ~15 eV, dipolar dissociation (DD) characterizes a direct excitation process of the target molecule and it takes place at higher energies [11]. DD involves dissociation of an electronically excited state into an ion-pair, *i.e.*, it dissociates into a positively and negatively charged fragment [12]:



Its electron energy dependence usually consists of a monotonically increase from a threshold of the anion yield (in this example,  $B^{-}$ ) [12].

### 2.4.3. Electron transfer

The processes of collisional ionisation include every interaction between neutral particles in which an electron transfer occurs. From the many reactions possible, the reactions below resume the different electron transfer types studied in the present thesis:



One way of performing electron transfer experiments is to make use of an electron donor, *i.e.*, an atom that has a weakly bound valence electron and under particular experimental conditions can transfer it to a target molecule. Examples of this kind of atoms are the alkaline metals (Na, K, Cs...) with particular low-ionisation energies. In the present work an experiment concerning electron transfer was used where the electron donor atom was potassium (K). Potassium has a relatively low ionisation energy, 4.34 eV [13], making it a good electron donor.

The electron transfer in atom-molecule collisions depends on the crossing of the potential energy surfaces of the neutral complex  $A + BC$  and the ionic  $A^+ + BC^-$  involved in the collision process. According to Kleyn *et al.* [14], for large atom - molecule distances, the ionic potential energy curve lies above the covalent, however due to the Coulombic potential of the collision complex  $(A^+BC^-)^*$  there is a crossing point in which two curves have the same value ( $R_c$ ). This interaction gives rise to a positive ion formation and a molecular anion, i.e. ion-pair formation. During the molecular anion formation, the internuclear equilibrium distance corresponding to the state that leads to dissociation is in general always higher than the equilibrium distance of the neutral molecule, since the capture of an excess electron reduces the bonding energy [6]. In the Lisbon laboratory, potassium - molecule collisions are typically performed in the lab-frame range 15 – 300 eV, meaning that in the low energy collision regime ( $< 50$  eV), the collision time (defined as the transit time of  $K^+$  after electron transfer and before leaving the strong Coulomb interaction with the TNI) is of the same order as the vibrational period of particular modes (typically stretching). As a consequence, during the collision the target molecule may experience a gradual increasing of a particular bond ( $R_m$ ), meaning that the electron affinity (see next sub-chapter) is not limited to a fixed value. This process is known as bond-stretching [15].

Considering that the crossing point between covalent and ionic potential energy curves in the case of diatomic molecules (or surfaces in the case of polyatomic molecules) takes place at large atom-molecule distances, van der Waals and polarization interactions can be ignored, meaning that the ionic potential can be represented by a Coulombic potential only. Since in this point both potential energy curves (or surfaces) have the same value, the crossing point ( $R_c$ ) in units of Å can be given by the following equation [14]:

$$R_c \approx \frac{e^2}{\Delta E} = \frac{14.41}{IE - EA(R_m)} \quad 2.16$$

where  $IE$  corresponds to the ionisation energy of the donor atom and  $EA$  corresponds to the electron affinity of the target atom (or molecule) [16], both in units of eV. The increase of the electron affinity results in an increase of the crossing distance.

The collision interaction can be depicted in a simple cartoon as presented in Figure 2.6. For simplicity, it is assumed an atom-atom collision scheme. In the case of atom-molecule collisions we cannot restrict ourselves to simple potential energy curves but rather

potential energy surfaces involved in the interaction. In the case of ionic scattering, there are two crossing distances, *i.e.*, one during approach,  $R_{c1}$ , and the other at departure  $R_{c2}$  ( $>R_{c1}$ ), see Figure 2.6.  $R_{c2}$  depends on the collision velocity, which reflects the electron affinity behaviour with  $R_m$ .

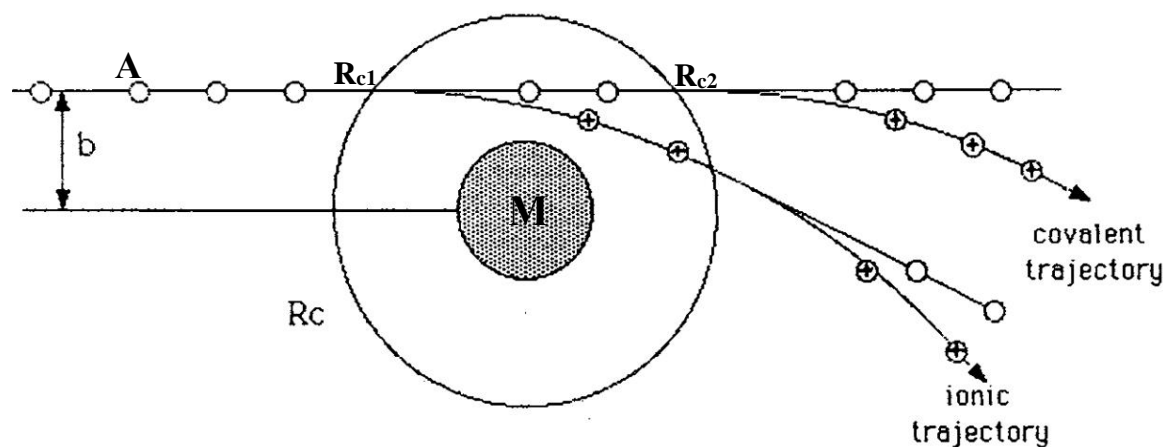


**Figure 2.6 – Representation of the collision trajectories between an alkaline atom (A) and a molecule (M). The crossing radius corresponds to the external circle and the repulsive potential region is represented by the dashed area. When the electron is transferred at  $R_{c1}$  the trajectory is known as ionic, whereas at  $R_{c2}$  the trajectory is termed covalent. Adapted from [14,17].**

The transition between ionic and covalent states is only possible if the adiabatic principle is satisfied, *i.e.*, if the collision partners get slowly closer to each other. In this case, the target electrons have enough time to adjust themselves to the internuclear separation due to electron transfer. However, if the collision is fast enough, there is no time for such changes and no electron transfer will occur. In this case the system will keep the same electronic configuration [14], *i.e.* known as covalent. In an electron transfer process, the probability of occurring a non-adiabatic transition ( $p$ ) is given by the Landau-Zener model (for a comprehensive description see ref. [14]).

#### 2.4.4. Electron affinity

The capability of a molecule to form a stable anion is denoted by the electron affinity (EA). It is defined as the energy difference between the molecule in its neutral ground state (M) and its anionic state ( $M^-$ ) [18]. Adiabatic electron affinity ( $EA_{ad}$ ) refers to

both, the neutral and the anion, in their ground electronic, vibrational and rotational states [19].

$$EA(M) = E(M) + E(M^-) \quad 2.17$$

Per definition the EA is negative if the electronic state  $M^-$  lies above the neutral  $M$ , and it is positive if it lies below [1]. A positive value indicates the presence of a stable anion. In order to have a stable anion, the excess energy given by the attachment of the extra electron has to be dissipated by the molecule.

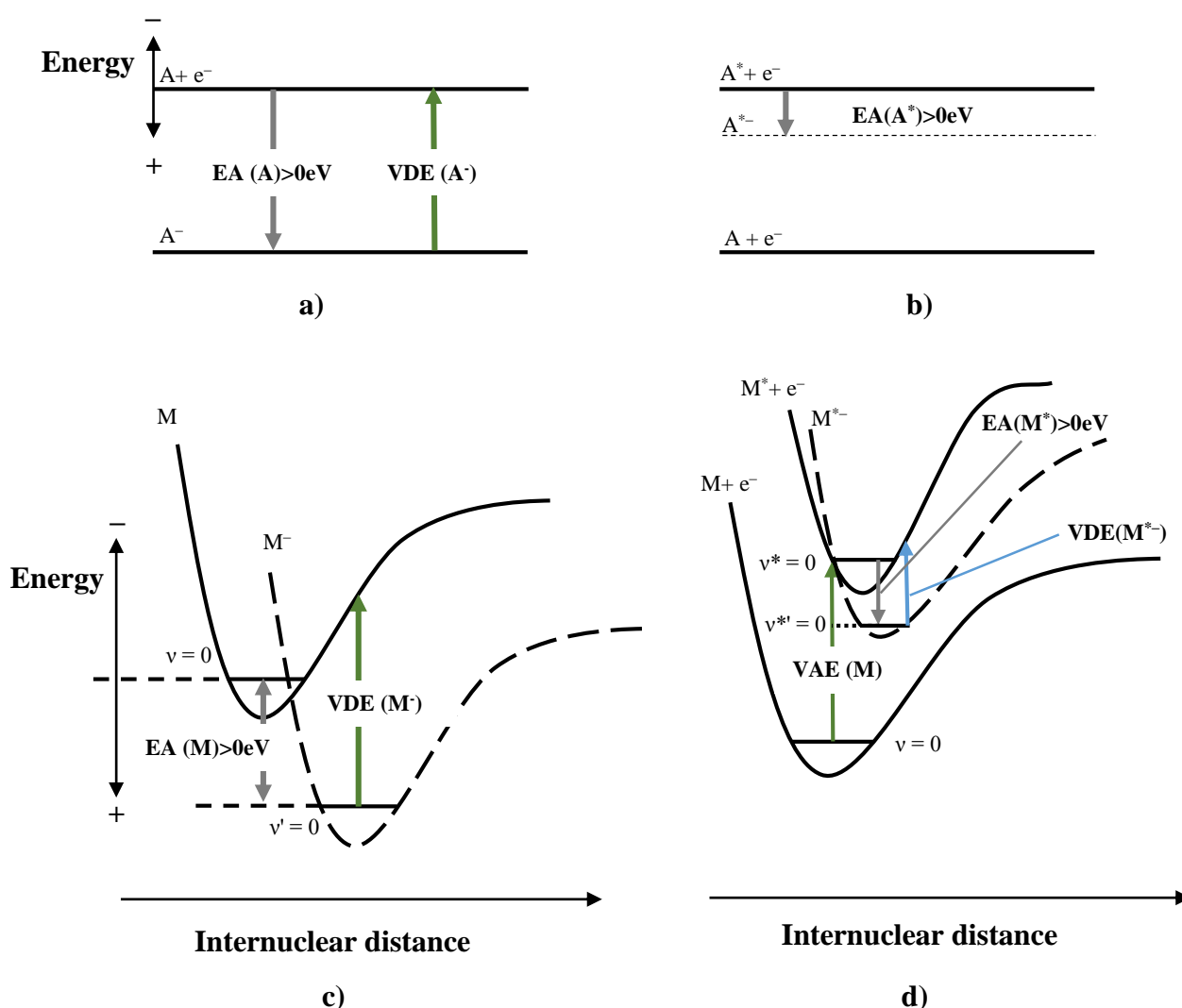


Figure 2.7 - Schematic diagrams of potential energies. Representation of the electron affinity (EA), vertical detachment energy (VDE) and vertical attachment energy (VAE). Adapt from [6].

It is also important to define vertical attachment energy (VAE) and vertical detachment energy (VDE). VDE is the minimum energy necessary to detach the additional electron from the ground state of the negative ion [18]. No changes in the internuclear distance occur (see sub-chapter 2.3). On the other hand, the VAE corresponds to the difference in energy between the neutral molecule in its ground electronic state with an electron at infinity, and the formed anion. As in the case of VDE, in VAE no changes in the internuclear distance occur. Figure 2.7 shows a schematic of the EA, VDE and VAE representation. In Figure 2.7 a) and b) examples of when an atom captures an extra electron are shown. Figure 2.7 c) and d) show examples of when an electron is captured by a diatomic molecule. In Figure 2.7 a) it is possible to observe that the EA(A) and VDE(A<sup>-</sup>) are the same. This is the case where all transitions occurring in atoms are vertical. The internuclear distance cannot change, as there is only one nucleus. Figure 2.7 b) and d) represent the case where a Feshbach resonance is formed. The excess electron is attached to an excited atom or molecule, forming the anionic specie A<sup>\*-</sup>, M<sup>\*-</sup>. Feshbach resonances and other types of resonances will be briefly described in the next sub-chapter.

### 2.4.5. One particle and two particle-one hole resonances

When an electron is captured by a molecule into its lowest unoccupied molecular orbital (LUMO) a resonance is formed. The LUMO usually has anti-bonding character [8].

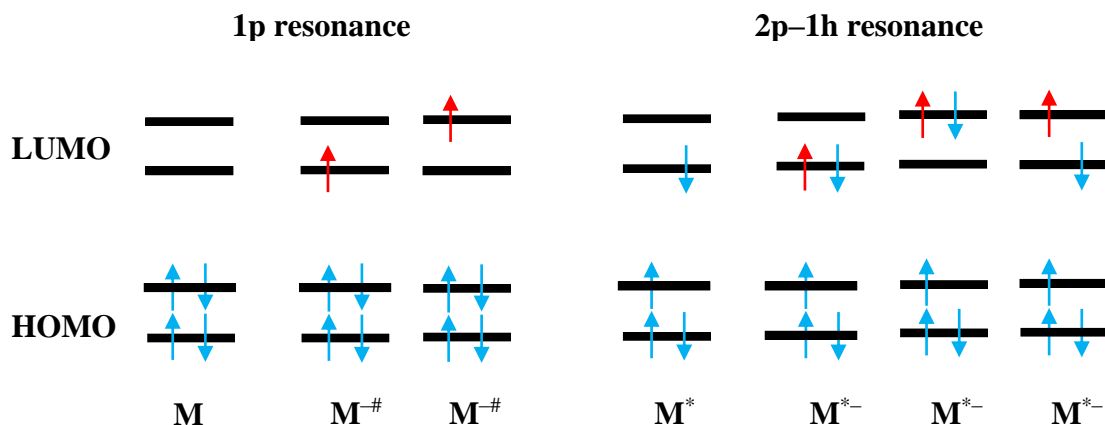
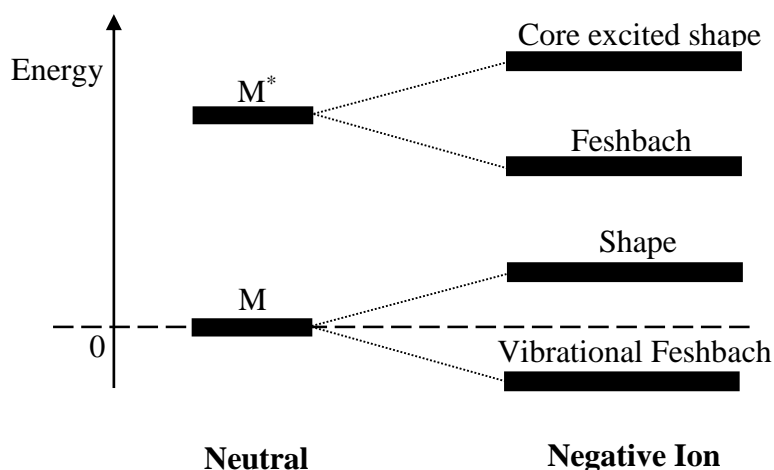


Figure 2.8 - 1p resonance and 2p-h resonance electronic configuration. The red arrows represent the captured electron. Adapted from [20].

The types of TNI observed in the present study are described by single particle (1p) and two particle-one hole (2p-1h) resonances (Figure 2.8). A 1p resonance is formed when the incoming electron occupies the LUMO. On the other hand, in a (2p-1h) resonance the incoming electron will excite at least one of the electrons of the molecule. Hence a hole is created in the electronic configuration as two electrons will occupy the LUMO [21].



**Figure 2.9 - Classification of the different types of resonance according to their energy in comparison to the neutral parent (M). Adapted from [1].**

A way to categorize the resonances can be done through the difference in energy between the neutral and the excited molecule (Figure 2.9). In a one particle resonance, the interaction between the incident electron and the neutral in the ground state origins a potential well where the incident electron will be trapped. This mechanism is described by the effective potential, which consists of the attractive polarization interaction and repulsive centrifugal potential. The attractive polarization interaction is given by [22]:

$$V_a(r) = -\frac{\alpha q^2}{2r^4} \quad 2.18$$

where the induced dipolar attraction ( $V_a(r)$ ) is defined by the polarization ( $\alpha$ ) of the target molecule, the distance between the incoming electron and the molecule ( $r$ ) and by the elementary charge ( $q$ ).

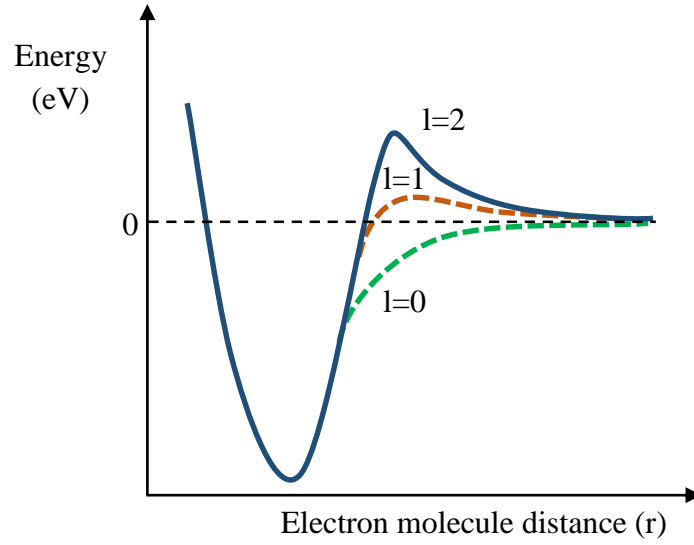


**Figure 2.10 - Representation of the effective potential of the electron-molecule interactions depending on their distance ( $r$ ). Depending on the angular momentum, different potential barriers are formed.**

**For  $l = 0$ , no potential barrier is formed, while for  $l \neq 0$  a centrifugal barrier is created and the electron can be momentarily trapped inside the effective potential. Adapted from [21].**

The repulsive centrifugal potential ( $V_l(r)$ ) is given by [22]:

$$V_l(r) = \frac{\hbar^2 l(l+1)}{2r^2\mu} \quad 2.19$$

where  $l$  represents the electron angular momentum and  $\mu$  is the reduced mass of the molecule-electron system. This will originate a centrifugal barrier in which the extra electron can be momentarily confined. Thus, the effective potential has the form:

$$V_{eff}(r) = V_l(r) + V_a(r) = \frac{\hbar^2 l(l+1)}{2r^2\mu} - \frac{\alpha q^2}{2r^4} \quad 2.20$$

The effective potential for different angular momentum quantum numbers ( $l = 0, 1$  and  $2$ ) is represented in Figure 2.10. When  $l \neq 0$  a centrifugal barrier is created and an electron can be momentarily trapped inside it. These are known as shape resonances [23,24], since the extra electron is trapped by the shape of the potential. In a shape resonance the electronic state of the TNI lies above (in energy) the neutral state (Figure 2.9). The lifetime of this resonance is short ( $10^{-15} - 10^{-10}$  s) [23], due to the possible

tunneling of the electron through the potential barrier. The TNI decay is further dictated by the competition of dissociation with autodetachment. The TNI decays back to the parent electronic state, which frequently includes vibrational excitation [24]. These resonances are also referred as one particle resonances. The energies of these resonances in electron-molecule experiments are usually found below 4 eV [23]. On the other hand for the case where the angular momentum is zero ( $l = 0$ ) no barrier is created.

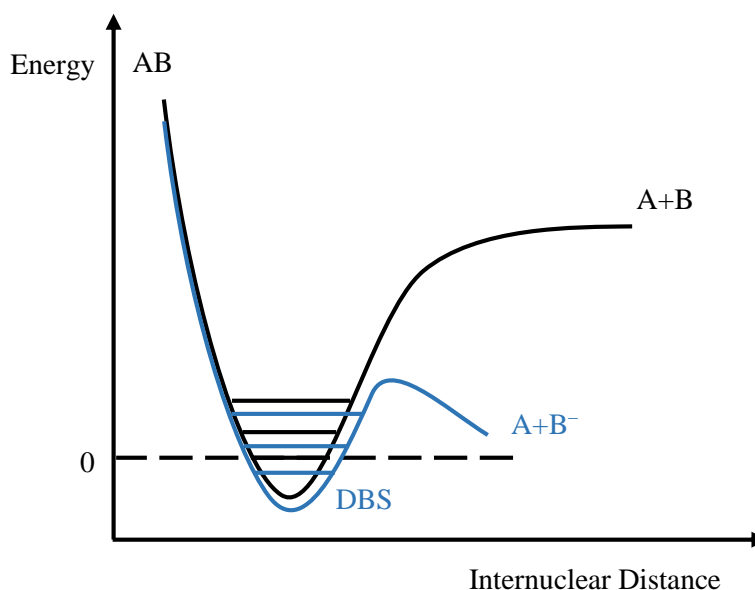


**Figure 2.11 – Representation of a dipole bound state or also called vibrational Feshbach resonance, since its vibrational levels are below the corresponding levels of the neutral. Adapted from [25].**

A vibrational or nuclear Feshbach resonance (Figure 2.11) is still a 1p resonance, however in this type of resonance the energy of the TNI produced is below the ground state of the neutral [8]. This means that molecules with this type of resonances have a positive electron affinity (EA) and are likely to have large polarizability or a very large dipole moment ( $>2.5$  D) [21].

In a core-excited resonance or two particle-one hole (2p-1h) resonance, the energy of the incoming electron is high enough to induce an electronic excitation. Two electrons will occupy molecular orbitals (MO) which are typically empty [26] (see Figure 2.8). These resonances take place at energies near to the electronic excitation energies and usually lead to TNIs that lie energetically above the electronically excited parent state of the neutral molecule [21]. A centrifugal barrier is bounding the electron as in the 1p resonance case [21]. As seen before, the potential barrier is dependent on the  $l$  value of the occupied excited



state orbital, therefore no electrons with zero angular momentum can be attached (at least by such barrier). This type of resonances can decay by autodetachment or dissociative attachment, having a typical lifetime of the order of  $10^{-3} - 10^{-2}$  s [20].

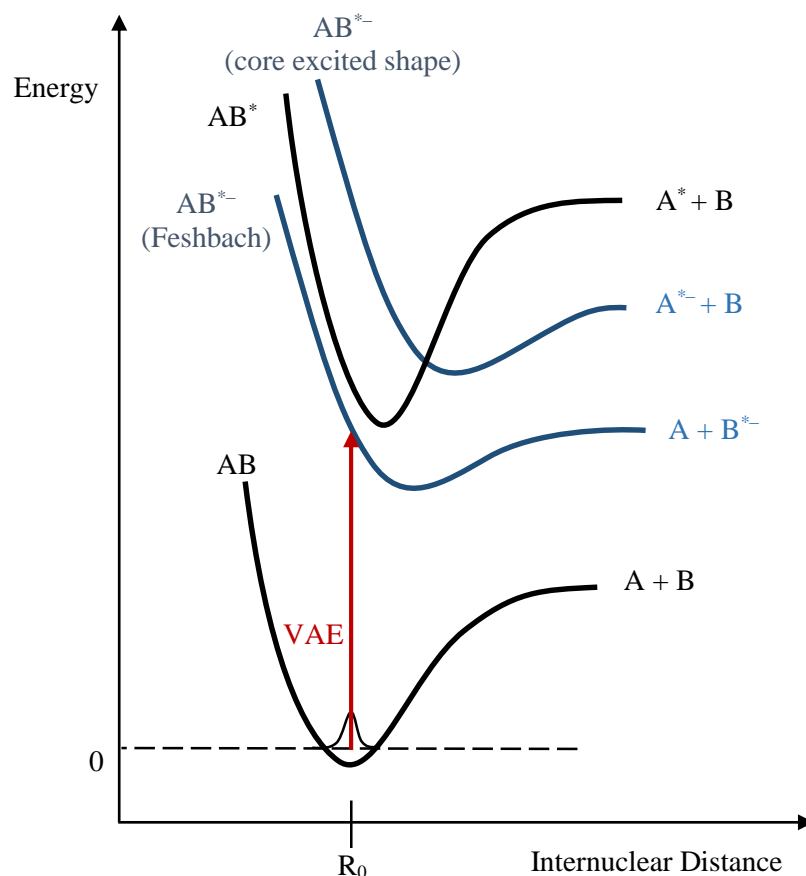


**Figure 2.12 – Scheme of a potential energy diagram where the neutral ground state and electronically excited state of molecule AB is visible. Core excited shape and Feshbach resonances are also represented. Adapted from [21].**

A Feshbach resonance (Figure 2.9 and Figure 2.12) is characterized by the TNI having a lower energy than the excited neutral [8]. The electron affinity of the excited neutral is thus positive. In order to dissociation take place, the captured electron needs to get the energy before reemission becomes energetically available. For a decay process into the neutral ground state a change of the electronic configuration is required. The autodetachment lifetime of the anion is thus significantly longer [9].

#### **2.4.6. Metastable ions**

When an ion is formed, it can have enough internal energy to dissociate before being detected. Concerning the ions stability, in mass spectrometric time scale there is a terminology that categorize three different types of ions: stable, unstable and metastable ions [5]. Stable ions are those that do not decompose or have decomposing rates  $\lesssim 10^5 \text{ s}^{-1}$ , therefore they will reach the detector without being fragmented [5]. On the other hand unstable ions decompose before reaching the detector, having dissociating rates  $> 10^6 \text{ s}^{-1}$  [5]. They are unable to be detected. The third type of ions are known as metastable and have decomposing rates of  $10^5 - 10^6 \text{ s}^{-1}$  [5,18]. They are defined as ions that are formed in the ion source (parent ions), but decay into fragments (daughter ions) while on their transit through the mass analyser system. This process is called metastable decomposition [27].

The origin of metastable formation can be due to several mechanisms, varying with the electronic structure and size of the precursor ion [7,18]. Processes such as, vibrational predissociation, tunneling through a barrier and rearrangement transitions will prompt to ion metastability [18]. Due to the distribution of internal energy, this type of ions have low peak intensities representing about  $< 1\%$  of the parent signal [7]. Naturally, excessive internal energy will lead to fragmentation while low internal energy leads to the formation of a parent ion [18], as long as it may accommodate this energy through its internal degrees of freedom.

## References

- [1] E. Illenberger, J. Momigny, Gaseous Molecular Ions. An Introduction to Elementary Processes Induced by Ionization, Steinkopff/Springer, New York, 1992.
- [2] S. Denifl, PhD thesis, University of Innsbruck, Innsbruck, 2004.
- [3] <http://de.wikipedia.org/wiki/Franck-Condon-Prinzip#mediaviewer/Datei:Franck-Condon-Prinzip.svg>, (Accessed on June 2014).
- [4] E. Condon, Phys. Rev. 28 (1926) 1182.
- [5] J.H. Gross, Mass Spectrometry, Springer Verlag, Germany, 2004.
- [6] L.G. Christophorou, Electron-Molecule Interactions and Their Applications, Academic Press, London, 1984.
- [7] T.D. Märk, G.H. Dunn, Electron impact ionization, Springer Verlag, Vienna, 1984.
- [8] H. Hotop, M.W. Ruf, M. Allan, I.I. Fabrikant, Advances In Atomic, Molecular, and Optical Physics, Academic Press, 2003.
- [9] A. Edtbauer, PhD Thesis, University of Innsbruck, Innsbruck, 2010.
- [10] S. Ptasinska, S. Denifl, V. Grill, T.D. Mark, E. Illenberger, P. Scheier, Phys. Rev. Lett. 95 (2005) 4.
- [11] E. Szymanska, N.J. Mason, E. Krishnakumar, C. Matias, A. Mauracher, P. Scheier, S. Denifl, Int. J. Mass Spectrom. 365 (2014) 356.
- [12] M. Bazin, S. Ptasinska, A.D. Bass, L. Sanche, Phys. Chem. Chem. Phys. 11 (2009) 1610.
- [13] R.L. Kelly, J. Phys. Chem. Ref. Data 16 (1987) 1.
- [14] A.W. Kleyn, J. Los, E.A. Gislason, Phys. Rep.-Rev. Sec. Phys. Lett. 90 (1982) 1.
- [15] J.A. Aten, J. Los, Chem. Phys. 25 (1977) 47.

- [16] D. Almeida, PhD, Universidade Nova de Lisboa, Lisboa, 2013.
- [17] A.W. Kleyn, A.M.C. Moutinho, *J. Phys. B-At. Mol. Opt. Phys.* 34 (2001) R1.
- [18] F. Ferreira-da-Silva, PhD thesis, University of Innsbruck, Innsbruck, 2009.
- [19] E. Illenberger, *Chem. Rev.* 92 (1992) 1589.
- [20] F.R. Ferreira-da-Silva, PhD thesis, University of Innsbruck, Innsbruck, 2009.
- [21] I. Bald, J. Langer, P. Tegeder, O. Ingolfsson, *Int. J. Mass Spectrom.* 277 (2008) 4.
- [22] O. Ingolfsson, F. Weik, E. Illenberger, *Int. J. Mass Spectrom. Ion Process.* 155 (1996) 1.
- [23] G.J. Schulz, *Rev. Mod. Phys.* 45 (1973) 423.
- [24] M. Allan, *J. Electron Spectrosc. Relat. Phenom.* 48 (1989) 219.
- [25] I. Bald, Doktors der Naturwissenschaften thesis, Freien Universität Berlin, Berlin, 2007.
- [26] Y. Yildirim, M. Balcan, A. Kinal, A.D. Bass, P. Cloutier, L. Sanche, *Eur. Phys. J. D* 66 (2012) 12.
- [27] R.G. Cooks, J.H. Beynon, R.M. Caprioli, G.R. Lester, *Metastable Ions*, Amsterdam, Netherlands, 1973.

## 3. Experimental set-up

---

In this chapter a brief description of the experimental set-ups used to perform the experimental work presented in this thesis is done. In order to study dissociative electron attachment (DEA) processes as well as electron transfer processes, two set-ups were used: a double focusing mass spectrometer at the institute for Ion Physics and Applied Physics, University of Innsbruck, Austria and a crossed molecular beam apparatus equipped with a time of flight mass spectrometer at the Atomic and Molecular Collisions Laboratory, Universidade Nova de Lisboa, Portugal.

### 3.1. Apparatus used to perform DEA experiments

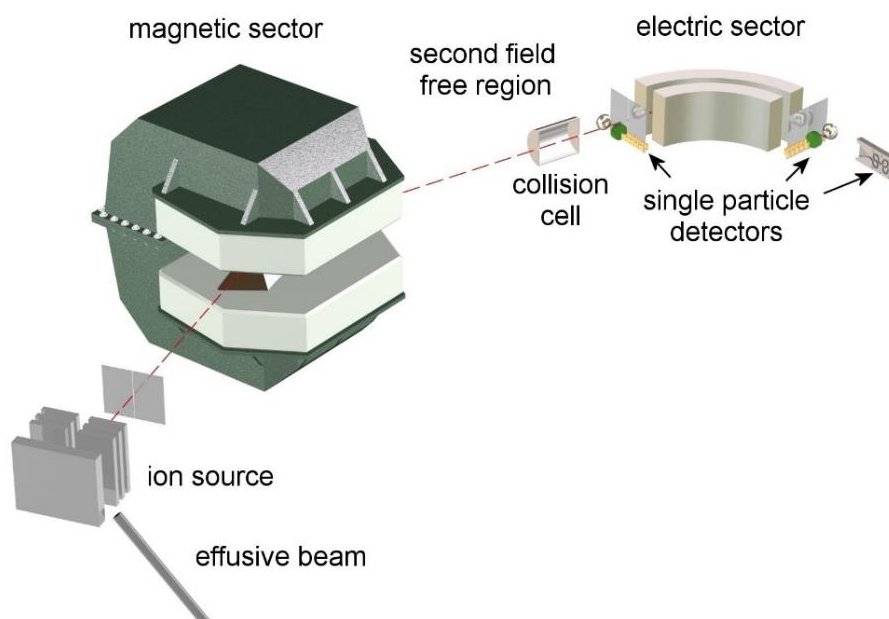


Figure 3.1 – Schematics of the double focusing spectrometer used to perform DEA experiments [1].

All DEA experiments were carried out at the Institute for Ion Physics and Applied Physics, University of Innsbruck, Austria. The mass and energy spectra for all the DEA studies were obtained using a double focusing mass spectrometer in a reverse Nier-Johnson geometry. In Figure 3.1 a schematics of the experimental set-up can be found. The mass

spectrometer is named double focusing because it combines both directional focusing and energy focusing. It is said to have a reversed geometry because, contrary to a standard double focusing spectrometer, the magnetic sector is prior to the electric sector. Briefly, this apparatus consists of an ion source, a first field free region, a magnetic field, a second field free region, an electric field and a channeltron detector. The set-up works in high vacuum conditions (typical base pressure of  $\approx 2 \times 10^{-7}$  mbar), which is secured by turbo pumps connected to rotatory pumps. Under normal circumstances this apparatus presents a mass resolution of  $\sim 1100$  and an energy resolution of  $\sim 1$  eV. The next sub-chapters present some of the main sector field components.

### 3.1.1. Introducing a sample in the chamber

Prior to sample interaction with the beam of electrons, the sample has to be transferred into highly diluted gas phase [2]. Taking into account the primitive phase of the compound (solid, liquid or gas) different inlet systems were used.

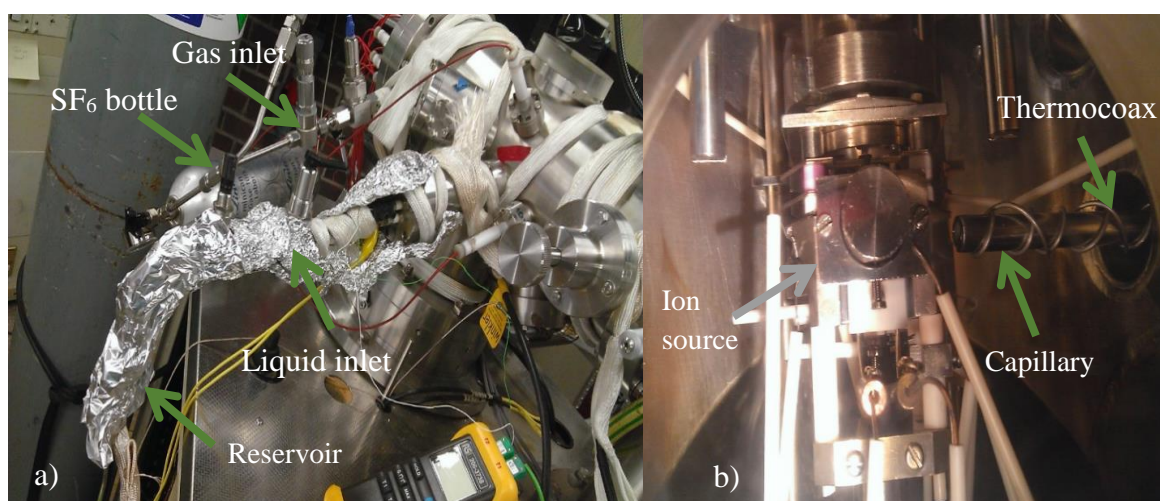


**Figure 3.2 – a) Picture of the VG-ZAB ion source chamber and gas and liquid inlets. A heating band and aluminium foil is wrapped around the liquid inlet. b) Detailed view of the ion source and capillary.**

#### 3.1.1.1. Gas phase sample

When in the gas phase, a gas sample is considered highly diluted when the mean free path for the particles is so long that bimolecular interactions are barely happening [2].

This is usually the case for background pressures in the chamber of the order of  $< 10^{-5}$  mbar.

All the samples studied in the gas phase were introduced in the ion source chamber through an inlet as shown in Figure 3.2. The inlet is attached to the ion source chamber. Through two valves (that are part of the inlet system) it is possible to control the gas pressure in the ion source chamber. These two valves allow safety (bellow-seal valve) and sensitive (needle valve) control of the pressure. SF<sub>6</sub> is also introduced in the chamber through this inlet. SF<sub>6</sub> is the gas used to calibrate the energy and mass scales (for more information about calibration see sub-chapter 3.1.8).

### **3.1.1.2. Liquid phase sample**

In order to measure liquid samples an inlet as the one shown in Figure 3.2 a) was used. The liquid sample is kept in a reservoir and is introduced in the ion source chamber by opening the set of valves in the inlet liquid system. As in the gas inlet (sub chapter 3.1.1.2), the liquid inlet also has two valves. The valves allow safety (bellow-seal valve) and sensitive (needle valve) control of the pressure in the ion source chamber. The flange where this line is attached has an incorporated capillarity that is aligned to end directly to one of the holes of the ion source block, as shown in Figure 3.2 b). The distance between the ion block and the end of the capillarity is less than 0.5 cm.

Not all liquids have a high vapour pressure and thus a heating system is required to increase their vapour pressures. Outside the chamber the heating system is composed of a heating band, while the capillarity is heated by thermocoax wire. Both temperatures are monitored by thermocouple sensors.

Before opening the valve and introducing the sample into the ion source chamber, several freeze-pump-cycles must be done. This procedure is done in order to get rid of volatile contaminations within the sample.

### **3.1.1.3. Solid phase sample**

Most solids have low vapour pressures at room temperature. Thus, in order to get a higher amount of sample to evaporate the solid samples are inserted into an oven. Heating wires heat the walls of the oven and are isolated from the oven by ceramics. The oven's

temperature is measured by a thermocouple. The oven is placed inside the ion chamber and the exit hole is facing a slit of the ion block by less than 0.5 cm apart.

### 3.1.2. Ion source

In the ion source, an effusive beam of molecules is introduced and made to cross with an electron beam. In Figure 3.3 a schematic drawing of the ion block is shown. The electron beam is produced by the heating of a tungsten rhenium filament with a diameter of 0.178 mm by means of an electric current of around 3-4 A and by applying an acceleration voltage. The electron beam energy distribution is given by [3]:

$$dN(E) \propto e^{\left[-\frac{W+E}{kT}\right]} dE \quad 3.1$$

where  $dN(E)$  is the number of electrons emitted per second between energies  $E$  and  $E + dE$ ,  $W$  represents the work function of the metal,  $T$  is the absolute temperature, whereas  $k$  is the Boltzmann constant. This means that electrons have a Maxwell-Boltzmann distribution, which in the current geometry they show an energy spread of  $\sim 1\text{eV}$  at full width at half maximum (FWHM).

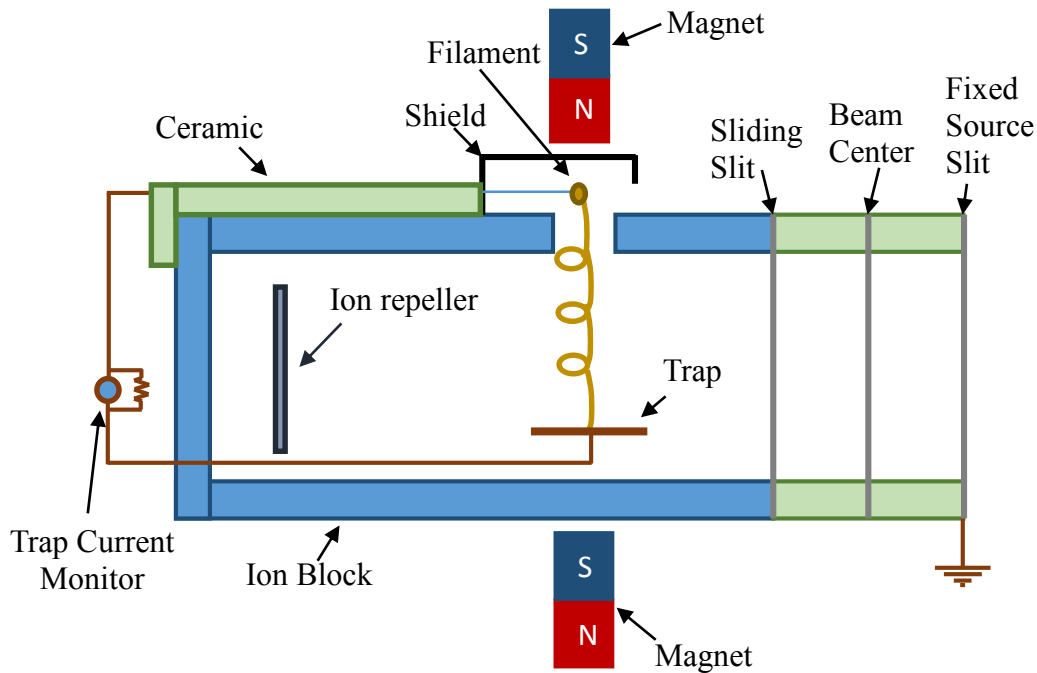


Figure 3.3 - Schematics of the ion block. Adapted from [4].



## Experimental Set-up

After electrons being produced, they are accelerated towards the ion source block by applying a potential difference between the filament and the ion source block (see Figure 3.3). The electron beam is collected at the so called trap, where the trap current regulation is used to control and monitor the filament current, i.e. the electron emission performance. In order to prevent, as much as possible, the electron beam spreading in the ion block, outside the source there are two magnets placed so as to attract each other [4]. The electron beam will then follow the magnetic flux lines created by the set of magnets. The ions are extracted from the source by means of an electric field (a potential difference of 6 kV is applied between the ion source block and the fixed source slit, which is at ground potential).

The usual background pressure in the ion source chamber is  $\approx 2 \times 10^{-7}$  mbar (sometimes lower  $\approx 7 \times 10^{-8}$  mbar). This value depends on how clean the chamber is and for how long it has been pumped out. When measurements are performed, pressures up to  $5 \times 10^{-5}$  mbar are used upon sample admission. The typical pressure value used in the ion source will strongly depend on the sample being probed. The ion source chamber is isolated from the mass analyser by a valve. This allows opening the ion source chamber without breaking the vacuum in the other parts of the set-up.

### 3.1.3. Mass analysis of ions

After the production of the ions upon electron-molecule interactions, they will enter a first field free region and will be analysed by their momentum in a magnetic sector. The following equation describes the kinetic energy of the ion when entering the magnetic field [4]:

$$qU = \frac{1}{2}mv^2 \quad 3.2$$

where  $U$  corresponds to the potential difference applied in the ion block in order to remove the ions from it;  $m$ ,  $q$  and  $v$  are the mass, the charge and the velocity of the ion, respectively. The next equation describes the magnetic force imposed to a charged particle:

$$\vec{F}_m = q\vec{v} \times \vec{B} \quad 3.3$$

with  $B$  the magnetic field. Since the velocity is perpendicular to the magnetic force, ions will have a circular trajectory with a radius  $r$  along the source:

### Experimental Set-up

$$\frac{mv^2}{r} = qvB \Leftrightarrow r = \frac{mv}{qB} \quad 3.4$$

Considering that the ions have a specific kinetic energy, the final equation can be shown as:

$$\frac{m}{q} = \frac{B^2 r^2}{2U} \quad 3.5$$

Bearing in mind equation 3.5, if a constant field strength and a constant voltage are applied and considering that the ions produced are singly charged, then the mass will be directly proportional to the square radius of the arch of the ions. Hence, for a given  $B$ , ions can be differentiated by their mass over charge ratio. It is possible to measure the different masses just by changing the magnetic field or the voltage.

The magnet also allows focusing a diverging ion beam that enters the field. The magnet is known to be directional focusing. However, so far, it was assumed that all ions entering the magnetic field have exactly the same kinetic energy. This is not entirely true, since there is some energy spread. Consequently, if the ions would be detected after the magnetic field, the result would be a blurred image. If the equation for the kinetic energy and equation 3.5, are taken into account:

$$r = \frac{\sqrt{2mE_k}}{qB} \quad 3.6$$

Then it is possible to see that for ions with the same mass and charge, can be dispersed by their kinetic energy ( $E_k$ ). Thus what is in need (after the momentum is selected) is an energy focus, since the magnet has no energy focusing effect.

#### 3.1.4. The Electrostatic Analyser and Magnet Combination

As presented in the previous sub-chapter 3.1.3, the ions that leave the ion source do not have the same kinetic energy. This will lead to an energy dispersion effect. To correct this, an electrostatic analyser (ESA) is present in combination with the magnet, resulting in a double focusing system: direction and energy. After the ions pass the magnet they will enter a second field free region and then the ESA. The electric force ( $\vec{F}_e$ ) in an electric field ( $\vec{E}$ ) is expressed by:

$$\vec{F}_e = q\vec{E} \quad 3.7$$

The present ESA has a radial electric field, hence the velocity of the ions that enter the ESA is always perpendicular to the electric field. As a result, equation 3.7 can be rewritten as:

$$qE = \frac{mv^2}{r} \quad 3.8$$

Knowing that the kinetic energy is expressed as  $E_k = \frac{1}{2}mv^2$ ,  $r$  is then given by:

$$r = \frac{2E_k}{qE} \quad 3.9$$

From equation 3.9 it can be seen that an ESA does not analyse masses, it analyses the kinetic energy of the ions. The combination of a magnet with an electrostatic analyser will allow an inherent energy spread of the beam to be compensated, *i.e.* although with different energies, ions with the same mass re-converge and can then be detected by the channeltron.

### 3.1.5. Detection: Channeltron

The ions are detected by a channeltron (or channel electron multiplier) schematically represented in Figure 3.4. A channeltron is an electron multiplier device operated in the single pulse counting regime. This means that when primary charged particles enter and hit the high surface resistance of the channeltron's walls, they will produce the emission of secondary electrons [5]. The secondary electrons will then be accelerated through the channel (see Figure 3.4) by a positive bias (potential difference between the entrance and output) hitting the wall and producing additional secondary electrons. This secondary electrons formation will keep on until an output pulse charge with up to  $10^8$  electrons is reached [5]. This pulse has a duration at FWHM of 8 ns, passes through a discriminator to allow setting a signal-to-noise ratio, and is finally combined with a pulse preamplifier and fed into a counter [5,6]. This signal then enters a desktop computer where a spectrum can be visualized according to the installed software.

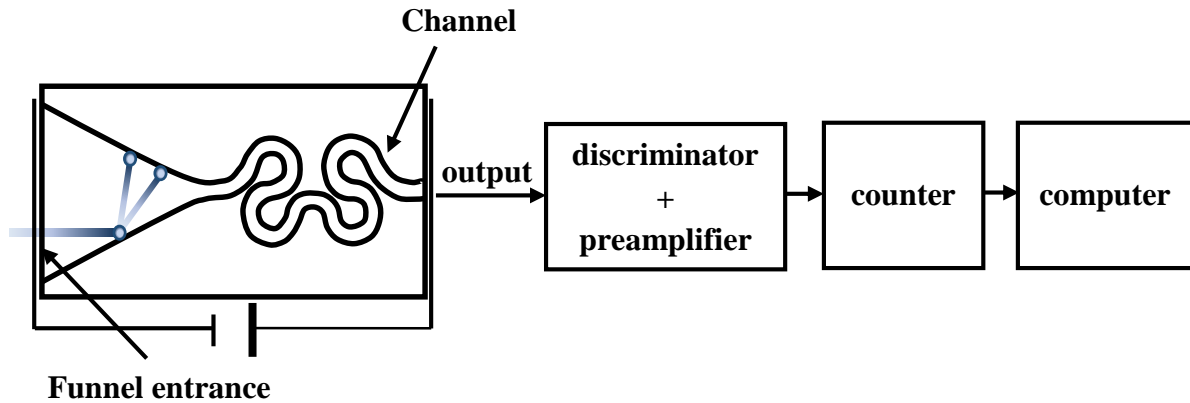


Figure 3.4 - Production of secondary electrons in a channel electron multiplier. The output will be amplified and discriminated by a preamplifier discriminator unit which will trigger a counter. This signal will be processed by a computer. Adapted from [5,6].

### 3.1.6. Mass resolution

According to Marshall's [7] definition of mass resolution, two peaks are said to be resolved if the valley between them is equal to 10% of either peak height. The ability that a mass analyser has to distinguish between two ions with a small  $m/z$  difference ( $\delta m$ ) is given by the mass resolving power ( $R_m$ ) [8]:

$$R_m = \frac{m}{\delta m} \quad 3.10$$

However, it is also possible to define the mass resolution of an isolated peak by using the peak width  $\delta m$  at 50% of the peak maximum yield i.e. the full width at half maximum (FWHM) [8].

### 3.1.7. Measurements

#### 3.1.7.1. Energy and mass scans

In order to perform energy scans for a certain ion, the mass of that ion has to be fixed and the electron energy is scanned over the intended range. The energy is scanned over several runs, and the runs are averaged over the total number. The number of runs performed and the time gate used depends on the signal statistics. Just for curiosity, in the

particular case of  $\text{SF}_6^-$ , for a pressure of  $1 \times 10^{-6}$  mbar in the ion source (background pressure:  $5 \times 10^{-7}$  mbar) an ion yield of around 20000 a.u. is obtained and thus 3 runs with a time gate of 0.5 s are enough to obtain a  $\text{SF}_6^-$  energy scan, where a distinguishable signal from the background noise is obtained.

In the case of performing mass scans, the electron energy is fixed, and the m/z ratio is scanned over the intended range. Again, here the time gate used will also depend on the signal intensity obtained in respect to the background noise.

### **3.1.7.2. Metastable ions**

As pointed out before, to extract the ions from the ion source they are accelerated by some kV before entering the electric or magnetic sector. The parent ions have velocities on the order of  $\sim 10^5$  m/s and thus, a metastable ion that is able to survive the flight time from the source to detection must have a lifetime in the  $\mu\text{s}$  timescale [9]. Bearing in mind that direct electronic dissociation along a repulsive potential energy surface takes place on vibration periods scale ( $10^{-13}$  to  $10^{-14}$  s), lifetimes on the order of  $\mu\text{s}$  are considered long enough.

With a double-focusing mass spectrometer with reversed Nier-Johnson geometry it is possible to detect metastable ions. A metastable ion decomposition peak is not detected at an integral m/z value. The peak of a daughter ion  $m_2$  formed from an ion  $m_1$  upon decomposition in the field-free-region before the magnetic analyser appears in a mass position designated as the apparent mass ( $m^*$ ). This mass is defined by the following equation [2]:

$$m^* = \frac{m_2^2}{m_1} \quad 3.11$$

On the other hand, if the ion selected decays in the second field free region before entering the electric sector, the decomposed ion will enter the electric sector with a different kinetic energy than the parent. The technique used to investigate the metastable dissociation of anions in the field free region between the magnetic sector and the electric sector is known as mass analysed ion kinetic energy (MIKE) [2]. This technique consists of selecting a mass  $m_0$  by the magnet and then scanning the electric sector field voltage ( $U$ ) [10]. The daughter ion in the second field free region will keep its velocity, however the kinetic

energy is different from the one owned by the parent ion ( $m_0$ ). Therefore, the daughter ion with a mass  $m_1$  will only be detected if the electric sector field voltage is decreased:

$$U_1 = U_0 \frac{m_1}{m_0} \quad 3.12$$

where  $U_0$  corresponds to the voltage applied at the electric sector to observe the parent ion and  $U_1$  is the voltage that needs to be applied so the daughter ion with a mass equal to  $m_1$  is observed. The peaks recorded in a MIKE scan are dependent on  $\frac{U}{U_0}$ . Information about the kinetic energy release (KER) during a metastable decay is obtained by the width of the peak of the fragment ion.

### **3.1.8. Calibration**

When performing measurements one of the main challenges result from fluctuations on energy and mass positions, which are due to the background pressure in the chamber not being the same for every set of measurements and contact potentials drifting electric potentials arising from the use of particular substances that change these metal surfaces properties. Therefore one of the most important aspects before taking conclusions out of the obtained data is to perform a set of calibration procedures.

In an energy scan the obtained values do not correspond to the absolute ones, instead are relative to a reference system. So why not set the reference system to 0 eV? This would mean that the voltage applied between the filament and the ion block would have been zero. However, this imposes a serious limitation because such value is not sufficient to give a measurable electron current in the ion block. This is certainly due to instrumental reasons. In order to solve this limitation the ion repeller is set to have an offset so the 0 eV electrons are detected at higher energies ( $\sim 2\text{eV}$ ). This implies that an energy shift is always present in all energy spectra recorded. There is then the need of calibrating the spectra.

In order to calibrate the energy spectra,  $\text{SF}_6$  is used. As said before, DEA is a resonant process that generally occurs below  $\sim 15\text{ eV}$  [11]. The ion yields obtained after an electron interacts with  $\text{SF}_6$  are well-known [12] and they have several peak resonances in the 0 – 12 eV region (see Figure 3.5). This allows having more than one point to calibrate the spectra and thus a better and more precise calibration procedure is achieved. The

electron energy distribution is determined by measuring the resonances of  $\text{SF}_6^-$ ,  $\text{F}^-$  and  $\text{F}_2^-$ . The electron energy resolution is obtained by measuring the  $\text{SF}_6^-$  FWHM peak.

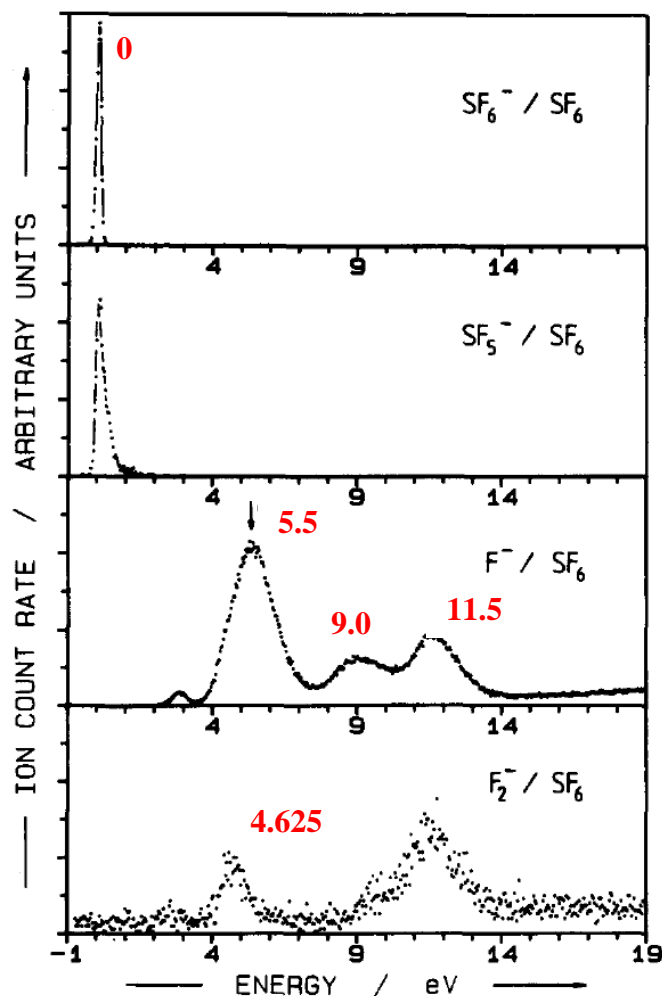
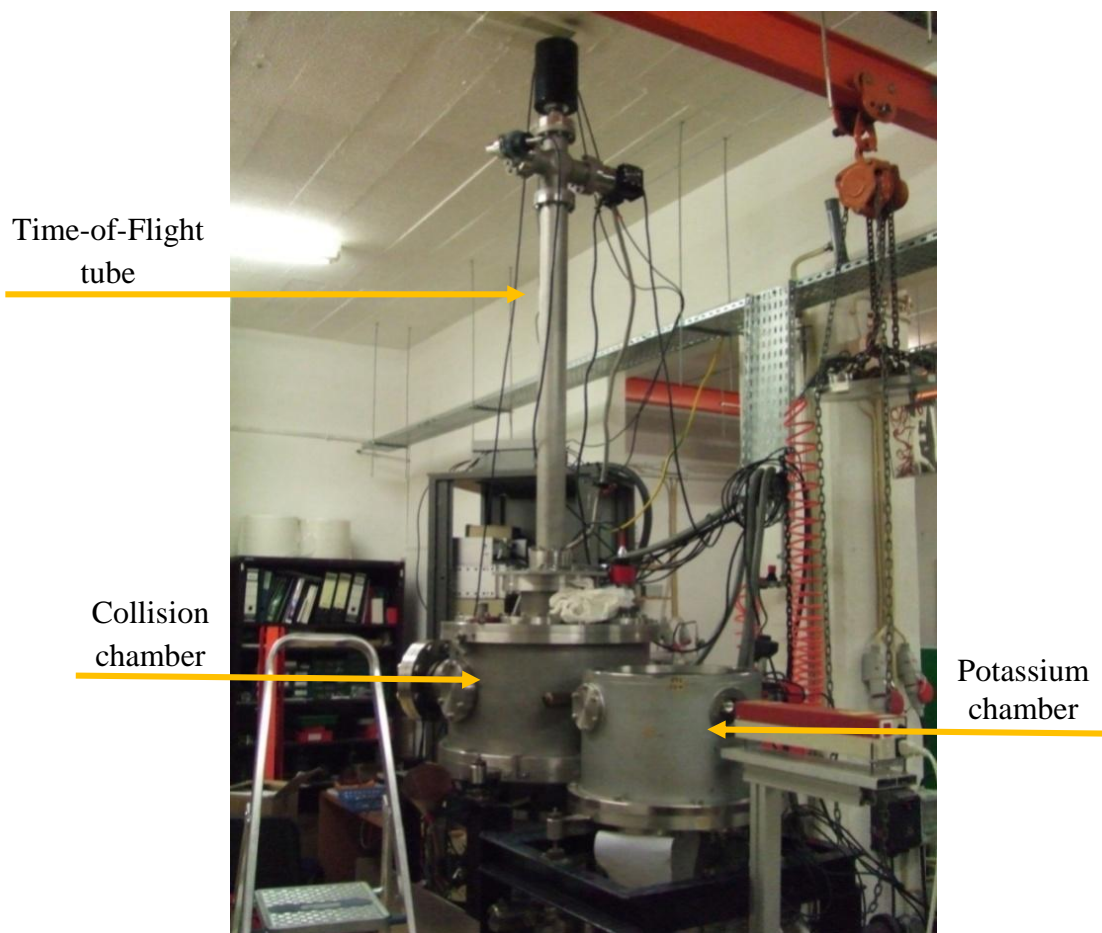


Figure 3.5 – Negative ion formation of  $\text{SF}_6^-$ ,  $\text{SF}_5^-$ ,  $\text{F}^-$  and  $\text{F}_2^-$  from the collision of electrons with  $\text{SF}_6$ . The energies used to calibrate energy spectra are identified in the graph. Adapted from [12].

During a mass scan a mass shift also occurs. Although the accelerating voltage, magnetic and electric field are set for the desirable  $m/z$  detection, there is a shift in the detected mass spectra. This is due to experimental reasons. The applied fields in the lenses system comprising the electron gun and analysers are not homogenous as they should be and hysteresis effects are also something to account for. Hence, in order to calibrate the mass spectra of  $\text{SF}_6^-$ , its fragment ions and corresponding isotopes are used. As such, a mass scan of the calibration gas and the sample under study has to be performed. The detected species are plotted against their known literature values (for the case of  $\text{SF}_6$ ) and

the unknown species are obtained by relative comparison in the mass scale. After, a quadratic fit is performed to the plotted data, and the values obtained for the fit are then used to plot the correct mass spectrum.

### **3.2. Apparatus used to study electron transfer**



**Figure 3.6 - Photograph of the experimental set-up used to perform electron transfer experiments.**

The mass spectra of anionic species produced through the interaction of neutral potassium atoms with biomolecules were obtained by a time-of-flight (TOF) mass technique, Figure 3.6, installed at the Atomic and Molecular Collisions Laboratory, Universidade Nova de Lisboa, Portugal. In Figure 3.7 a schematic representation of the set-up is shown. Briefly, the apparatus comprises two high vacuum chambers, being secured by diffusion pumps connected with rotatory pumps. The chambers are interconnected by



## Experimental Set-up

an inter-chamber valve. The typical base pressure in both chambers is of the order of  $5 \times 10^{-7}$  mbar. The next sub-chapters present some of the main components present in this set-up.

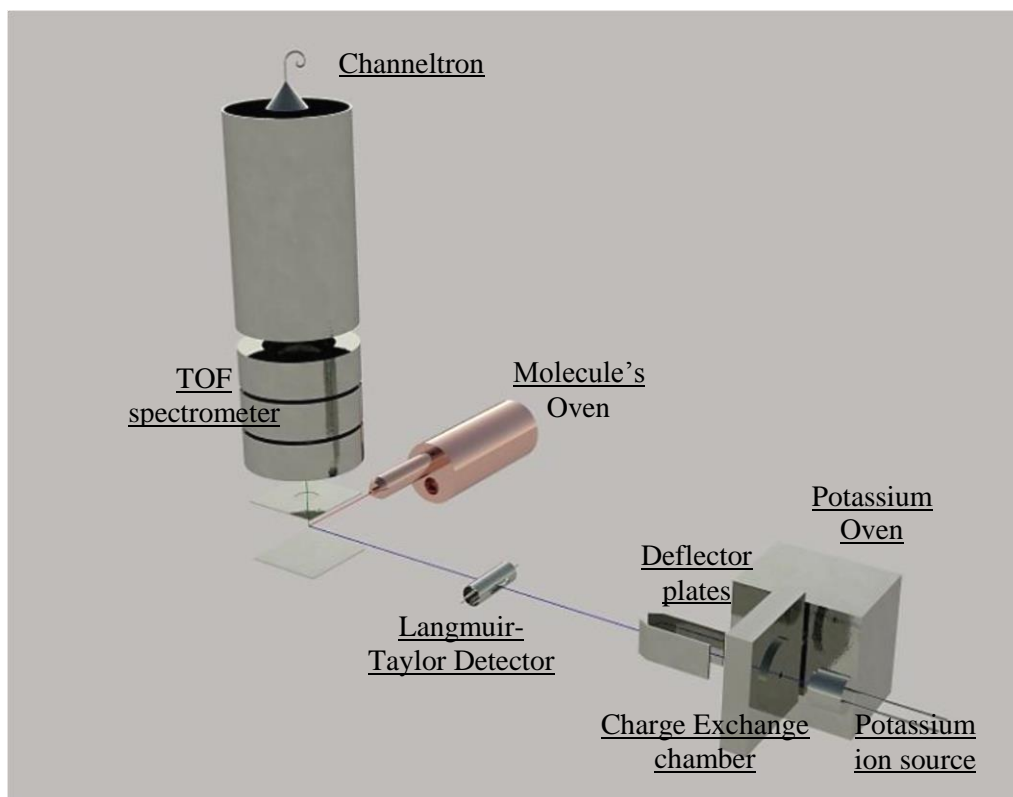


Figure 3.7 - Schematics of the charge transfer set-up. Adapted from [13].

### 3.2.1. Introducing the samples

The samples studied were solids and had to be admitted into vacuum by heating them in a cylinder copper oven. By heating the oven with the sample, it is possible to increase their vapour pressure and create a neutral effusive molecular beam. This beam passes through a 1 mm collimation slit. A thermocouple is used to monitor the oven's temperature, where temperature control is a very important parameter in order to avoid the molecule's thermal decomposition.

### 3.2.2. Production of the neutral potassium beam and ions

In Figure 3.8 a schematic of the neutral potassium beam formation is shown. In the potassium chamber there is a potassium ion source, where the hyperthermal potassium ions ( $K_{hyper}^+$ ) are produced. The potassium oven is heated to  $\sim 420$  K, where previously solid potassium has been introduced, forming neutral thermal potassium atoms ( $K_{ther}^0$ ). The  $K_{hyper}^+$  will be accelerated until they pass through a circular slit interacting with a  $K_{ther}^0$  beam produced in the potassium oven. When interacting, the neutral potassium atoms  $K_{ther}^0$  may transfer an electron to  $K_{hyper}^+$  in a resonant charge exchange process. The final result will be the formation of  $K_{hyper}^0 + K_{ther}^+$ . The hyperthermal projectile does not lose kinetic energy [14] and the reaction can be described as:

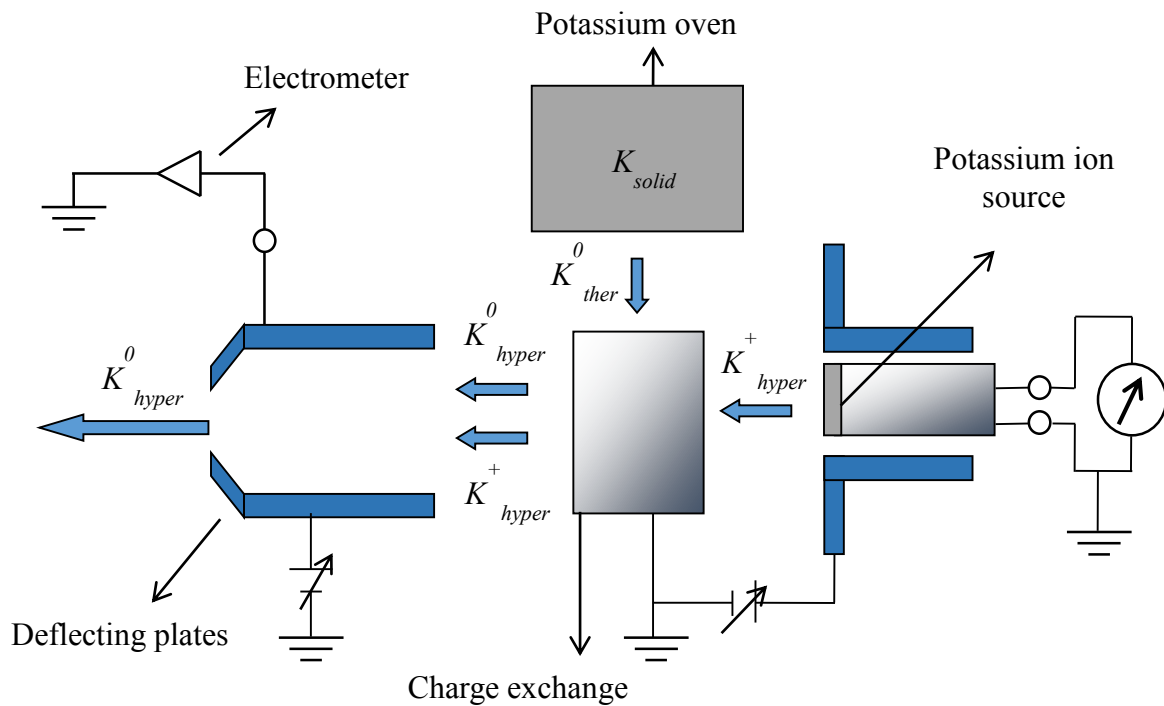
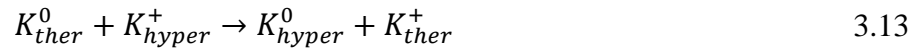


Figure 3.8 – Schematics of the charge exchange beam formation. Adapted from [13].

Not all the  $K_{hyper}^+$  produced by the ionic source will charge exchange during their passage through the charge exchange chamber. The deflecting plates outside the charge

exchange chamber allow the removal of these  $K_{hyper}^+$  that did not exchange their charge, by applying a potential difference in between the plates. Such is enough to deflect the  $K_{hyper}^+$  ions. All the potassium atoms that are not charged will not be affected by this deflector field. One of the deflecting plates is connected to an electrometer so the ionic current can be measured. This also allows controlling the ion ( $K^+$ ) production rate at the source.

After the hyperthermal alkaline beam has been produced, it will enter the collision chamber where its intensity is monitored by a Langmuir-Taylor detector. This detector allows the neutral beam intensity control, however it does not affect the beam passage to the collision region [13]. A Langmuir-Taylor detector consists on a cylindrical collector that has an iridium ionising filament (0.125 mm thickness and a purity over 99%). The filament is set slightly above the beam direction and the collector has two openings that allow the passage of the neutral beam into the collision zone. When a current is applied to the iridium filament electrons are produced with enough energy to ionise particles that pass near the filament. The positive voltage applied in the filament relative to the collector will deflect the ionised particles outwards hitting the collector. The collector is connected to an electrometer. The deflected ionised particles will produce a current in the collector, which is proportional to the neutral beam intensity. The usual currents applied to the filament and voltage drop are 0.63 A and 60 V, respectively. An effusive molecular beam is introduced in the collision region by a slit with 1 mm of diameter, where it intersects with the hyperthermal neutral potassium beam. The collision region is localized between two parallel plates with a 1.2 cm mutual distance. The negative ions formed in the interaction region are extracted in the normal direction to the crossing plane of the two beams by an electric field. The ions enter an Einzel lens system and then to the interior of the time-of-flight drift tube (with an effective length of 1.4 m) [13]. At the top end the ions will be detected by a channeltron.

### **3.2.3. Time of flight spectrometer**

In 1932, Smythe and Mattauch [15] created the first time-of-flight (TOF) mass spectrometers [16]. These kind of mass spectrometers are based on the principle that different masses ( $m/z$ ), exposed to the same force, acquire different velocities and therefore reach the detector at different times. However, these spectrometers had some shortcomings,

for example, the time-of-flight spectrometers did not select correctly the intended velocities [16]. These devices would introduce extra peaks, not allowing the correct analysis of the mass spectra. There have been several improvements to Smythe and Mattauch's TOF concept; one example is the introduction of a reflectron, which increases the TOF's resolution significantly. The linear TOF used at Atomic and Molecular Collisions Laboratory is based on the Wiley and McLaren geometry. In 1955 Wiley and McLaren [17] proposed the introduction of a second acceleration field [16]. This allowed to have a better resolution (in mass and time) and the potential of TOF spectrometry was then increased [10,17].

Take the example of a negative ion being accelerated in the direction of a positive electrode. Considering a uniform electric field is applied between two parallel metal plates separated by a distance  $d$ . The electric field  $E$  is  $E = \Delta U/d$ , being  $\Delta U$  the potential difference between the plates. Knowing that the electric force is given by  $F = eE$ , one ion formed at rest will be accelerated along the electric field  $E$  according to Newton's second law:

$$a = \frac{F}{m} = e \frac{E}{m} = \text{const} \quad 3.14$$

with  $e = 1.6 \cdot 10^{-19}C$ . If the positive electrode is replaced by a grid, the ion will pass through it and will continue its trajectory out of the collision (or interaction) region. This is called an extraction grid. The electrode opposite to the grid will repel the ions and thus is known as a repeller.

In a TOF spectrometer with only one acceleration field, if two ions start with the same axial velocity but with opposite directions, the ion that was ejected in the opposite direction of the applied field will be decelerated; the ion which is ejected in the same direction as the applied field will be accelerated in the detector direction. The ion that initially moved contrary to the applied field, will pass the starting point with the same speed as the ion which goes towards the field, but with a time delay that will persist throughout the flight path to the detector. This delay must be less than the time difference between two adjacent masses, otherwise it will not be possible to distinguish between a real mass and this kind of 'defect'. This fault can be partially corrected by the introduction of a second accelerating field. Thus, ions which have a lower speed will remain longer in the acceleration region, thus acquiring greater acceleration and decreasing the time delay (see Figure 3.9 - solid lines are repeller plates and dashed lines represent extraction grids).

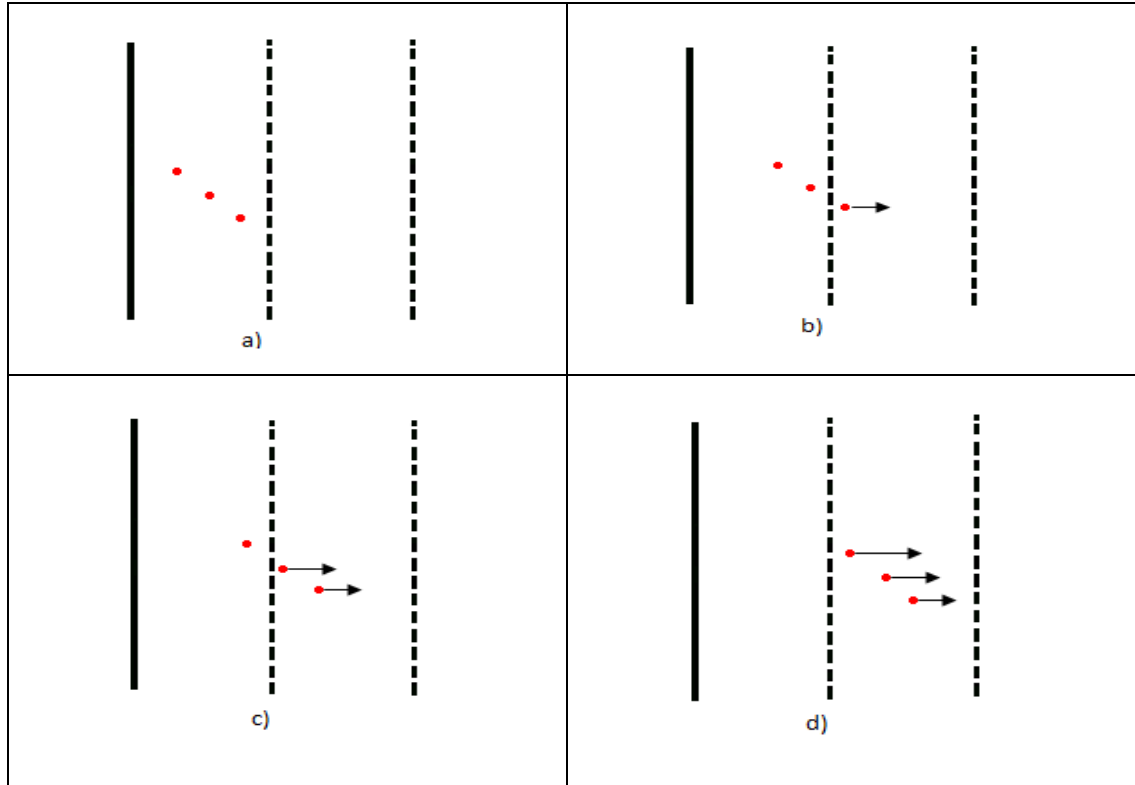


**Figure 3.9 - Representation of the ions acceleration in the acceleration region.**

The ions formed in the collision region are removed by a first electric field ( $E_1$ ), and then accelerated by a second ( $E_2$ ) field before entering the flight tube (which has no electric field applied, known as drift region), reaching the detector.

The flight times for each region can be obtained by solving the respective equation of motion and kinetic energy. Considering that the particle is in the xx axis, the motion equation is given by:

$$x = x_0 + v_0 t_s + \frac{1}{2} a t_s^2 \quad 3.15$$

$s$  is the distance between the plates (depending on the region,  $s = s_1, s_2$ , or  $s_3$ ). In the case of the collision region  $s_1$  represents the distance between the ion formation and the plate that separates the collision and acceleration region.

From the equation of kinetic energy it is possible to calculate the velocity of the ion:

$$E_k = \frac{1}{2} m v^2 \Leftrightarrow v = \sqrt{\frac{2E_k}{m}} \quad 3.16$$

Where  $E_k$  is the kinetic energy of an ion.

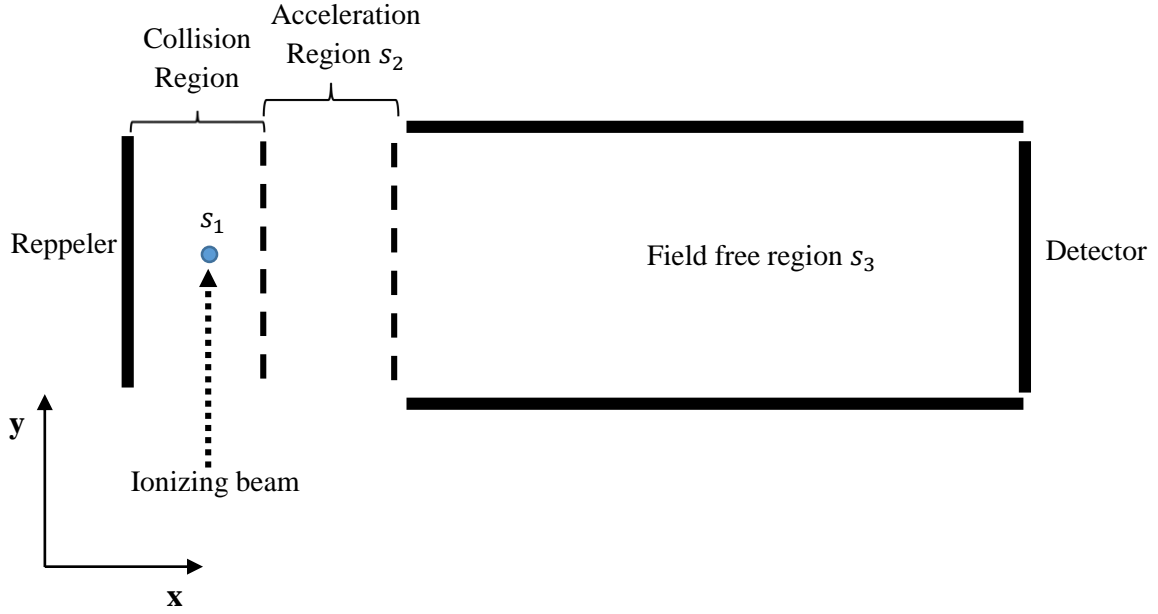


Figure 3.10 - Generic schematics of a time-of-flight mass spectrometer.

Taking into account the formulation in Figure 3.10, the total time-of-flight ( $t_m$ ) of an ion is given by the sum of the time spent in all regions. In the ideal case where all ions start moving in a plane  $s_1$  and have zero initial kinetic energy, the total flight time will be given by [10]:

$$t_m = \left( \frac{m}{ze(E_1 s_1 + E_2 s_2)} \right)^{1/2} \left( 2k^{1/2} s_1 + \frac{2k^{1/2} s_2}{k^{1/2} + 1} + s_3 \right) \quad 3.17$$

with  $k$  being a constant:

$$k = \frac{E_1 s_1 + E_2 s_2}{E_1 s_1} \quad 3.18$$

The mass resolution is given by the difference between the flight times of two consecutive masses,  $m$  and  $m + 1$ . Thus, assuming that the ions were created with the same value in module of  $s$  and  $E_{k_0}$ , the mass resolution can be calculated by [10]:

$$\Delta T_m = t_m \left[ \left( 1 + \frac{1}{m} \right)^{1/2} - 1 \right] \quad 3.19$$

In the case where  $m$  is much larger than 1, the mass resolution calculation can be approximated by [10]:

### Experimental Set-up

$$\Delta T_m \approx \frac{t_m}{2m} \quad 3.20$$

In summary, ions are formed in the collision region after the interaction of the neutral potassium beam with the molecular target. These ions are accelerated by electric fields and they are projected through a free field region until they reach the detector. The home made TOF assembled in the Lisbon laboratory has a mass resolution of  $\sim 150$ .

In Table 3.1 a resume of the main experimental specifications in the crossed molecular beam set-up is shown.

Potassium chamber	Oven and Charge Exchange Chambers temperatures	420; 435 K
	Background pressure	$\sim 5 \times 10^{-7}$ mbar
	Working pressure	$\sim 9 \times 10^{-7}$ mbar
Collision chamber	Background pressure	$\sim 5 \times 10^{-7}$ mbar
	Working pressure	$\sim 9 \times 10^{-6}$ mbar
TOF and detection system	Repeller voltage	-3900 V
	Extraction voltage grid	-3500 V
	Einzel lens	-1500 V
	Channeltron $V_{in}$	0 V
	Channeltron $V_{out}$	2250 V

**Table 3.1 – Specifications of the system.**

## References

- [1] A. Mauracher, Doctor rerum naturalium thesis, University of Innsbruck, Innsbruck, 2009.
- [2] J.H. Gross, Mass Spectrometry, Springer Verlag, Germany, 2004.
- [3] L.G. Christophorou;, Electron-Molecule Interactions and Their Applications, Academic Press, London, 1984.
- [4] M.A. Huels, B. Boudaïffa, P. Cloutier, D. Hunting, L. Sanche, Journal of the American Chemical Society 125 (2003) 4467.
- [5] [http://www.sjuts.com/Introduction\\_Principles.html](http://www.sjuts.com/Introduction_Principles.html), (Accessed August 2014).
- [6] A. Edtbauer, PhD Thesis, University of Innsbruck, Innsbruck, 2010.
- [7] A.G. Marshall, C.L. Hendrickson, S.D.H. Shi, Anal. Chem. 74 (2002) 253A.
- [8] E.D. Hoffmann, V. Stroobant, Mass Spectrometry: Principles and Applications, John Wiley & Sons Ltd, Chichester, 2007.
- [9] R.G. Cooks, J.H. Beynon, R.M. Caprioli, G.R. Lester, Metastable Ions, Amsterdam, Netherlands, 1973.
- [10] E. Illenberger, J. Momigny, Gaseous Molecular Ions. An Introduction to Elementary Processes Induced by Ionization, Steinkopff/Springer, New York, 1992.
- [11] E. Szymanska, N.J. Mason, E. Krishnakumar, C. Matias, A. Mauracher, P. Scheier, S. Denifl, Int. J. Mass Spectrom. 365 (2014) 356.
- [12] M. Fenzlaff, R. Gerhard, E. Illenberger, J. Chem. Phys. 88 (1988) 149.
- [13] R. Antunes, PhD Thesis, Universidade Nova de Lisboa, Lisboa, 2011.
- [14] J.A. Aten, J. Los, Chem. Phys. 25 (1977) 47.
- [15] W.R. Smythe, J. Mattauch, Phys. Rev. 40 (1932) 0429.
- [16] J.T. Watson, O.D. Sparkman, Introduction to Mass Spectrometry, John Wiley & Sons, Ltd, 2008.



*Experimental Set-up*

- [17] W.C. Wiley, I.H. McLaren, Rev. Sci. Instrum. 26 (1955) 1150.

## 4. Results and discussion

---

Useful information on the mechanisms initiated by the collision of electrons/atoms with molecules can be obtained by using mass spectrometry techniques. The majority of the experiments performed throughout this thesis have made use of a double sector field mass spectrometer regarding DEA processes. With this set-up free low energy electrons were made to interact with different molecular targets, and the different formed anions have been detected. The anion formation proceeds essentially via two distinct processes, viz. dissociative electron attachment (DEA) and dipolar dissociation (DD) [1]. As discussed in Chapter 2, the DEA process comprises the capture of an electron by a molecule forming a transient negative ion (TNI) and then fragmenting into a stable anion and (one or more) neutral species. Additionally, a study concerning electron transfer with biomolecules was also performed. In this case a TNI is formed by the collision of an electron donor atom with the target molecule. This study was performed in a crossed molecular beam machine equipped with a linear TOF.

In this chapter it is presented an introduction to the work done throughout this thesis followed by the proofs of publication of the papers published in international peer review journals. As it was mentioned before different types of molecules were studied, and so this chapter will be divided into two sub-chapters devoted to each set of targets: biomolecules and technologically relevant molecules.

### 4.1. Biomolecules

The harmful effects of exposure to ionisation radiation are known for several decades [2], where the interaction of high energy radiation/particles (*e.g.*: X-rays,  $\beta$ ,  $\alpha$  particles, ions) [3] with the physiological medium produces secondary species (ions, radicals, electrons) along its/their ionisation track(s). From the secondary species produced, the most abundant are secondary electrons ( $\sim 5 \times 10^4$  per MeV of incident radiation) with kinetic energies lower than 20 eV [2]. It is known that the interaction of secondary electrons with living cells represents an important step towards radiation damage [4,5]. The ballistic

electrons before reaching thermalization, lose their kinetic energies through successive inelastic interactions (e.g. ionisation, electronic excitation, ro-vibrational excitation, dissociation, etc.) or can alternatively, attach to atoms and molecules in the medium, or hydrate in the medium itself to induce further chemical changes. Within the context of this thesis a focus is made in negative ions formation and their detection. For the electron energies used in the experiments (typically below 15 eV), electron induced dissociation of the TNI results in anion formation and radical species. These latter are particularly relevant regarding the sort of damage they can produce in the biological environment.

#### **4.1.1. Comparative studies upon potassium and electron collisions with biomolecules: site selectivity**

The changes triggered by the ionising radiation in the physiological environment are not merely instantaneous, they may occur in a time window that extends from the interaction moment up to several years and even decades [6,7] (see Figure 4.1). The physiological damages incited by the direct and indirect radiation action may have severe consequences. The interaction of the radiation with the cell's deoxyribonucleic acid (DNA) can cause genome alterations leading to cell death [8] or in the worst case it may boost the development of a cancer [9]. However, the fact that radiation can cause cell death can also be seen as an advantage. In radiotherapeutic treatment, the fact that it is possible to kill cells by the use of radiation can be taken as a tool in order to destroy the cancer cells. Though the use of radiation in radiotherapeutic treatment is expected to be as much effective as possible, it may also cause damage to the surrounding healthy cells, which in turn may develop an oncologic condition [10-12]. Other techniques that minimize this side-effect rely on the use of proton and ion beams. Beams of heavy ionized particles have a fundamental advantage over ordinary radiation therapy with photons. The energy transferred to the tissue can be deposited on very well-defined positions (known as the Bragg peak), which may have a reduced effect on adjacent tissue.

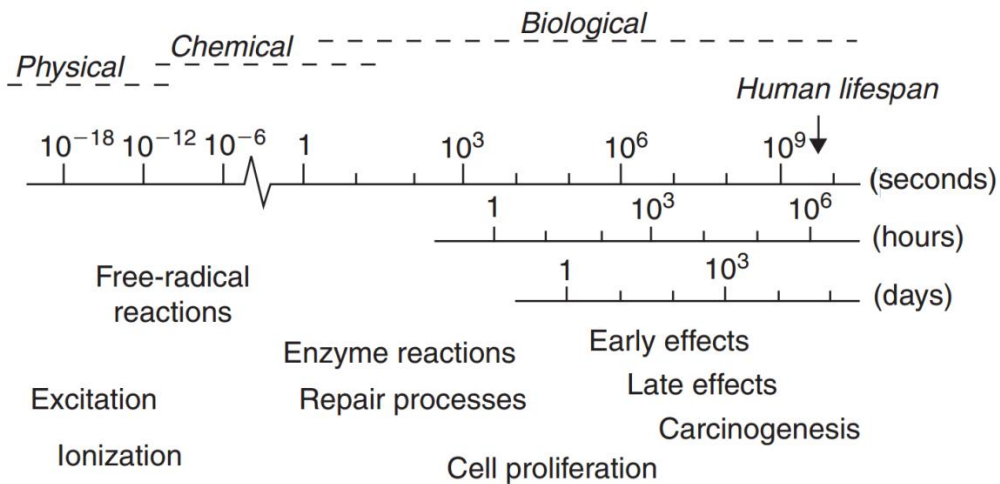


Figure 4.1 – Time-scale schematic of radiation exposure on biological systems. From [7].

To date it is not yet known how excess electrons in the physiological medium induce strand breaks in the DNA, i.e. what are the biological effective mechanisms and their related response to such “attack”. It is then of great interest to study the processes that lead to cell degradation caused by radiation or by products of the interaction with the physiological medium. The information obtained may give useful hints on the benefits and dangers of radiation consisting of correctly assessing heavy ionised particles and to allow a responsible medical use of the same techniques.

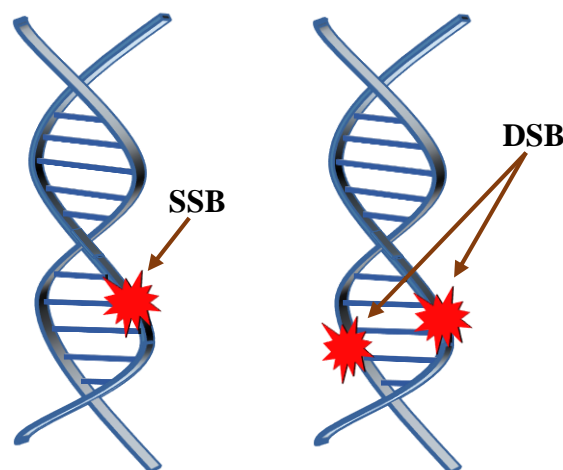
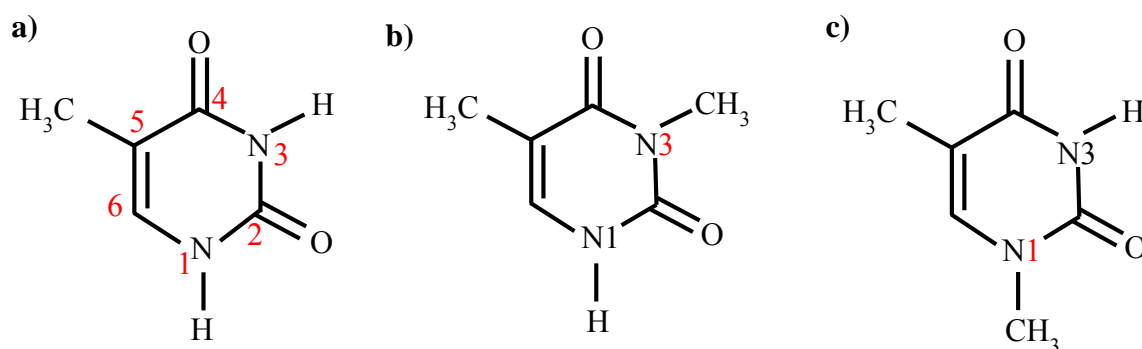


Figure 4.2 - Schematics of a single and a double strand break.

Studies performed by Boudaiffa *et al.* [2] show that electrons with energies below the ionisation threshold can trigger damages in the DNA strands, leading to simple (SSB) and double (DSB) strand breaks [2,13-15] (Figure 4.2). The interaction of secondary

electrons with energies below ionisation threshold of several molecular components, such as DNA/RNA molecular bases (or units) gives rise to a transient negative ion (TNI) formation that will further decay into dissociative anions and neutral radicals [16]. These processes may lead to strand breaks in DNA [10]. Other processes, besides DEA, can influence the electron collisional process with the DNA. Molecules or atoms present in the physiological medium can act as electron donors. Thus, it is also important to study electron transfer processes as another possible route to induce damage.



**Figure 4.3** –a) schematic drawing of a thymine molecule with atom labelling numbers (in red). b) and c) represents the possible N-methylated sites of thymine, 3-methylthymine and 1-methylthymine, respectively.

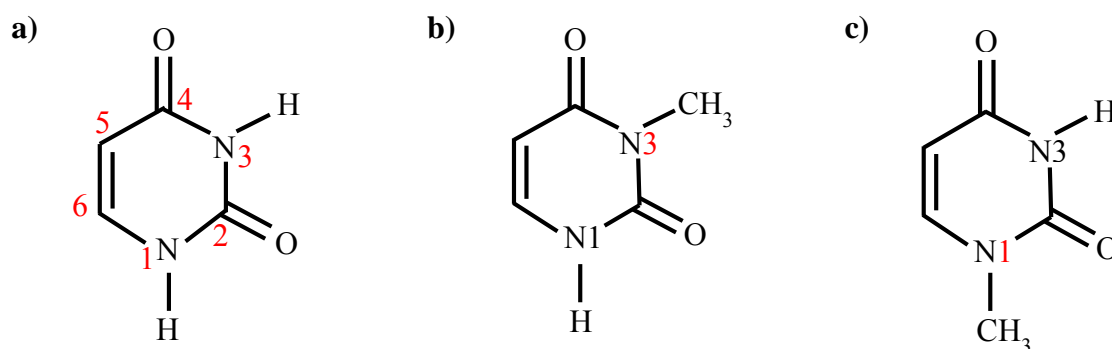


**Figure 4.4** – a) schematic drawing of a uracil molecule with atom labelling numbers (in red). Uracil replaces thymine in the transcription of DNA and is also present in the RNA. b) and c) represents the possible N-methylated sites of uracil, 3-methyluracil and 1-methyluracil, respectively.

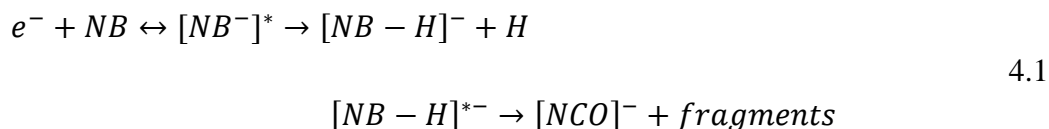
DNA is formed by four nucleobases (NB): thymine, adenine, cytosine and guanine, whereas in RNA, thymine is replaced by uracil. Thymine and uracil have a very similar

structural resemblance, where the only difference is a methyl group in the C5 position present in thymine and absent in uracil (see Figure 4.3 and Figure 4.4).

The main contribution to the paper presented below concerns the electron transfer studies to pyrimidine bases performed at the Atomic and Molecular Collisions Laboratory, Universidade Nova de Lisboa, Portugal. Atom-molecule interactions were investigated in the collision energy range from 30 – 100 eV and the resulting anion formation was TOF mass analysed. The electron donor atom used to perform such atom-molecule collisions was potassium.

Previous DEA and electron transfer studies in thymine (126 a.m.u.) and uracil (112 a.m.u.) have been thoroughly investigated [15,17-21]. In electron transfer experiments with nucleobases thymine and uracil,  $\text{NCO}^-$  is the most dominant fragment anion for collision energies above 30 eV (in the lab frame). Worth mentioning that in the centre-of-mass frame the collision energy is about 20.6 eV for potassium-thymine and 20.0 eV for potassium-uracil. However, in the electron transfer process we have to account for the ionisation energy of the potassium atom (4.34 eV) and the electron affinity of the molecular target (see  $\Delta E$  in equation 2.17). Generally speaking the EA of the pyrimidine bases is close to 0 eV and so the energy available in the system for 30 eV lab frame is about 15.7 eV for potassium-uracil and 16.3 eV for potassium-thymine collisions. This means that at this available energy we may only be able to access the resonances available up to this energy value. This is valid as long as the ground state covalent and ionic potential energy curves are involved [21]. From the DEA studies it was observable that for electron energies below  $\sim 4$  eV the most abundant fragment is the dehydrogenated parent anion. However, in the DEA studies, for electron energies above  $\sim 4$  eV the formation of  $\text{NCO}^-$  turns out to be the most dominant signal too. While the formation of the dehydrogenated parent anion results from a single bond break in the molecule,  $\text{NCO}^-$  formation implies a complete break of the pyrimidine ring. In order to form  $\text{NCO}^-$ , two bonds of the ring and one N – H bond have to be broken.

Previous DEA measurements with partially deuterated molecules showed that in order to form the dehydrogenated parent anion, exclusively hydrogen atoms from the N sites are removed [19]. Other DEA studies with nucleobases embedded in helium nanodroplets [22] showed the exclusive formation of the dehydrogenated parent anion  $(\text{NB} - \text{H})^-$ . All other channels in this cold environment are quenched. In the gas-phase this may imply that after the formation of the dehydrogenated parent anion, the excess energy can be deposited into the available reaction products leading to further fragmentation.



Thus, the formation of  $(NB - H)^-$  is considered to be the most probable intermediate step for  $NCO^-$  formation. In Figure 4.5 and Figure 4.6 it is shown a schematic representation of the possible pathways in thymine leading to  $NCO^-$  formation upon electron capture. In order to form  $NCO^-$  there are three possible pathways. Note that further reaction steps occur upon the loss of  $NCO^-$ , but those are not discussed here (see publication below).

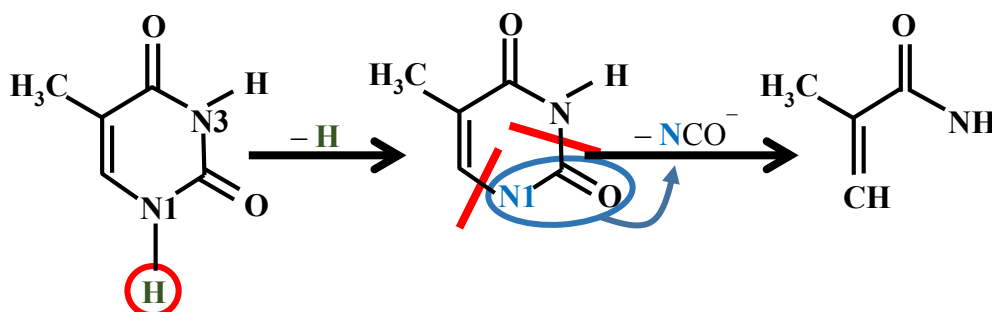


**Figure 4.5 - Schematic representation of  $NCO^-$  path formation when a hydrogen atom is removed from position N1. Further reaction steps occur upon the loss of  $NCO^-$  (see publication below).**

The present work is focussed on the study of the DNA base thymine and RNA base uracil and their N-methylated derivatives (Figure 4.3 and Figure 4.4). By methylation of the N-sites it is possible to follow the fragmentation pathway(s) that leads to  $NCO^-$  formation upon hydrogen loss.

The following publication contains a set of three joint studies on DEA, electron transfer and matrix assisted laser desorption/ionisation (MALDI) for pyrimidine bases (thymine and uracil) and for partially methylated pyrimidine bases (1- and 3-methyl thymine and 1- and 3-methyl uracil). The use of DEA and electron transfer techniques to perform this studies was already explained before. MALDI is a technique that allows studying the role of the deprotonation site. Since the formation of  $(NB - H)^-$  can be seen as the first step for the  $NCO^-$  formation, the use of MALDI can be used to determine the fragmentation path. However, MALDI is outside the scope of the present thesis and no further explanation will be given here.

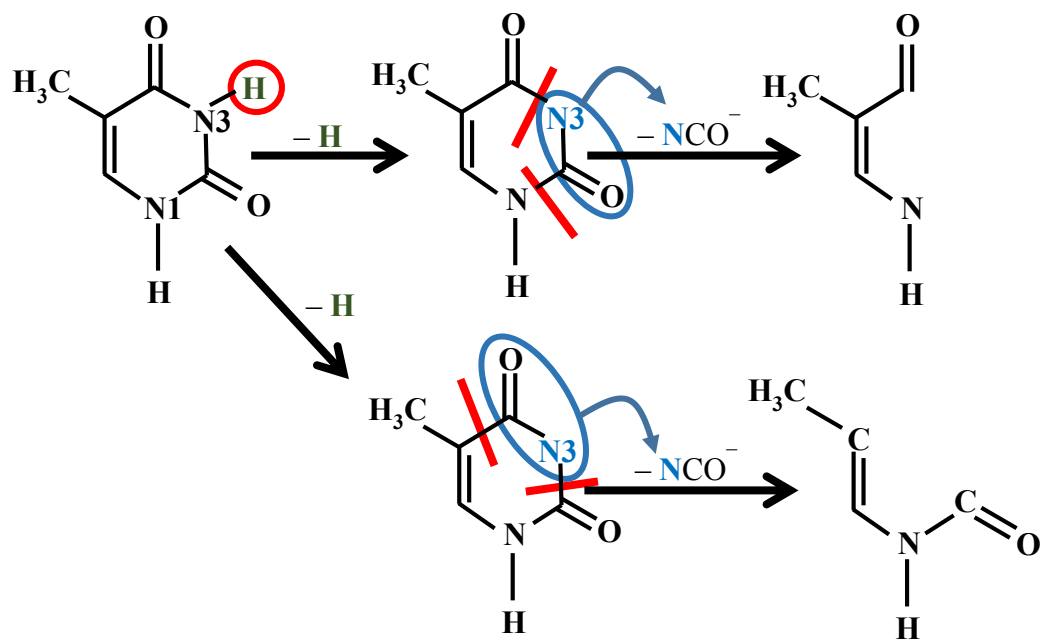


Figure 4.6 – Schematic representation of the different NCO<sup>-</sup> path formation when a hydrogen atom is removed from position N3. Further reaction steps occur upon the loss of NCO<sup>-</sup> (see publication below).





## RESEARCH ARTICLE

## NCO<sup>-</sup>, a Key Fragment Upon Dissociative Electron Attachment and Electron Transfer to Pyrimidine Bases: Site Selectivity for a Slow Decay Process

Filipe Ferreira da Silva,<sup>1</sup> Carolina Matias,<sup>1,2</sup> Diogo Almeida,<sup>1</sup> Gustavo García,<sup>3</sup> Oddur Ingólfsson,<sup>4</sup> Helga Dögg Flosadóttir,<sup>4</sup> Benedikt Ómarsson,<sup>4</sup> Sylwia Ptasinska,<sup>5</sup> Benjamin Puschnigg,<sup>2</sup> Paul Scheier,<sup>2</sup> Paulo Limão-Vieira,<sup>1</sup> Stephan Denifl<sup>2</sup>

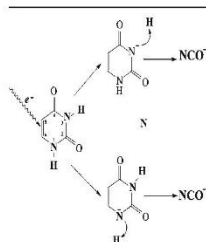
<sup>1</sup>Laboratório de Colisões Atômicas e Moleculares, CEFITEC, Departamento de Física, Faculdade de Ciências e Tecnologia, Universidade Nova de Lisboa, Campus de Caparica, 2829-516, Caparica, Portugal

<sup>2</sup>Institut für Ionenphysik und Angewandte Physik and Center for Biomolecular Sciences Innsbruck, Leopold-Franzens Universität Innsbruck, Technikerstr. 25, 6020, Innsbruck, Austria

<sup>3</sup>Instituto de Física Fundamental, Consejo Superior de Investigaciones Científicas (CSIC), Serrano 113-bis, 28006, Madrid, Spain

<sup>4</sup>Department of Chemistry and Science Institute, University of Iceland, Dunhagi 3, 107, Reykjavik, Iceland

<sup>5</sup>Department of Physics and Radiation Laboratory, University of Notre Dame, Notre Dame, IN 46556, USA



**Abstract.** We report gas phase studies on NCO<sup>-</sup> fragment formation from the nucleobases thymine and uracil and their N-site methylated derivatives upon dissociative electron attachment (DEA) and through electron transfer in potassium collisions. For comparison, the NCO<sup>-</sup> production in metastable decay of the nucleobases after deprotonation in matrix assisted laser desorption/ionization (MALDI) is also reported. We show that the delayed fragmentation of the dehydrogenated closed-shell anion into NCO<sup>-</sup> upon DEA proceeds few microseconds after the electron attachment process, indicating a rather slow unimolecular decomposition. Utilizing partially methylated thymine, we demonstrate that the remarkable site selectivity of the initial hydrogen loss as a function

of the electron energy is preserved in the prompt as well as the metastable NCO<sup>-</sup> formation in DEA. Site selectivity in the NCO<sup>-</sup> yield is also pronounced after deprotonation in MALDI, though distinctly different from that observed in DEA. This is discussed in terms of the different electronic states subjected to metastable decay in these experiments. In potassium collisions with 1- and 3-methylthymine and 1- and 3-methyluracil, the dominant fragment is the NCO<sup>-</sup> ion and the branching ratios as a function of the collision energy show evidence of extraordinary site-selectivity in the reactions yielding its formation.

**Key words:** NCO anion, Electron transfer, Negative ion formation, Metastable decay, DEA, Collision dynamics, Matrix assisted laser desorption/ionization (MALDI)

Received: 6 May 2013/Revised: 26 June 2013/Accepted: 27 June 2013

### Introduction

Electron driven reactions are of interest in many areas of science and technology, including low-temperature plasmas, the interstellar and planetary atmospheres and dense interstellar clouds, as well as biological processes and medicine, just to mention a few. Pioneering studies by Sanche and coworkers [1, 2] have shown that low-energy electrons (<15 eV) can efficiently damage DNA by inducing single- and double-strand breaks. These alterations are

**Electronic supplementary material** The online version of this article (doi:10.1007/s13361-013-0715-9) contains supplementary material, which is available to authorized users.

Correspondence to: Stephan Denifl; e-mail: stephan.denifl@uibk.ac.at; Paulo Limão-Vieira; email: plimaovieira@fet.unl.pt

Published online: 17 September 2013

initiated by dissociative electron attachment (DEA) processes with the initial capture of an electron leading to a temporary negative ion (TNI), which may then decompose by spontaneous ejection of the electron (autodetachment) or by dissociation into neutral and anionic fragments. Since these landmark studies on the resonant formation of DNA strand breaks by 3-15 eV electrons, several experimental and theoretical DEA studies with segments and building blocks of DNA and RNA, in the gas phase and deposited as thin films, have been reported [3–10]. Furthermore, previously site-selective bond cleavage upon DEA to biologically relevant molecules was demonstrated for the nucleobases, thymine (T) and uracil (U) [11–13], as well as for smaller molecules such as methanol and some simple organic acids [14]. These experiments demonstrated that precise control of chemical reactions in DEA can be achieved by just tuning the initial electron energy. Electron-induced dissociation was shown to be controllable not only for gas phase molecules but also by scanning tunneling electrons in molecules deposited on a surface [15–17].

Meanwhile, such site selective bond cleavage upon low-energy electron attachment in the gas phase has also been observed for a number of other biomolecular systems like thymidine [18], ribose [19, 20], clusters of a few base pairs of DNA embedded in He droplets [21], amino acids [22–25], and peptides [26]. In the majority of these studies, the discussion has been focused on single bond cleavage reactions leading to the formation of the dehydrogenated closed-shell anion  $[M - H]^-$  [11, 13, 18, 19, 22–26] and the complementary reaction leading to  $H^-$  [12, 14]. The loss of a hydrogen atom is fast compared with ring cleavage and the excision of heavier fragments and, hence, this reaction can compete efficiently with autodetachment (see also a recent study on time-resolved dynamics of the TNI for uracil [27]). In the case of the pyrimidine bases, hydrogen abstraction is observed at electron energies close to 1 eV through site selective loss of the H atom from the N1 position, whereas electrons with incident energies between 1 and 3 eV are required to induce hydrogen loss from the N3 position. In contrast,  $H^-$  formation is observed at higher electron energies between 5 and 12 eV and with a much lower cross section than the  $H^-$  neutral loss. It was further shown that other product anions are also formed upon DEA to the nucleobases thymine (T) and uracil (U) in this energy range, with  $NCO^-$  being the most abundant [28]. In this context, it is worth mentioning that the neutral precursor  $NCO$  is a pseudo-halogen with high electron affinity ( $\sim 3.6$  eV) that exceeds those of halogen atoms. In addition to the experimental efforts, extensive theoretical studies have also been performed in order to better understand the mechanism of DEA in nucleobases. These include calculations of potential energy surfaces as a function of the appropriate internal coordinates by Li et al. [29] and Takayanagi et al. [30] using density functional theory (DFT) and more recently by González-Ramírez et al. using CASSCF/CASPT2 methodology [31]. Furthermore, Burrow et al.

[32] have studied valence and dipole-bound anion formation, while Winstead and McKoy [33, 34] and Gianturco et al. [36] have performed theoretical calculations on the LEE interaction with uracil, revealing resonant features in the elastic scattering cross section (formed via shape resonances). More recently, also resonant features in inelastic scattering from thymine [36] and uracil [37] have been reported. These resonances represent excited states from electron capture with simultaneous valence shell excitation (so-called core excited resonances). Nevertheless, for nucleobases the assignment of DEA resonances at higher electron energies to either higher lying shape resonances [36] or core excited resonances [38] is still debatable.

For isolated cases, there have been theoretical predictions of complex, concerted one-step fragmentation after electron attachment, with even four-bonds breaking quasi-simultaneously [39]. As discussed below in detail, however,  $NCO^-$  formation from the nucleobase anions is a complex unimolecular decomposition process, which is expected to occur on longer time scales and in more than one step. For few polyatomic molecules like valine or nitrobenzene a delayed (metastable) fragmentation extending to several microseconds after the attachment process has been reported recently [23, 40–43]. In the context of the metastable decomposition of biomolecular anions, a number of decay studies have also been reported on deprotonated biologically relevant anions formed in matrix assisted laser desorption/ionization (MALDI). These include studies on the metastable decay of the deprotonated nucleobases, nucleosides and the ribophosphate [44–47], as well as the sugars ribose [47] and fructose [47, 48]. In these studies, the focus resides on the role of the deprotonation site in determining the fragmentation path as reviewed in a recent colloquium [44]. It has been found that for thymine,  $NCO^-$  is the most significant fragmentation channel, which strongly depends on the deprotonation site.

Elementary ionization processes other than direct electron attachment and deprotonation are also active in biological systems and recently, several studies have been performed in order to understand how electron transfer in atom-molecule collisions can dictate the fragmentation pattern of biological components [49]. Thereby, also remarkable site and bond selectivity have been shown (i.e., by tuning the collision energy, a selectivity for  $H^-$  abstraction from the N1 site versus the N3 site in the pyrimidine bases, as well as clear selectivity for the N–H versus the C–H bonds [49] were achieved). Furthermore, in recent potassium–uracil collision studies [50], we have shown that for intermediate energies (above 30 eV in the lab frame), the most intense fragment anion formed is  $NCO^-$ , whereas for DEA studies in the low energy region ( $< 4$  eV), the loss of an hydrogen atom from the parent anion (i.e.,  $[U - H]^-$  formation, is the most prominent [51, 52]).

A prerequisite in the formation of  $NCO^-$  from a pyrimidine base, irrespective if the initial ion formation process is electron attachment, electron transfer, or MALDI, is the loss of at least one hydrogen atom from a nitrogen site

F. F. da Silva et al: Site Selectivity for a Slow Decay Process

and a 2-fold cleavage of the ring. This reaction sequence represents a complex unimolecular decomposition process, which occurs on a much longer time scale than simple bond cleavage. In the present study, we report the  $\text{NCO}^-$  formation from thymine, uracil, and their N-methylated counterparts upon DEA and collisions with potassium atoms, as well as in the unimolecular decomposition of  $[\text{M} - \text{H}]^-$  after hydrogen abstraction in DEA and deprotonation in MALDI. To get insight into the fragmentation pathways and to elucidate site selective bond cleavage processes, 1-methylthymine (1-meT), 3-methylthymine (3-meT), 1-methyluracil (1-meU), and 3-methyluracil (3-meU) were used to clearly distinguish between different sites.

## Experimental

The present work has been carried out using three different crossed beam apparatus, two at the Institute for Ion Physics and Applied Physics in Innsbruck and one at the Atomic and Molecular Collisions Laboratory in Lisbon as well as a MALDI instrument at the Science Institute of the University of Iceland. In both Innsbruck experiments, a molecular effusive beam of thymine and the partially methylated analog were formed by evaporation of their pristine powder (purchased from Sigma Aldrich, Vienna, Austria or synthesized as described in [44]) from an electrically heated oven kept in vacuum. The effusive beam of molecules was crossed with an electron beam from a standard Nier-type ion source [26] in one of the instruments and from a hemispherical monochromator in the other [12]. In the latter setup, the electron current was about 30 nA with a resolution of about 120 meV full width at half maximum (FWHM). In that setup, anions formed were mass analyzed with a quadrupole mass spectrometer and detected with a channeltron type secondary electron multiplier. In the setup with the Nier type ion source, the electron current was about 10  $\mu\text{A}$  with a resolution of about 1 eV (FWHM) and the anions formed were accelerated by an 8 kV potential into a sector field mass spectrometer. After passing the first field-free-region (ff1), the anions were analyzed by their momentum in a magnetic sector before entering a second field-free-region (ff2). After ff2, the anions were analyzed by their kinetic energy in an electric sector. The mass- and energy-analyzed anions were detected with a channeltron type secondary electron multiplier. This instrument was utilized to probe the stability of anions on the  $\mu\text{s}$  time scale. A metastable decay of a precursor anion with mass  $m_p$  in the ff1 is determined by variation of the acceleration voltage  $U$ . A metastable decay product in the ff1 (with mass  $m_d$ ) will keep its velocity; however, the kinetic energy is different from that of the parent anion. Thus, a decay product with  $m_d$  will only reach the detector if the high voltage is increased to  $U_f = U m_p/m_d$ . Decay reactions in the second field-free region ff2 between the magnetic and electric sector are probed using the mass analyzed ion kinetic energy (MIKE) scan method [43]. The following relationship between the ratio of the precursor mass  $m_p$  and the resulting fragment ion mass  $m_f$  and the ratio of the corresponding electric sector field voltages allows the

unambiguous assignment of the mass of the fragment ion:

$$\frac{E}{E_0} = \frac{m_f}{m_p} \quad (1)$$

In the Lisbon laboratory, the negative ion time of flight (ToF) mass spectra were obtained by neutral potassium atom collisions with 1- and 3-methylthymine and 1- and 3-methyluracil in a crossed beam experimental set-up described elsewhere [53]. Briefly, an effusive molecular beam crosses a primary beam of neutral potassium (K) atoms. In this setup,  $\text{K}^+$  ions produced in a potassium ion source were accelerated to 30–100 eV before passing through an oven, where they resonantly charge-exchange with neutral potassium to produce a beam of hyperthermal atoms. Residual ions from the primary beam were removed by electrostatic deflecting plates outside the oven. The intensity of the neutral potassium beam was monitored using a Langmuir-Taylor ionization detector, before and after the ToF mass spectra collection, with typical values on the order of tens of pA. The effusive beam of methylated uracil or thymine was introduced into a 1-mm diameter capillary where it was crossed with the neutral hyperthermal potassium beam between two parallel plates with 1.2-cm separation. The anions produced were extracted by a  $250 \text{ Vcm}^{-1}$  pulsed electrostatic field. The  $\text{K}^+$  beam was pulsed with 2  $\mu\text{s}$  width and an adjusted frequency depending on the collision energy, typically 222 kHz for 100 eV. The typical base pressure in the collision chamber was  $8 \times 10^{-6}$  Pa and the working pressure did not rise significantly upon heating the powder samples. Mass spectra were obtained by subtracting the background measurements (without heated sample) from sample measurements. The mass calibration was carried out on the basis of the well-known anionic species formed after potassium collisions with the nitromethane molecule [53]. The solid samples were purchased from Sigma-Aldrich with a minimum purity of  $\geq 99\%$  or synthesized as described in reference [44]. They were used as delivered and evaporated at temperatures between 393 and 413 K depending on the sample. The heating temperature was controlled using a PID unit. In order to test for any thermal decomposition, the spectra were recorded at different temperatures. No differences were observed in relative peak intensities as a function of the temperatures. The extraction region and the ToF system were heated to approximately 393 K throughout the measurements in order to prevent any sample deposition and thence charge accumulation on the electrodes.

Metastable decay of the deprotonated thymine and thymine derivatives was measured in a negative ion, post source decay (PSD) mode with a UV MALDI mass spectrometer (MALDI-MS) (Reflex IV; Bruker Daltonics, Bremen, Germany). The instrument and its operation have been described in detail elsewhere [54]. In brief, ions were generated in the MALDI process with an  $\text{N}_2$ -laser at 337 nm. The repetition rate was 10 Hz and the power was kept about 20 % above the detection threshold for the corresponding

parent ions. Negative ions were extracted in pulsed delay extraction mode with a delay time of 200 ns and accelerated into a reflectron ToF mass spectrometer. The parent ions were selected and gated into the field-free region of the mass spectrometer for PSD spectra recording. The mass gate was set at  $\pm 5$  Da in all experiments. The total acceleration voltage into the field-free linear region was 25 kV, resulting in about 6–9  $\mu$ s flight time. The observed metastable decay occurs within this time window. After the linear flight, the ions were reflected using a grid-less ion mirror and detected with a double micro-channel plate detector. The reflectron voltage was stepped down in seven segments to assure collection of all fragments. Individual segments are the sum of 500 individual shots, which were recorded by using the fragmentation analyses and structural ToF method FAST, within the instrumental control software FlexControl provided by the instrument manufacturer. The alignment of individual segments and the mass calibration of the spectra were carried out with the FlexAnalyses software also provided by the instrument manufacturer.

The sample molecules thymine and 1-methylthymine were acquired from Sigma-Aldrich, Germany, as high purity samples (>98 %) and used without further purification. The thymine derivative 3-methylthymine was prepared in-house from thymine. The preparation and purification was performed as described by Breeger et al. [55] and the structure was verified by H-NMR. Samples were prepared for measurements by co-spotting 0.5  $\mu$ L of a 1 mg/mL aqueous solution of the matrix bisbenzimidazole hydrochloride;  $C_{25}H_{24}N_6O \cdot 3HCl$  ( $\geq 98$  %, Sigma-Aldrich, Germany) and 0.5  $\mu$ L of a 10 mg/mL solution of the nucleobase in methanol on a stainless steel sample carrier.

## Results and Discussion

The most abundant fragment anion upon DEA to isolated thymine in the electron energy range above  $\sim 4$  eV is  $NCO^-$ . This is also the most abundant fragment ion in metastable decay of deprotonated thymine and the other pyrimidine bases, such as uracil and cytosine, when these are formed in MALDI [44, 46], as well as in potassium-uracil and -thymine collisions in the energy range from 30–100 eV [50]. Since  $NCO^-$  is formed efficiently upon attachment of a free electron, the dominant role of the  $NCO^-$  formation in potassium collision may seem obvious. However, in potassium collisions, this channel is even enhanced compared with DEA since  $K^+$  can efficiently delay autodetachment in the collision complex due to considerable Coulomb interaction. Therefore, the energy can be redistributed through the different degrees of freedom yielding a rather statistical dissociation in detriment of direct dissociation [50].

Figure 1 shows the three possible pathways leading to  $NCO^-$  formation, from  $[M - H]^-$ , formed after hydrogen abstraction upon electron attachment. Also given are the threshold energies,  $E_{th}$ , for each reaction step calculated at the B2PLYP/ma-TZVP level of theory [56, 57]. In our

calculations for reaction paths c and d the energy minimization of the open chain neutral moiety spontaneously finds its way to a local minimum four-membered ring structure. For clarity, the open chain geometries are also shown, though these are not necessary intermediates or transition states on these reaction paths. In addition to the threshold energies, also the height of the reaction barrier,  $E_{TS}$  associated with the opening of this four-membered ring to form the lowest energy open chain structure, is shown. This barrier is calculated at the B3LYP/6-311G(d,p) [58, 59] level of theory using the nudged elastic band method [60], and the single point energy of the transition state geometry is then calculated at the B2PLYP/ma-TZVP level of theory. For further detail on the calculations, please see Online Resource 1. In good agreement with the energy dependency of the observed hydrogen abstraction [32], we find the thermochemical threshold for loss of the H atom from the N1 and N3 position to be 0.89 and 1.38 eV, respectively. The reaction enthalpy for the  $NCO^-$  formation through electron attachment to the neutral thymine is equal to the sum of the threshold energies for reaction paths b and e (i.e., 3.47 eV). The threshold energy for the formation of the local minima four-membered ring, on the other hand, is 3.88 eV, independent of the route, and the opening of the four-membered ring is associated with a barrier of 0.35 eV.

### *$NCO^-$ Formation upon DEA to Thymine and 1- and 3-Methylthymine*

Figure 2a shows the anion efficiency curve of  $NCO^-$  formed upon free electron attachment to the pyrimidine base thymine (T). The anion yield exhibits a rich spectrum composed of a number of overlapping resonances. The corresponding resonant features are located at about 2.3, 4.4, 6.1, 6.8, 8.1, and 9.7 eV. The ion yield shown represents the “prompt” ion yield (i.e., the decay of the TNI has occurred in the ion source and thus on a time scale  $< \sim 1$   $\mu$ s). The thermochemical threshold calculated for the formation of  $NCO^-$  through the sequential decay mechanism shown in Figure 1 matches very well with the experimental onset of the second resonance at 4.4 eV. From the vibrational frequencies calculated here, we derive an internal energy of about 0.4 eV for the neutral precursor (i.e., the first weak resonance observed at 2.3 eV (onset  $\sim 1.5$  eV) must be formed by another reaction). The prompt  $NCO^-$  ion yields for 1-meT and 3-meT, shown in Figure 2b and c, respectively, exhibit similarities to the anion efficiency curve of  $NCO^-$  from T (i.e., a series of resonances up to about 12 eV). Remarkably, though the resonance energies seem to be very similar for the three molecules, the relative yield through these resonances varies strongly between the three molecules (e.g., the most abundant resonance in T at about 6.8 eV becomes less pronounced relative to the yield at higher energies when going from T  $\rightarrow$  1-meT  $\rightarrow$  3-meT).

For the pyrimidine bases the most abundant DEA fragment is the dehydrogenated closed-shell anion (here for

F. F. da Silva et al: Site Selectivity for a Slow Decay Process

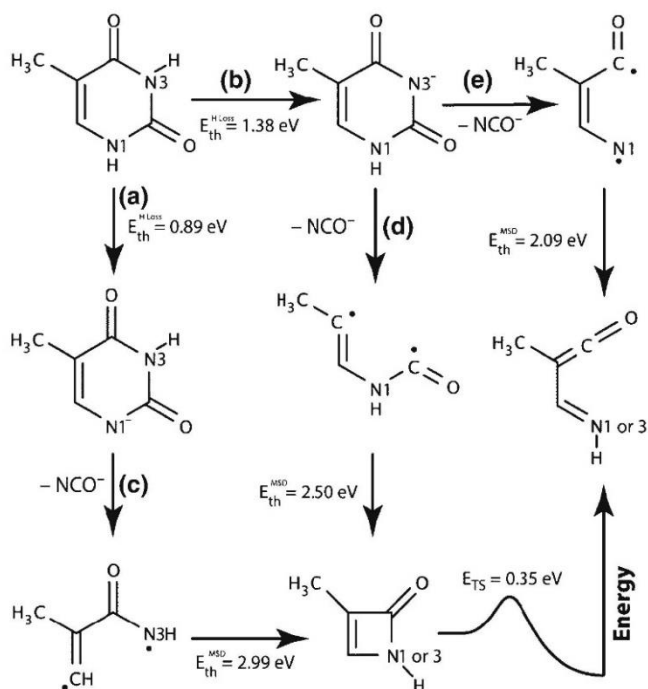


**Figure 1.** Reaction scheme showing the three different possible reaction pathways leading to  $\text{NCO}^-$  formation in thymine upon electron capture, along with the threshold energies for individual reaction steps calculated at the B2PLYP/ma-TZVP level of theory [56, 57]. **(a)** H loss from N1; **(b)** H loss from N3; **(c)**, **(d)**, and **(e)** pathways leading to  $\text{NCO}^-$  formation. For reaction paths **(c)** and **(d)**, energy minimization of the neutral moiety leads to a local minimum four-membered ring structure. For clarity, the open chain geometries along these reaction paths are also shown, though these are not necessarily intermediates or transition states on these paths. The energy barrier,  $E_{TS}$ , calculated with the nudged elastic band method [60] for the opening of this four-membered ring structure to form the lowest energy open chain structure is also given

thymine referred to as  $[\text{T} - \text{H}]^-$ ). It is formed via a series of narrow features at electron energies below 3 eV, which are assigned to vibrational Feshbach resonances (VFRs) [32, 61]. Figure 3a shows the measurement of  $[\text{T} - \text{H}]^-$  with the sector field instrument where VFRs are not resolved because of the lower energy resolution compared with the electron monochromator used in the previous study [32]. Measurements with partially deuterated molecules showed further that in the  $[\text{T} - \text{H}]^-$  formation through DEA, exclusively hydrogen atoms from the nitrogen sites are removed [11]. In the case of 1-methylthymine, hydrogen can only be removed from the N3 position and the  $[1\text{-meT} - \text{H}]^-$  anion efficiency curve showed a smooth asymmetric resonance with a threshold at about 1.4 eV [32]. Thus the VFRs result only in H loss from the N1 site, whereas the broad resonance at 1.6 eV leads to loss of hydrogen from the N3 position and is ascribed to a resonance involving a mixing of the  $\pi_2^*$  and  $\sigma_2^*$  virtual orbitals of the neutral precursor [32]. Similarly, the relative intensity of resonances in the  $\text{NCO}^-$  ion yield

changes through the N1 and N3 methylation (see Figure 2). The most abundant resonance in T at about 6.8 eV becomes much less pronounced relative to the resonances at 4.4, 6.1, and 9.7 eV when going from T  $\rightarrow$  1-meT. In the case of 3-meT, the resonance at 6.8 eV is almost suppressed. The resonance at 8.1 eV disappears upon both N1 and N3 methylation, while the resonances at about 6.8 and 9.7 eV seemingly remain unaffected. The low signal/noise ratio of the measurements for the methylated sample prevents deriving the tendency for the weak resonance at 2.3 eV.

Assuming a partly sequential decay mechanism for the  $\text{NCO}^-$  formation, the dehydrogenated parent anion  $[\text{T} - \text{H}]^-$  is the most probable intermediate (see Figure 1). Figure 3a compares the ion yield of the two prompt anions  $[\text{T} - \text{H}]^-$  and  $\text{NCO}^-$  formed upon DEA to T. The relative abundance of these two anions depends strongly on the initial electron energy. At electron energies  $< 4\text{ eV}$ ,  $[\text{T} - \text{H}]^-$  is more abundant than  $\text{NCO}^-$ . At higher electron energies, however, the internal energy of  $[\text{T} - \text{H}]^-$  becomes sufficiently large

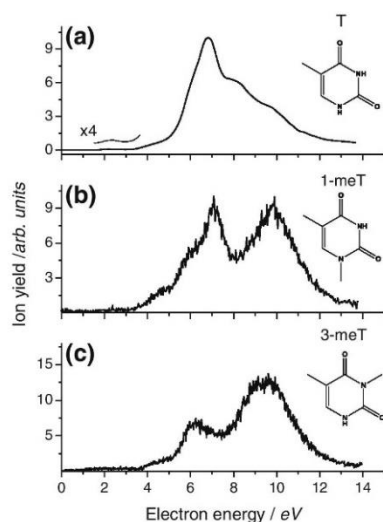


**Figure 2.** Prompt anion yields for  $\text{NCO}^-$  formed upon DEA to **(a)** thymine (T), **(b)** thymine methylated at N1 (1-meT), and **(c)** thymine methylated at N3 (3-meT), measured with the electron monochromator

that decomposition into  $\text{NCO}^-$  and other low-mass anions with much weaker abundance (not discussed here) dominates. Hence, at higher incident energies,  $\text{NCO}^-$  can be formed through prompt dissociation of the TNI or through further metastable decay of  $[\text{T} - \text{H}]^-$ . Polyatomic molecules can accommodate a substantial amount of internal energy in their vibrational degrees of freedom and vibrational predissociation leads often to a delayed decomposition of these ions extending to the microsecond regime. In the case discussed here the metastable decomposition of  $[\text{T} - \text{H}]^-$  into low-mass fragments including  $\text{NCO}^-$  can be observed mass spectrometrically. Indeed, in the present experiment, we obtain direct evidence for metastable decays into  $\text{NCO}^-$  using the scan techniques introduced in the experimental section. Figure 3b and c show the electron energy dependence of the  $\text{NCO}^-$  formation through metastable decay of  $[\text{T} - \text{H}]^-$ ,  $[\text{1-meT} - \text{H}]^-$ , and  $[\text{3-meT} - \text{H}]^-$  formed through DEA. In the first and second field-free region of the mass spectrometer the  $\text{NCO}^-$  yield shows 3 peaks located at 3.5, 5.5, and 8.8 eV. For the presently set acceleration voltage of 8 kV the time that elapsed from the formation of  $[\text{M} - \text{H}]^-$  and the ion entering and exiting the two field-free regions are 1 and 10  $\mu\text{s}$  for the first field-free region and 19 and 31.6  $\mu\text{s}$  for the second field-free region, respectively. The broad high-energy peak between about 8 and 11 eV is weaker for the formation of  $\text{NCO}^-$  at later times, which reflects a reduced stability of the precursor ion  $[\text{T} - \text{H}]^-$  at higher electron energies (i.e., faster fragmentation).

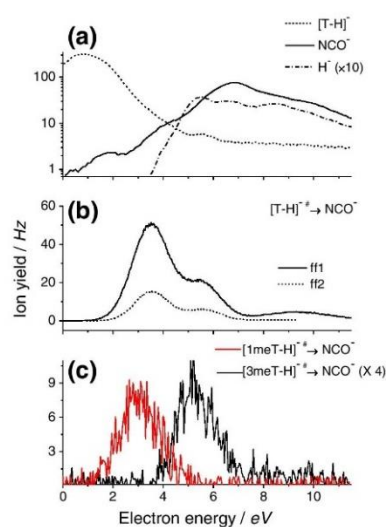


**Figure 3.** **(a)** Prompt ion yields for  $[\text{T} - \text{H}]^-$  (dotted line),  $\text{NCO}^-$  (solid line) and  $\text{H}^-$  (dash-dotted line) formed upon DEA to thymine. **(b)** Metastable anion yields for the decomposition of  $[\text{T} - \text{H}]^-$  from thymine (T) into  $\text{NCO}^-$  in the first (solid) and second (dotted line) field free region of the double-sector field mass spectrometer. **(c)** Same decay channel like for middle panel for 1-methylthymine (1-meT) and 3-methylthymine (3-meT). All anion yields shown were measured with the sector field instrument

Remarkably, for 1-meT the metastable  $\text{NCO}^-$  yield from  $[\text{M} - \text{H}]^-$  only shows a contribution in the low energy range which, within the accuracy of the measurement, we ascribe to the metastable decay peak observed here at 3.5 eV for T. In addition, this metastable yield coincides well with the high energy part of the  $[\text{M} - \text{H}]^-$  yield from 1-meT through initial occupation of the anti-bonding  $\pi_2^*/\sigma_2^*$  molecular orbitals (MO) [32]. In 3-meT, on the other hand, the metastable decay of  $[\text{M} - \text{H}]^-$  to form  $\text{NCO}^-$  is confined to the two resonances at higher electron energies observed in the metastable decay of  $[\text{T} - \text{H}]^-$ . The resonance close to 5.5 eV coincides with a resonance observed in the  $[\text{M} - \text{H}]^-$  yield from T (see Figure 3a). The resonant metastable yields observed for 1-meT and 3-meT (Figure 3c) show clearly that both the N1 and N3 dehydrogenation sites in the thymine anion contribute to the formation of  $\text{NCO}^-$  in the metastable decay of  $[\text{M} - \text{H}]^-$  formed through DEA. Furthermore, it is also clear from Figure 3 and the thermochemical thresholds in Figure 1 that the site selectivity of the energy dependency of the  $\text{NCO}^-$  formation after dehydrogenation from N1 and N3, respectively, is not due to thermochemical restrictions of the respective processes. On the contrary, this site selectivity in the metastable  $\text{NCO}^-$  formation is clearly the result of the

F. F. da Silva et al: Site Selectivity for a Slow Decay Process

different nature of the resonances leading to the initial hydrogen abstraction. The respective contribution from both sites can thus be tuned by the initial electron energy. One may also correlate the three metastable peaks observed in Figure 3b with the prompt  $\text{NCO}^-$  ion yield shown for T in Figure 2a. Assuming that the prompt peaks are shifted slightly by few hundred meV upwards compared with the corresponding metastable peaks (attributable to a higher excess energy responsible for the prompt decay), we assign the prompt resonances at 4.4, 6.1, and 9.7 eV to the electronic states decaying also in the metastable time regime.

#### *$\text{NCO}^-$ Formation upon Deprotonation of Thymine, 1- and 3-Methylthymine in MALDI*

Figure 4 compares the metastable decay spectra of  $[\text{T} - \text{H}]^-$ ,  $[\text{1-meT} - \text{H}]^-$ , and  $[\text{3-meT} - \text{H}]^-$  formed through deprotonation in MALDI. The figure shows that  $\text{NCO}^-$  formation in MALDI only proceeds from T and 1-meT, but is not observed from 3-meT.

Hence, initial deprotonation at the N3 site is a prerequisite for the  $\text{NCO}^-$  formation in MALDI and no further decay is observed after deprotonation at N1. This is very different from the metastable decay of T, 1-meT, and 3-meT after hydrogen loss upon DEA, where  $\text{NCO}^-$  formation is observed from  $[\text{1-meT} - \text{H}]^-$  as well as  $[\text{3-meT} - \text{H}]^-$ . Furthermore, similar to the MALDI experiments, classical dynamics simulations of the decay of the deprotonated species in their electronic ground state [44, 46] show  $\text{NCO}^-$  formation nearly exclusively after deprotonation from the N3 site. Hence, the classical dynamics simulations showed  $\text{NCO}^-$  formation in four out of 10 of the trajectories simulated for thymine deprotonation at N3, but for

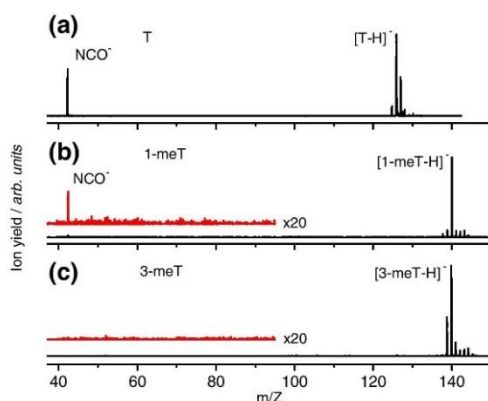


**Figure 4.** MALDI post source decay spectra of the metastable decay of deprotonated (a) thymine (T), (b) 1-methylthymine (1-meT), and (c) 3-methylthymine (3-meT). While  $\text{NCO}^-$  is observed from the native thymine and from 1-meT, no such fragmentation is observed from 3-meT. Adapted from reference [46]

thymine deprotonation at N1, only one out of 10 simulations resulted in  $\text{NCO}^-$  formation. Similarly, nine out of 10 trajectories simulated for  $[\text{1-meT} - \text{H}]^-$  resulted in  $\text{NCO}^-$  formation but no fragmentation was observed for  $[\text{3-meT} - \text{H}]^-$ . In MALDI the deprotonated anion is formed through proton transfer under multiple collision condition in the expanding plume of matrix and analyte molecules, and the resulting internal energy of small deprotonated molecular anions produced in this process is estimated to be around 4–5 eV [62, 63]. Consequently, these deprotonated ions are formed in their electronic ground state but with considerable internal energy. Similarly, the classical dynamics simulations are based on the condition that the anions have reached the thermally equilibrated electronic ground state before dissociation occurs and considerable internal energy is added to accelerate the trajectories. In the case of thymine, and its methylated analogs, the internal energy added was 8 eV (above room temperature). Hence, both in the MALDI experiment and in the classical dynamics simulations, the internal energy of the deprotonated parent ions is considerably higher than the thermochemical threshold for their metastable decay, independent of the deprotonation site (see step c, d, and e in Figure 1). Nonetheless, in MALDI and in our classical dynamics simulations,  $\text{NCO}^-$  is only observed after deprotonation from N3 (with the exception of one trajectory in the simulations). We note that such statistical decay model was previously applied successfully for the metastable decay of the amino acid valine [23]. In the study for valine, the decomposition process  $[\text{M} - \text{H}]^- \rightarrow \text{HCOO}^- + \text{neutrals}$ , was examined for  $[\text{M} - \text{H}]^-$  formed through DEA and in MALDI, and it was found to be independent of the formation mechanism of  $[\text{M} - \text{H}]^-$  (i.e., if it was formed by deprotonation in MALDI or DEA). In the presently studied decay for thymine, a purely statistical decay model seems to be applicable only in a limited way for  $[\text{M} - \text{H}]^-$  formed in the DEA process since it misses the metastable decay starting from H-loss from the N1 position. As mentioned above, in the case of hydrogen loss from the N3 position in DEA, the TNI is initially formed through a single electron occupying the low lying  $\pi_2^*$  orbital, mixing with the repulsive  $\sigma_2^*$ . The TNI then relaxes through hydrogen loss to the electronic ground state of  $[\text{M} - \text{H}]^-$ . The bulk of the excess energy brought in by the attaching electron and through the electron affinity of  $[\text{M} - \text{H}]^-$  (3.5 eV) [11] is distributed within the internal degrees of freedom of the  $[\text{M} - \text{H}]^-$  fragment. Correspondingly, the metastable  $\text{NCO}^-$  formation is observed from the higher energy side of the resonance where sufficient internal energy is available for further fragmentation. Metastable decay from  $[\text{M} - \text{H}]^-$  formed through hydrogen loss from N1, on the other hand, proceeds exclusively when the TNI leading to the precursor ion,  $[\text{M} - \text{H}]^-$ , is formed through a core excited resonance located close to 5.5 eV. Hence, here the TNI leading to hydrogen loss is formed in an electronically excited state with two electrons in a formerly unoccupied MO and a single vacancy in a previously occupied MO. This may also lead to the formation of  $[\text{M} - \text{H}]^-$ , an electronically excited state of the dehydrogenated molecular ion. In that case, further

fragmentation to  $\text{NCO}^-$  after hydrogen loss from N1 proceeds from an electronically excited state, which in turn explains the absence of this channel in metastable decay of the ground state precursor ions. We also note that the metastable peak at about 5.5 eV matches well with the DEA resonance for  $\text{H}^-$  formation from the N1 position (see Figure 3a). Thus, we tentatively assign a common electronically excited TNI state as a precursor for the fragment anions formed at this energy.

#### *$\text{NCO}^-$ Formation upon Collisions of Potassium Atoms with 1- and 3-Methyluracil and 1- and 3-Methylthymine*

Figure 5 shows the negative ion ToF mass spectrum of 1-methyluracil recorded at 30 eV (lab frame) potassium impact energies, where the most intense anion is assigned to  $\text{NCO}^-$ . Apart from  $\text{NCO}^-$ , also a number of other, lower intensity fragment anions have been observed in potassium collisions with pyrimidine bases as thymine and uracil at 30, 70, and 100 eV collision energies (see e.g., Almeida et al. [64]). In this contribution, however, we limit our discussion to  $\text{NCO}^-$ . In order to have a conclusive set of data on the  $\text{NCO}^-$  formation, several mass spectra of the four different methylated pyrimidine bases have been recorded in the energy range from 30 to 100 eV. These provide information on the site and bond selectivity of fragmentation pathways involved in the decomposition of the TNI of the pyrimidine bases, when these are formed in potassium collisions. Recently, we have shown that in potassium collisions with methylated pyrimidine bases,  $\text{H}^-$  formation can be completely inactivated when the N-H bond is replaced by N- $\text{CH}_3$  [49]. Accordingly, the mechanism leading to  $\text{NCO}^-$  formation can be interpreted as a multiple-step mechanism initiated by the loss of the hydrogen atom from the N1 and/or the N3 positions. In electron transfer experiments on potassium collisions with thymine (T) and uracil (U), it was proposed that the dehydrogenated parent anion  $[\text{M} - \text{H}]^-$  is indeed a precursor in the formation of the fragments like  $\text{NCO}^-$  that require bond cleavages in the ring [50]. Thus, the initial position of the hydrogen loss will dictate the fragmentation yield as we shall show here.

In the present discussion, we concentrate on the possible fragmentation pathways shown in Figure 1 and will not explore reactions initiated by hydrogen loss from the C5 and/or C6 positions, which are energetically much less favorable (threshold energy  $>2$  eV) [29]. However, initial hydrogen loss from the carbon positions, while requiring a more complex mechanism for the  $\text{NCO}^-$  formation, may be dominating at higher collision energies ( $>100$  eV) [50].

We see from the possible pathways in Figure 1 that after electron transfer and formation of a TNI, the system can evolve through paths a and/or b with H loss from the N1 and/or the N3 position, respectively. In the case that the loss of hydrogen stems from the N3 position,  $\text{NCO}^-$  formation may further proceed along d and/or e, whereas abstraction from the N1 position leads to a  $\text{NCO}^-$  formation through c

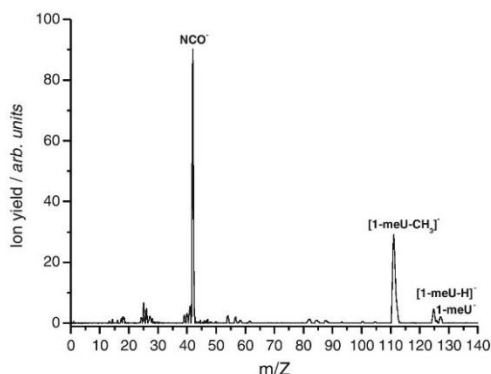


Figure 5. Negative ion Time-of-flight mass spectrum of ions formed in collisions of potassium atoms with 1-meU at 30 eV lab frame collision energy

only. In order to evaluate the contribution of such paths,  $\text{NCO}^-$  branching ratios (i.e.,  $\text{NCO}^- / \sum X^-$  where the denominator corresponds to the sum of the ion yields of all fragment anions) were obtained as function of the collision energy for the four methylated pyrimidines 1- and 3-meT, and 1- and 3-meU. The resulting ratios are plotted in Figure 6. In the case of 1-meU and 3-meU, the relative difference between the two molecules is approximately 0.1 for all collision energies with the exception of 70 eV. Therefore,  $\text{NCO}^-$  formation from potassium collisions with 1-meU is more favorable than in the case of 3-meU. In the case of 1-meU, the decomposition process is initiated by the loss of hydrogen from the N3 position leading to the intermediate  $[\text{1-meU} - \text{H}]^-$  anion formation. The reaction will then follow path d and/or e, whereas path c will remain blocked. In contrast, for 3-meU the only pathway that is opened is c since methylation in the N3 position suppresses  $\text{NCO}^-$  formation from paths d and e. As a result we observe a lower  $\text{NCO}^-$  branching ratio for 3-meU in comparison with 1-meU.

In the lower panel of Figure 6, we show the results from collisions of potassium atoms with 1-meT and 3-meT. A close inspection of this figure shows remarkably similar  $\text{NCO}^-$  branching ratios for collision energies up to 50 eV, indicating very limited site selectivity at low collision energies. For higher collision energies ( $>50$  eV), on the other hand, a distinct site selectivity, favoring  $\text{NCO}^-$  formation from 1-meT, appears.

For collision energies below 50 eV, which correspond to collision times longer than 40 fs, the potassium cation formed after electron transfer to the target molecule may be present sufficiently long in order to stabilize the TNI through Coulomb interaction within the collision complex. This ensures that pathways d and e are open together with pathway c. This rationale can be interpreted in terms of the spatial orientation of the molecular orbitals. The incoming electron can be trapped in



F. F. da Silva et al: Site Selectivity for a Slow Decay Process

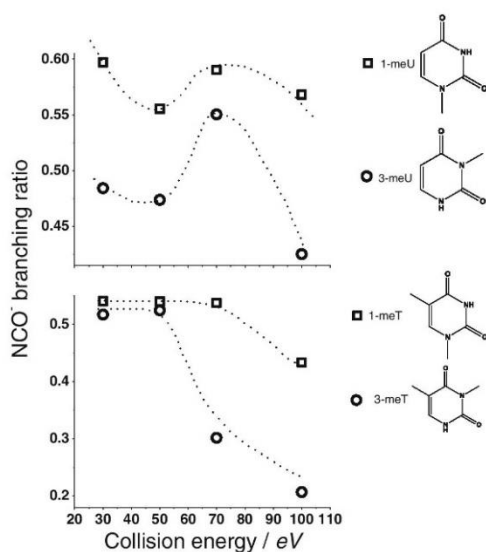


**Figure 6.** NCO<sup>-</sup> branching ratios in collisions of potassium atoms with N-site methylated uracil and thymine molecules. The dotted lines are just to guide the eye

the C5 methyl group position  $\pi^*$  orbital, with time enough to be transferred to  $\sigma^*$  N-CH<sub>3</sub> from the N3 position methyl group. This assumption seems reasonable since a similar transition has been described recently by Almeida et al. [64], in context to the loss of a methyl group in potassium collisions with 1-meT and 3-meU. Therefore, in this unimolecular decomposition such coupling will allow accessing the three pathways c, d, and e in Figure 1, which in turn means similar NCO<sup>-</sup> branching ratio for energies up to 50 eV. For higher collision energies (70 and 100 eV), the K<sup>+</sup> stabilizing effect will not be effective enough because of its reduced transit time, and this coupling may no longer hold. In this energy range, the relative difference between the NCO<sup>-</sup> branching ratios from 1-meT and 3-meT is, thus, increased to about 0.2 in favor of NCO<sup>-</sup> formation from 1-meT. This effect is mostly noticeable for energies above 50 eV and these results show an unprecedented site- and bond-selectivity regarding the concerted fragmentation mechanism yielding NCO<sup>-</sup> formation in DNA pyrimidine bases upon electron transfer.

## Conclusion

In this work, we presented negative ion formation in N-site methylated pyrimidine derivatives through DEA, MALDI, and potassium–molecule collision experiments, with particular focus on NCO<sup>-</sup> formation. This is the dominant fragment anion formed upon DEA to gas phase thymine at electron

energies of  $\sim 4$  eV, the only fragment observed in metastable decay of deprotonated thymine in MALDI and, in the case of potassium-N-site methylated pyrimidine collisions, NCO<sup>-</sup> is the most abundant fragment anion for collision energies above 30 eV.

A previous free electron attachment study with thymine embedded in cold helium droplets [65] showed that [T – H]<sup>-</sup> is the only fragment anion formed when an electron attaches to thymine in the droplet. In addition, the anion efficiency curve of [T – H]<sup>-</sup> upon DEA to superfluid helium droplets doped with thymine matches well with the total anion yield obtained for DEA to gas phase thymine. This led to the conclusion that because of the highly efficient energy dissipation to the surrounding matrix, the formation of all low-mass anions is quenched in helium droplets in favor of the [T – H]<sup>-</sup> formation [65]. The present DEA results directly confirm that NCO<sup>-</sup> is formed in a sequential decay reaction with the dehydrogenated closed shell anion as the intermediate product. Previously, it was assumed that multistep bond cleavage reactions, such as the NCO<sup>-</sup> formation studied here are less selective than single bond dissociations [39]. Here, we show that the remarkable site selectivity in the H<sup>-</sup> and [M – H]<sup>-</sup> reaction channels in the pyrimidine bases is preserved for the subsequent decay reaction into NCO<sup>-</sup>. Furthermore, this is true even if the decay takes place several tens of microseconds after the initial electron attachment process. Comparison with MALDI shows that the contribution to the metastable anion yield at  $\sim 5.5$  eV in the DEA experiments (and thus also in the prompt ion yields of H<sup>-</sup> and [M – H]<sup>-</sup>) results from a core excited resonance and is thus not observable in the statistical decay of the electronic ground state in MALDI and in classical dynamics simulations. The present results show that not only the total amount of internal energy determines the extent of this metastable decay channel but also the initial electronic state of the TNI leading to the formation of the [T – H]<sup>-</sup> precursor ion.

From the electron transfer experiments in potassium collisions with N-site methylated pyrimidines, NCO<sup>-</sup> branching ratios obtained show remarkable site- and bond-selectivity in this decay channel. In the case of N-site methylated uracil, the selectivity is verified for all collision energies. However for N-site methylated thymine the selectivity depends strongly on the collision energy. The dwell time of the potassium cation in the Coulomb complex will dictate the fragmentation pathways leading to the NCO<sup>-</sup> formation. For longer collision times, some fragmentation channels are not accessible without cation stabilization, whereas for shorter collision times, they are blocked. In the latter situation, the selectivity of the NCO<sup>-</sup> formation is clearly visible. To our knowledge, the study presented here shows for the first time that site-selectivity in molecular fragmentation upon electron transfer can be conserved, even in complex, concerted reaction mechanisms that require multiple bond breaking.

## Acknowledgments

The authors acknowledge support for this work from the FWF, Wien (P-22665) and the European Commission, Brussels.

F.F.S. and D.A. acknowledge the Portuguese Foundation for Science and Technology (FCT-MEC) for post-doctoral and post-graduate scholarships SFRH/BPD/68979/2010 and SFRH/BD/61645/2009, respectively. D.A. together with P.L.-V. acknowledge the PEst-OE/FIS/UI0068/2011 and PTDC/FIS-ATO/1832/2012 grants. O.I. acknowledges support from the Icelandic Centre for Research (RANNIS) and the Research Fund of the University of Iceland, and H.D.F. acknowledges a Ph.D. grant from the Eimskip University Fund. G.G. acknowledges support from the Spanish Ministerio de Economía y Productividad (Project FIS2009-10245). This work also forms a part of the EU/ESF COST Actions Electron Controlled Chemical Lithography (ECCL) CM0601, The Chemical Cosmos CM0805, and the Nanoscale Insights into Ion Beam Cancer Therapy (Nano-IBCT) MP1002.

## References

- Boudaiffa, B., Cloutier, P., Hunting, D., Huels, M.A., Sanche, L.: Resonant formation of DNA strand breaks by low-energy (3 to 20 eV) electrons. *Science* **287**, 1658–1660 (2000)
- Martin, F., Burrow, P.D., Cai, Z., Cloutier, P., Hunting, D., Sanche, L.: DNA strand breaks induced by 0–4 eV electrons: The role of shape resonances. *Phys. Rev. Lett.* **93**, 068101-1–068101-4 (2004)
- Alizadeh, E., Sanche, L.: Precursors of solvated electrons in radiobiological physics and chemistry. *Chem. Rev.* **12**, 5578–5602 (2012)
- Baccarelli, I., Bald, L., Gianturco, F.A., Illenberger, E., Kopyra, J.: Electron-induced damage of DNA and its components: experiments and theoretical models. *Phys. Rep.* **508**, 1–44 (2011)
- Bald, L., Langer, J., Tegeder, P., Ingólfsson, O.: From isolated molecules through clusters and condensates to the building blocks of life. A short tribute to Professor Eugen Illenberger's work in the field of negative ion chemistry. *Int. J. Mass Spectrom.* **277**, 4–25 (2008)
- Sanche, L.: Role of secondary low energy electrons in radiobiology and chemoradiation therapy of cancer. *Chem. Phys. Lett.* **474**, 1–6 (2009)
- Baccarelli, I., Gianturco, F.A., Scifoni, E., Solov'yov, A.V., Surduovich, E.: Molecular level assessments of radiation biodamage. *Eur. Phys. J. D* **60**, 1–10 (2010)
- Simons, J.: How do low-energy (0.1–2 eV) electrons cause DNA-strand breaks? *Acc. Chem. Res.* **39**, 772–779 (2006)
- Gu, J., Leszczynski, J., Schaeffer III, H.F.: Interactions of electrons with bare and hydrated biomolecules: from nucleic acid bases to DNA segments. *Chem. Rev.* **112**, 5603–5640 (2012)
- Orlando, T.M., Oh, D., Chen, Y., Aleksandrov, A.B.: Low-energy electron diffraction and induced damage in hydrated DNA. *J. Chem. Phys.* **128**, 195102-1–195102-7 (2008)
- Abdoul-Carime, H., Gohlke, S., Illenberger, E.: Site-specific dissociation of DNA bases by slow electrons at early stages of irradiation. *Phys. Rev. Lett.* **92**, 168103-1–168103-4 (2004)
- Ptasinska, S., Denifl, S., Grill, V., Märk, T.D., Illenberger, E., Scheier, P.: Bond- and site-selective loss of H- from pyrimidine bases. *Phys. Rev. Lett.* **95**, 093201-1–093201-4 (2005)
- Ptasinska, S., Denifl, S., Grill, V., Märk, T.D., Scheier, P., Gohlke, S., Huels, M., Illenberger, E.: Bond-selective H-ion abstraction from thymine. *Angew. Chem. Int. Ed.* **44**, 1647–1650 (2005)
- Prabhudesai, V.S., Kelkar, A.H., Nandi, D., Krishnakumar, E.: Functional group-dependent site-specific fragmentation of molecules by low energy electrons. *Phys. Rev. Lett.* **95**, 143202-1–143202-4 (2005)
- Sloan, P.A., Palmer, R.E.: Two-electron dissociation of single molecules by atomic manipulation at room temperature. *Nature* **434**, 367–371 (2005)
- Riedel, D., Bocquet, M.-L., Lesnard, H., Lastapis, M., Lorente, N., Sonnet, P., Dujardin, G.: Selective scanning tunnelling microscope electron-induced reactions of single biphenyl molecules on a Si(100) surface. *J. Am. Chem. Soc.* **131**, 7344–7352 (2009)
- Ning, Z., Polanyi, J.C.: Charge delocalization induces reaction in molecular chains at a surface. *Angew. Chem. Int. Ed.* **52**, 320–324 (2013)
- Ptasinska, S., Denifl, S., Gohlke, S., Scheier, P., Illenberger, E., Märk, T.D.: Decomposition of thymidine by low-energy electrons: Implications for the molecular mechanisms of single-strand breaks in DNA. *Angew. Chem. Int. Ed.* **45**, 1893–1896 (2006)
- Baccarelli, I., Gianturco, F.A., Grandi, A., Sanna, V., Lucchese, R.R., Bald, L., Kopyra, J., Illenberger, E.: Selective bond breaking in beta-D-ribose by gas-phase electron attachment around 8 eV. *J. Am. Chem. Soc.* **129**, 6269–6277 (2007)
- Bald, L., Kopyra, J., Illenberger, E.: Selective excision of C5 from D-ribose in the gas phase by low-energy electrons (0–1 eV): implications for the mechanism of DNA damage. *Angew. Chem., Int. Ed.* **45**, 4851–4855 (2006)
- Denifl, S., Zappa, F., Mähr, I., Lecointre, J., Probst, M., Märk, T.D., Scheier, P.: Mass spectrometric investigation of anions formed upon free electron attachment to nucleobase molecules and clusters embedded in superfluid helium droplets. *Phys. Rev. Lett.* **97**, 043201-1–043201-4 (2006)
- Papp, P., Urban, J., Matejcek, S., Stano, M., Ingólfsson, O.: Dissociative electron attachment to gas phase valine: a combined experimental and theoretical study. *J. Chem. Phys.* **125**, 204301-1–204301-8 (2006)
- Flosadottir, H.D., Denifl, S., Zappa, F., Wendt, N., Mauracher, A., Bacher, A., Jonsson, H., Märk, T.D., Scheier, P., Ingólfsson, O.: Combined experimental and theoretical study on the nature and the metastable decay pathways of the amino acid ion fragment [M-H]. *Angew. Chem. Int. Ed.* **46**, 8057–8059 (2007)
- Vasil'ev, Y.V., Figard, B.J., Voinov, V.G., Barofsky, D.F., Deinzer, M.L.: Resonant electron capture by some amino acids and their methyl esters. *J. Am. Chem. Soc.* **128**, 5506–5515 (2006)
- Vizcaino, V., Puschnigg, B., Huber, S.E., Probst, M., Fabrikant, I.I., Gallup, G.A., Illenberger, E., Scheier, P., Denifl, S.: Hydrogen loss in aminobutanoic acid isomers by the sigma\* resonance formed in electron capture. *New J. Phys.* **14**, 043017-1–043017-12 (2012)
- Gschliesser, D., Vizcaino, V., Probst, M., Scheier, P., Denifl, S.: Formation and decay of the dehydrogenated parent anion upon electron attachment to dialanine. *Chem. Eur. J.* **18**, 4613–4619 (2012)
- Yandell, M.A., King, S.B., Neumark, D.M.: Time-resolved radiation chemistry: photoelectron imaging of transient negative ions of nucleobases. *J. Am. Chem. Soc.* **135**, 2128–2131 (2013)
- Denifl, S., Ptasinska, S., Probst, M., Hrusak, J., Scheier, P., Märk, T.D.: Electron attachment to the gas-phase DNA bases cytosine and thymine. *J. Phys. Chem. A* **108**, 6562–6569 (2004)
- Li, X., Sanche, L., Sevilla, M.D.: Low energy electron interactions with uracil: the energetics predicted by theory. *J. Phys. Chem. B* **108**, 5472–5476 (2004)
- Takayanagi, T., Asakura, T., Motegi, H.: Theoretical study on the mechanism of low-energy dissociative electron attachment for uracil. *J. Phys. Chem. A* **113**, 4795–4801 (2009)
- González-Ramírez, I., Segarra-Martí, J., Serrano-Andrés, L., Merchán, M., Rubio, M., Roca-Sanjuán, D.: On the N-1-H and N-3-H bond dissociation in uracil by low energy electrons: a CASSCF/CASPT2 study. *J. Chem. Theory Comput.* **8**, 2769–2776 (2012)
- Burrow, P., Gallup, G., Scheer, A., Denifl, S., Ptasinska, S., Märk, T.D., Scheier, P.: Vibrational Feshbach resonances in uracil and thymine. *J. Chem. Phys.* **124**, 124310-1–124310-7 (2006)
- Winstead, C., McKoy, V.: Low-energy electron collisions with gas-phase uracil. *J. Chem. Phys.* **125**, 174304-1–174304-8 (2006)
- Winstead, C., McKoy, V.: Ring-breaking electron attachment to uracil: following bond dissociations via evolving resonances. *J. Chem. Phys.* **129**, 077101-1–077101-2 (2008); *J. Chem. Phys.* **128**, 174302 (2008)
- Gianturco, F. A.; Sebastianelli, F.; Lucchese, R. R.; Baccarelli, I.; Sanna, N.: Ring-breaking electron attachment to uracil: Following bond dissociations via evolving resonances. *J. Chem. Phys.* **128**, 174302-1–174302-8 (2008); Erratum: "Ring-breaking electron attachment to uracil: Following bond dissociations via evolving resonances". *J. Chem. Phys.* **131**, 249901-1–249901-2 (2008)
- Dora, A., Bryjko, L., van Mourik, T., Tennyson, J.: R-matrix study of elastic and inelastic electron collisions with cytosine and thymine. *J. Phys. B* **45**, 175203-1–175203-10 (2012)
- Dora, A., Tennyson, J., Bryjko, L., van Mourik, T.: R-matrix calculation of low-energy electron collisions with uracil. *J. Chem. Phys.* **130**, 164307-1–164307-8 (2009)
- Aflatooni, K., Scheer, A.M., Burrow, P.D.: Total dissociative electron attachment cross sections for molecular constituents of DNA. *J. Chem. Phys.* **125**, 054301-1–054301-5 (2006)
- Davis, D., Vysotskiy, V.P., Sajeev, Y., Cederbaum, L.S.: A one-step four-bond-breaking reaction catalyzed by an electron. *Angew. Chem. Int. Ed.* **51**, 8003–8007 (2012)

F. F. da Silva et al: Site Selectivity for a Slow Decay Process

40. Asfandiarov, N.L., Pshenichnyuk, S.A., Lukin, V.G., Pshenichnyuk, I.A., Modelli, A., Matejčík, S.: Temporary anion states and dissociative electron attachment to nitrobenzene derivatives. *Int. J. Mass Spectrom.* **264**, 22–37 (2007)
41. Mauracher, A., Denifl, S., Edtbauer, A., Hager, M., Probst, M., Echt, O., Märk, T.D., Scheier, P., Field, T.A., Graupner, K.: Metastable anions of dinitrobenzene: resonances for electron attachment and kinetic energy release. *J. Chem. Phys.* **133**, 244302-1–244302-9 (2010)
42. Shchukin, P.V., Muftakhov, M.V., Pogulya, A.V.: Study of fragmentation pathways of metastable negative ions in aliphatic dipeptides using the statistical theory. *Rapid Commun. Mass Spectrom.* **26**, 828–834 (2012)
43. Zappa, F., Beikircher, M., Mauracher, A., Denifl, S., Probst, M., Injan, N., Limtrakul, J., Bacher, A., Echt, O., Märk, T.D., Scheier, P., Field, T.A., Graupner, K.: Metastable dissociation of anions formed by electron attachment. *Chem. Phys. Chem.* **9**, 607–611 (2008)
44. Flosadóttir, H.D., Ómarsson, B., Bald, I., Ingólfsson, O.: Metastable decay of DNA components and their compositions—a perspective on the role of reactive electron scattering in radiation damage. *Eur. Phys. J. D* **66**, 13–32 (2012)
45. Flosadóttir, H.D., Jónsson, H., Sigurdsson, S.T., Ingólfsson, O.: Experimental and theoretical study of the metastable decay of negatively charged nucleosides in the gas phase. *Phys. Chem. Chem. Phys.* **13**, 15283–15290 (2011)
46. Bald, I., Flosadóttir, H.D., Ómarsson, B., Ingólfsson, O.: Metastable fragmentation of a thymidine-nucleotide and its components. *Int. J. Mass Spectrom.* **313**, 15–20 (2012)
47. Bald, I., Flosadóttir, H.D., Kopyra, J., Illenberger, E., Ingólfsson, O.: Fragmentation of deprotonated D-ribose and D-fructose in MALDI-Comparison with dissociative electron attachment. *Int. J. Mass Spectrom.* **280**, 190–197 (2009)
48. Flosadóttir, H.D., Bald, I., Ingólfsson, O.: Fast and metastable fragmentation of deprotonated D-fructose—a combined experimental and computational study. *Int. J. Mass Spectrom.* **305**, 50–57 (2011)
49. Almeida, D., Ferreira da Silva, F., Garcia, G., Limão-Vieira, P.: Selective bond cleavage in potassium collisions with pyrimidine bases of DNA. *Phys. Rev. Lett.* **110**, 023201-1–023201-5 (2013)
50. Almeida, D., Antunes, R., Martins, G., Eden, S., Ferreira da Silva, F., Nunes, Y., Garcia, G., Limão-Vieira, P.: Electron transfer-induced fragmentation of thymine and uracil in atom-molecule collisions. *Phys. Chem. Chem. Phys.* **13**, 15657–15665 (2011)
51. Hanel, G., Gstir, B., Denifl, S., Scheier, P., Probst, M., Farizon, B., Farizon, M., Illenberger, I., Märk, T.D.: Electron attachment to uracil: Effective destruction at subexcitation energies. *Phys. Rev. Lett.* **90**, 188104-1–188104-4 (2003)
52. Scheer, A.M., Silvernail, C., Belot, J.A., Aflatooni, K., Gallup, G.A., Burrow, P.D.: Dissociative electron attachment to uracil deuterated at the N-1 and N-3 positions. *Chem. Phys. Lett.* **411**, 46–50 (2005)
53. Antunes, R., Almeida, D., Martins, G., Mason, N.J., Garcia, G., Maneira, M.J.P., Nunes, Y., Limão-Vieira, P.: Negative ion formation in potassium-nitromethane collisions. *Phys. Chem. Chem. Phys.* **12**, 12513–12519 (2010)
54. Stano, M., Flosadóttir, H.D., Ingólfsson, O.: Effective quenching of fragment formation in negative ion oligonucleotide matrix-assisted laser desorption/ionization mass spectrometry through sodium adduct formation. *Rapid Commun. Mass Spectrom.* **20**, 3498–3502 (2006)
55. Breeger, S., von Meltzer, M., Hennecke, U., Carell, T.: Investigation of the pathways of excess electron transfer in DNA with flavin-donor and oxetane-acceptor modified DNA hairpins. *Chem. Eur. J.* **12**, 6469–6477 (2006)
56. Grimme, S.: Semiempirical hybrid density functional with perturbative second-order correlation. *J. Chem. Phys.* **124**, 034108-1–034108-16 (2006)
57. Zheng, J., Xu, X., Truhlar, D.G.: Minimally augmented Karlsruhe basis sets. *Theor. Chem. Acc.* **128**, 295–305 (2011)
58. Becke, A.D.: Density-functional thermochemistry. III. The role of exact exchange. *J. Chem. Phys.* **98** (7), 5648–5652 (1993)
59. Krishnan, R., Binkley, J.S., Seeger, R., Pople, J.A.: Self-consistent molecular orbital methods. XX. A basis set for correlated wave functions. *J. Chem. Phys.* **72**, 650–654 (1980)
60. Jónsson, H.: Simulation of surface processes. *Proc. Natl. Acad. Sci. U. S. A.* **108**, 944–949 (2011)
61. Gallup, G.A., Fabrikant, I.I.: Vibrational Feshbach resonances in dissociative electron attachment to uracil. *Phys. Rev. A* **83**, 012706-1–012706-7 (2011)
62. Greisch, F., Gabelica, V., Remacle, F., De Pauw, E.: Thermometer ions for matrix-enhanced laser desorption/ionization internal energy calibration. *Rapid Commun. Mass Spectrom.* **17**, 1847–1854 (2003)
63. Luo, G., Marginean, I., Vertes, A.: Internal energy of ions generated by matrix-assisted laser desorption/ionization. *Anal. Chem.* **74**, 6185–6190 (2002)
64. Almeida, D., Kinzel, D., Ferreira da Silva, F., Puschnigg, B., Gschliesser, D., Scheier, P., Denifl, S., Garcia, G., González, L., Limão-Vieira, P.: N-site demethylation in pyrimidine bases as studied by low energy electrons and ab initio calculations. *Phys. Chem. Chem. Phys.* **15**, 11431–11440 (2013)
65. Denifl, S., Zappa, F., Mauracher, A., Ferreira da Silva, F., Bacher, A., Echt, O., Märk, T.D., Böhme, D.K., Scheier, P.: Dissociative electron attachment to DNA bases near absolute zero temperature: freezing dissociation intermediates. *Chem. Phys. Chem.* **9**, 1387–1389 (2008)

#### 4.1.2. Dissociative electron attachment to dimethyl disulphide

A part from the DNA constituents, many other biomolecules are also interest of investigation concerning radiation damage studies. Sulphur containing compounds are examples of that. They are not only intrinsic constituents of essential biological compounds, *e.g.* amino acids and proteins; they are also compounds that play an important role in Earth's atmospheric chemistry [23-25], ocean and soil chemistry [26].

Figure 4.7, shows a representation of dimethyl disulphide ( $C_2H_6S_2$ , DMDS) molecule that was investigated by DEA experiments within the scope of this thesis. This molecule is one of the most widespread sulphur pollutants [27], and can be seen as a model system for the study of covalent disulphide bonds [26].

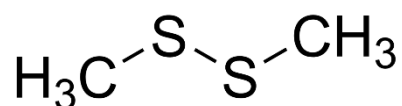


Figure 4.7 - Schematic drawing of a dimethyl disulphide. From [28].

As mentioned previously, the interaction of high-energy particles with biological matter creates secondary low-energy electrons that will interact with the physiological medium. This interaction does not resume itself to the interaction with DNA. The secondary electrons produced from the high-energy primary radiation can also interact and even fragment proteins. Proteins are very important constituents of a cell. They are the cell building blocks and carry out almost all cell functions [29]. Proteins are formed by polymers of amino acids, which are linked by peptide bonds ( $-CO-NH-$ ) and in a few cases by disulphide bonds ( $-S-S-$ ) [27]. Depending on the protein function in the body, they can be defined as: structural, signalling, gene regulatory, transport, enzymes and receptor. Some proteins are responsible for the replication of DNA. In order to occur cell replication the DNA contained in a cell has to be duplicated. As discussed before, if the DNA suffers some damages (*e.g.* single and double strand breaks) it can lead to cell mutation or death [9]. It is, however, possible for a cell to correct mistakes that occurred during DNA replication. Nevertheless, an abnormal correction or miscopying can be devastating for a cell. Thus, by damaging these proteins it may lead to their inhibition or to the change of their specific functionality. This can translate into malfunctions and misfoldings, that depending on the protein will have serious consequences in the physiological medium [27].

Hence, proteins can be a source of reactive radicals that may interact with the nearby DNA, provoking some damages [27].

The study of the disulphide bond is an important subject since its activation has been recognised as having a substantial role in biochemical processes that are connected to stabilising structures of some proteins [30]. The cellular functions [31,32] differ according to the disulphide-reduced against disulphide-oxidized forms of the disulphide containing peptides [33]. Disulphide redox systems have been acknowledged as being fundamental processes in cellular life. They regulate the cell growth and proliferation [31] and cancer development [32]. So any additional study, either theoretical or experimental, in particular of low-energy interactions with molecules with a sulphur-sulphur chemical bond is of the most importance to fully understand the underlying molecular mechanisms involved in these processes.

In the following publication the interest relied in how low-energy electrons interact with DMDS. DEA experiments have been performed to dimethyl disulphide by means of a crossed electron beam apparatus and anion efficiency curves of the formed fragments have been measured in the electron energy range from  $\sim 0 - 15$  eV.

Previous DEA experiments to  $C_2H_6S_2$  have been already performed by Modelli *et al.* [34]. In this study they report the presence of three fragment anions:  $CH_2S^-$  (46 u),  $CH_3S^-$  (47 u),  $CH_3S_2^-$  (79 u). In their experiments a quadrupole mass spectrometer was used to obtain negatively charged fragments upon electron capture. In a later work, Modelli and co-workers [35] focused on the importance of  $\sigma^*$  shape resonances involving the S–C and S–S antibonding orbitals in low-energy electron transmission spectroscopy experiments.

Comparing the present work and the previous by Modelli *et al.* [34], the most obvious difference is the experimental set-up and the electron source used. While in the present study a standard electron source was used, in Modelli *et al.* [34] work it was used a monochromator. A monochromator allows to cut out a small width of the broad energy distribution obtained by a filament heating. In the end this will lead to a FWHM in the range of few meV. As said previously (in the experimental set-up chapter 3.1.2), in the present study the electron beam used has a FWHM of 1 eV, while with the monochromator that Modelli *et al.* [34] used it was possible to achieve a resolution of 100 meV. Thus, although with the resolution obtained in the present work, the higher electron current allowed to gain better sensitivity – which allowed to detect other fragment anions that were not possible to detect in Modelli's *et al.* [34] work. In the present work eight fragment

## *Results and discussion*

anions were detected and measured as a function of the incident electron energy. From those eight fragments, five are being reported for the first time. In both studies, the by far dominant signal is assigned to the formation of  $\text{CH}_2\text{S}^-$ , which represents the break in half of a dimethyl disulphide molecule and the loss of a hydrogen atom.

The contribution presented below includes experimental results as well as thermochemical calculations that helped to identify the possible reaction pathways.



## Low-energy electron interactions with dimethyl disulphide

C. Matias<sup>a</sup>, A. Mauracher<sup>a</sup>, P. Scheier<sup>a</sup>, P. Limão-Vieira<sup>b,\*</sup>, S. Denifl<sup>a,\*</sup><sup>a</sup> Institut für Ionenphysik und Angewandte Physik and Center of Molecular Biosciences Innsbruck, Universität Innsbruck, Technikerstr. 25, A-6020 Innsbruck, Austria<sup>b</sup> Laboratório de Colisões Atômicas e Moleculares, CEFITEC, Departamento de Física, Faculdade de Ciências e Tecnologia, Universidade Nova de Lisboa, 2829-516 Caparica, Portugal

## ARTICLE INFO

## Article history:

Received 20 March 2014

In final form 6 May 2014

Available online 13 May 2014

## ABSTRACT

Electron attachment experiments have been performed with dimethyl disulphide, C<sub>2</sub>H<sub>6</sub>S<sub>2</sub>, in the gas phase by means of a crossed electron-molecular beam experiment. Ion yields for 8 anions have been measured in the energy range from ~0 to 15 eV. Many of the dissociative electron attachment products observed at low energy arise from surprisingly complex reactions associated with multiple bond cleavages as well as structural and electronic rearrangement. Quantum chemical calculations on the electronic properties of C<sub>2</sub>H<sub>6</sub>S<sub>2</sub> have been performed in order to complement the experimental investigations.

© 2014 Elsevier B.V. All rights reserved.

## 1. Introduction

Several studies concerning the role of sulphur containing molecular species in the field of atmospheric chemistry have been reported (e.g. see Refs. [1–3] and references therein), whilst disulphide bond activation has been identified as relevant within the context of biochemical processes closely related to the stabilizing role on the structure of several proteins [4]. Within the disulphide containing peptides, conformational structures vary according to the disulphide-reduced against disulphide-oxidized forms [5], which in turn means different cellular functions [6,7]. Reduction processes have been identified as crucial in biological systems, i.e. any additional theoretical and experimental studies will allow to fully understand the underlying molecular mechanisms of such processes. Here we are particularly interested in the role of resonant low-energy electron attachment to bare dimethyl disulphide (DMDS) molecules.

Dissociative electron attachment (DEA) experiments to DMDS yielding three fragment anions, namely CH<sub>2</sub>S<sup>-</sup> (46 u), CH<sub>3</sub>S<sup>-</sup> (47 u), CH<sub>3</sub>S<sub>2</sub><sup>-</sup> (79 u) have been performed by Modelli et al. [8]. All fragments observed were formed in a single resonance below the electron energy of 1 eV. The by far dominant signal can be assigned to SCH<sub>2</sub> formation. In a later study they further reported on the role of  $\sigma^*$  shape resonances involving S–C and S–S antibonding levels in low-energy electron transmission spectroscopy experiments [9]. Rydberg electron-transfer spectroscopy and quantum chemical calculations on a series of saturated disulphides have shown nondissociative electron transfer at 0.2 eV [10]. Recent

multireference calculations on DMDS revealed that in the ground state the extra electron occupies the  $\sigma^*(\text{S–S})$  molecular orbital (MO) and upper in energy, there are two states at 202 and 210 kJ mol<sup>-1</sup> (2.094 and 2.176 eV, respectively) whose singly occupied molecular orbitals are linear combinations of two non-bonding 3p-orbitals on each of the sulphur atoms [11]. These authors also point out evidence of another state at 278 kJ mol<sup>-1</sup> (2.881 eV) where the unpaired electron is mainly located in the  $\sigma(\text{S–S})$  MO.

In the present work we investigate the negative ion formation upon electron attachment to dimethyl disulphide at low energies (~0–15 eV). In the study by Modelli et al. [8] negatively charged fragments formed upon electron capture to DMDS were analysed with a quadrupole mass spectrometer, while in the present study we utilized a two-sector-field mass spectrometer. We note that the energy resolution in the previous experiment was substantially higher (~50 meV compared to ~1 eV in the present work); however due to the higher electron current used here we gain sensitivity, which allows us to detect other fragment anions that have not been detected before. In the present work five out of eight measured fragments are reported for the first time.

## 2. Experimental and quantum chemical calculations

A two-sector-field mass spectrometer equipped with a standard Nier-type ion source was used in the present study. The electron energy spread is about 1 eV (FWHM). The electron current is regulated to 10  $\mu\text{A}$ , which is reached for electron energies higher than 2 eV. A voltage drop of 6 kV is accelerating the ions to the sector fields. A liquid sample of DMDS, purchased from Sigma–Aldrich with a stated purity of >99%, was used for the present measurements. The sample was degassed by a repeated freeze–pump–thaw

\* Corresponding authors. Fax: +351 21 294 85 49 (P. Limão-Vieira), +43 512 507 2932 (S. Denifl).

E-mail addresses: [plimaovieira@fct.unl.pt](mailto:plimaovieira@fct.unl.pt) (P. Limão-Vieira), [Stephan.Denifl@uibk.ac.at](mailto:Stephan.Denifl@uibk.ac.at) (S. Denifl).

<http://dx.doi.org/10.1016/j.cpllett.2014.05.016>

0009-2614/© 2014 Elsevier B.V. All rights reserved.

cycle prior to the experiments. During measurements the sample was kept at room temperature. The effusive molecular beam (capillary orifice with 1 mm diameter) was crossed at an angle of  $60^\circ$  with the electron beam. The electron energy resolution and calibration were obtained by measuring the resulting ion yields as function of the electron energy for  $SF_6^-$ ,  $F^-$ , and  $F_2^-$  upon electron attachment to  $SF_6$  [12]. After mass selection in the magnetic sector field the ions pass a 1.4 m long field-free region before entering the electrostatic sector field. For the present investigation the mass resolution was kept at a minimum value of about  $m/\Delta m \sim 1000$  by opening all slits to their maximum. The anions are detected with a channel electron multiplier operated in a pulse counting mode. Mass spectra were recorded at different electron energies and for all anions, identified as products of dissociative electron attachment to dimethyl disulphide, anion efficiency curves from  $\sim 0$  to 15 eV were measured.

For a better interpretation of the experimental findings, we carried out quantum chemical calculations on the electronic properties of DMDS. Full geometry optimization was achieved by employing MP2 perturbation theory in combination with Dunning's correlation consistent triple- $\zeta$  basis set augmented with diffuse functions (aug-cc-pVTZ). Adiabatic electron affinities and reaction thresholds were determined by employing various extrapolation schemes. We compare the results of G4(MP2) [13], CBS [14], W1 [15] and W1BD [16], which are all considered being highly accurate. The most accurate results are obtained with the W1BD method, which yields a root-mean-square deviation from the experiment of  $(0.62 \pm 0.48) \text{ kcal mol}^{-1}$ , i.e.  $(26.886 \pm 20.815) \text{ meV}$ , in the G2/97 test set [16]. We find that all schemes yield very similar results. In Table 1 we list the reaction thresholds of all species involved, while in Table 2 we list the electron affinities. For the reaction thresholds listed in Table 1 we assumed the most simple single bond cleavages. These reaction thresholds can be lowered in case more stable neutral complexes are formed which will be discussed in the next section. The GAUSSIAN 09 C.01 suite of programs was employed to carry out the calculations [17].

### 3. Results and discussion

The ion efficiency curves of eight anions presently observed from dissociative electron attachment to dimethyl disulphide are shown in Figures 1–3. Five of them are reported for the first time. The possible chemical compositions of the fragment anions observed and their corresponding resonance positions are listed in Table 3.

Before measuring the ion efficiency curves mass scans were also performed at electron energies between  $\sim 0$  and 10 eV. For

**Table 1**  
Reaction thresholds calculated using various high-level extrapolation schemes. See text for further explanations.

$H_3CS_2CH_3 + e^- \rightarrow$	Reaction threshold (eV)			
	G4(MP2)	CBS	W1	W1BD
$H_3CS_2CH_3$	0	0	0	0
$H_3CS_2CH_2 + H$	2.33	2.38	2.46	2.46
$H_3CS_2CH + 2H$	6.76	6.44	6.53	6.55
$H_2CS_2CH_2 + 2H$	6.31	6.34	6.42	6.45
$CH_3S_2 + CH_3$	0.70	0.70	0.72	0.72
$CH_2S_2 + CH_3 + H$	4.43	4.45	4.46	4.46
$CHS_2^- + CH_3 + 2H$	7.28	7.38	7.43	7.43
$S_2 + 2CH_3$	2.86	2.85	2.86	2.87
$CH_3S^- + SCH_3$	0.88	0.88	0.90	0.90
$CH_2S^- + SCH_3 + H$	4.41	4.41	4.45	4.45
$SH^- + SCH_3 + CH_2$	4.65	4.32	4.63	4.64
$S^- + SCH_3 + CH_3$	3.81	3.79	3.78	3.78

**Table 2**  
(Adiabatic) Electron affinities for the molecular fragments forming anions observed in the experiment using various high-level extrapolation schemes. See text for further explanations.

	(Adiabatic) Electron affinity (eV)			
	G4(MP2)	CBS	W1	W1BD
$H_3CS_2CH_3$	0.18	0.20	0.08	0.08
$H_3CS_2CH_2$	1.69	1.73	1.63	1.63
$H_3CS_2CH$	0.65	1.04	1.02	1.00
$H_2CS_2CH_2$	1.19	1.24	1.20	1.17
$CH_3S_2$	1.76	1.81	1.78	1.77
$CH_2S_2$	1.04	1.09	1.12	1.13
$CHS_2$	3.08	2.98	2.86	2.87
$S_2$	1.70	1.70	1.66	1.67
$CH_3S$	1.86	1.90	1.87	1.87
$CH_2S$	0.46	0.50	0.51	0.51
$SH$	2.32	2.37	2.35	2.35
$S$	2.04	2.09	2.08	2.08

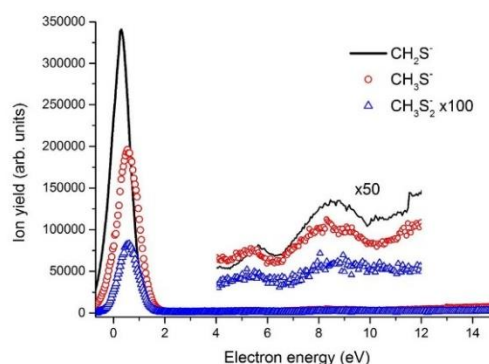


**Figure 1.** Anion efficiency curves for the most intense anions formed upon dissociative electron attachment to dimethyl disulphide assigned to  $CH_2S^-$  (black solid line),  $CH_3S^-$  (red circles) and  $CH_3S_2^-$  (blue triangles), respectively. (For interpretation of the references to colour in this figure legend, the reader is referred to the web version of this article.)

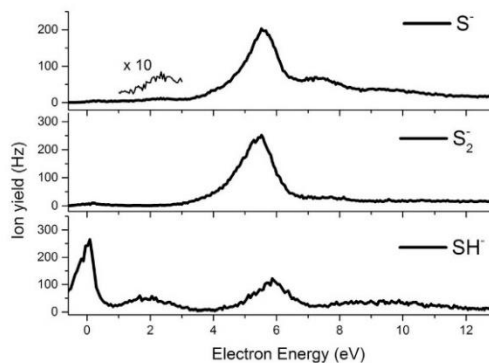


**Figure 2.** Anion efficiency curves of the fragment ions  $S^-$  (upper panel),  $S_2^-$  (middle panel),  $SH^-$  (lower panel), respectively.



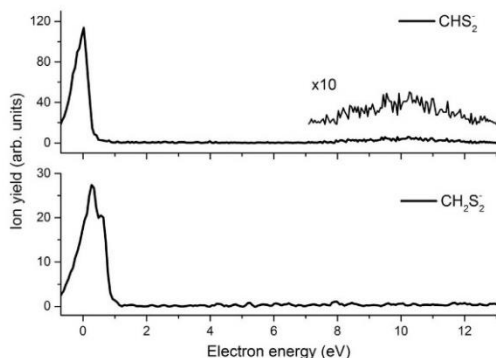


Figure 3. Anion efficiency curves of  $\text{CHS}_2$  (upper panel) and  $\text{CH}_2\text{S}_2$  (lower panel).

Table 3

Peak positions for all anions of dimethyl disulphide obtained in the present experiment compared to previous studies [8].

Mass (u)	Assignment	Peak position (eV)	[8]
79	$\text{CH}_2\text{S}_2^-$	0.6	5.1
78	$\text{CH}_2\text{S}_2^-$	0.3	9.2
77	$\text{CHS}_2^-$	0 <sup>a</sup>	10.0
64	$\text{S}_2^-$	0.2 <sup>a</sup>	5.4, 7.3
47	$\text{CH}_3\text{S}^-$	0.7	3.8, 5.3
46	$\text{CH}_2\text{S}^-$	0.3	3.7, 5.6
33	$\text{SH}^-$	0 <sup>a</sup>	1.9, 5.8
32	$\text{S}^-$	0.5 <sup>a</sup>	2.4, 5.5, 7.2

<sup>a</sup> This resonance is due to thermal decomposition (see text).

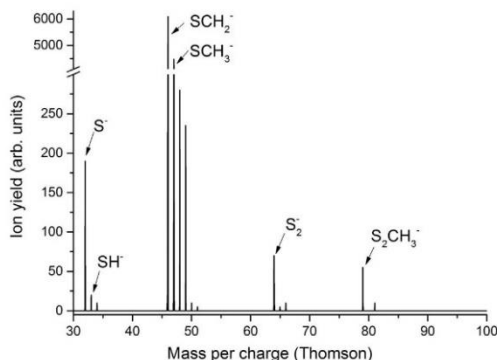


Figure 4. Mass spectrum obtained at the electron energy of 6 eV. The ion peaks are labelled according to their chemical composition. For further details see text.

illustration we show in Figure 4 a mass spectrum recorded at the electron energy of 6 eV. Anions are formed in high abundance at this energy and relative intensities can be compared. For the mass scan recorded at the electron energy close to 0 eV comparatively weak ion yields (around 1% of the anion  $\text{CH}_2\text{S}_2^-$ ) at masses 92 u, 93 u and 94 u are present. At a first glance, these masses were thought to correspond to anions resulting from electron attachment to dimethyl disulphide, i.e. to the fragments  $(\text{M}-2\text{H})^-$ ,  $(\text{M}-\text{H})^-$ , and the parent  $(\text{M})^-$ , respectively. If the formation of the non-dissociated molecular ion would be observable, it would

comprise the energy of the incoming electron and the electron affinity of the molecule, which could have resulted in a statistical intramolecular rearrangement delaying autodetachment [18]. The calculated adiabatic electron affinity of DMDS at W1BD level of theory is 0.08 eV (electronic and zero point energy), which is associated with a noticeable change in the S–S bond length from 2.06 Å to 2.92 Å. Moreover, both C–S–S angles change from 103.6° to ~92° by adding an additional electron. MP2/aug-cc-pVTZ yields a similar adiabatic electron affinity of 0.03 eV and a vertical detachment energy of 1.64 eV which is in good agreement with the experimental value of 1.75 eV [10]. However, the isotope pattern in the recorded mass spectra did not match any of the fragment anions proposed as well as the parent anion. In the latter case the ion yield at 94 u hence cannot be assigned to the parent anion. In addition, all of these anions showed a resonance around 0.6 eV. The comparison with the thresholds obtained in the present calculations (see Table 1) leads to the conclusion that the formation of  $(\text{M}-2\text{H})^-$  and  $(\text{M}-\text{H})^-$  is energetically not possible at the experimentally observed energies. In the calculation of the  $(\text{M}-2\text{H})^-$  reaction threshold we calculated two cases, (i) removal of the two hydrogen atoms from one methyl-group and (ii) removal of one hydrogen atom from both methyl-groups. In the latter case the threshold is 6.45 eV, which is 0.10 eV lower than the threshold to remove the hydrogen atoms from the same methyl-group. These reaction thresholds are lowered in case a hydrogen molecule is formed (binding energy of  $\text{H}_2$  is 4.48 eV, obtained with W1BD). Nevertheless the threshold energies values still show a discrepancy with the experimental observations (~0.6 eV) and the same occurs in the case of a dehydrogenated parent  $(\text{M}-\text{H})^-$ , where the calculations indicate an endothermic reaction with a thermodynamic threshold of 2.46 eV (W1BD energies). Hence the experimental appearance energies of these fragments are a second indication (in addition to the isotope pattern) that the presence of ion yield at these three masses is due to an unknown impurity in the gas inlet.

The fragmentation patterns observed can be classified into three different groups according to their structural similarities: (1) *Fragment anions*  $\text{CH}_n\text{S}_2^-$  – this group comprises masses 77 u ( $\text{CHS}_2^-$ ), 78 u ( $\text{CH}_2\text{S}_2^-$ ), 79 u ( $\text{CH}_3\text{S}_2^-$ ); (2) *Fragment anions*  $\text{CH}_n\text{S}^-$  – includes masses 46 u and 47 u that correspond to  $\text{CH}_2\text{S}^-$  and  $\text{CH}_3\text{S}^-$ , respectively, which are by far the most dominant fragment anions. The last group (3) *Fragment anions*  $\text{S}_2^-$ ,  $\text{SH}^-$ ,  $\text{S}^-$  – incorporates masses 64 u, 33 u and 32 u, respectively.

### 3.1. Ion efficiency curves

The formation of  $\text{CH}_2\text{S}_2^-$  (mass 78 u) ion is just restricted to a feature close to 0.3 eV, while all other fragment ions show more extended resonance profiles (see Table 3). This can be due to the fact that even the 0.3 eV resonance of  $\text{CH}_2\text{S}_2^-$  has a very weak yield (~1%) compared to the most intense resonances of other fragment anions. Hence any  $\text{CH}_2\text{S}_2^-$  signal at higher electron energies may be below the detection limit of the apparatus.

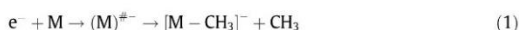
Within the variety of resonance structures in the entire energy range from 0 to 15 eV the anion intensity of most of the fragments is concentrated within three energy regions, in the range below 2, 4–6 and 6–10 eV. For example, the shape and position for the resonances of  $\text{S}^-$  and  $\text{S}_2^-$  fragments are very similar, which indicate that these anions may have common precursor transient anion states. Another group of anions that show a similar behavior are  $\text{CH}_2\text{S}^-$ ,  $\text{CH}_3\text{S}^-$  and  $\text{CH}_3\text{S}_2^-$ , which exhibit comparable values for the resonances, both at lower and higher electron energies.

The temporary negative ions (TNIs) generated at low energy (<2 eV) can be assigned as shape resonances involving  $\sigma^*$  antibonding orbitals. Modelli et al. [8] calculated that the lowest  $\sigma^*$  antibonding orbital of the (S–S) bond is at 1.04 eV, which is in good

agreement with our experimental results. Also, it is likely that the resonances at higher energies can be characterized as core-excited resonances with possible contributions of high-energy shape resonances. The states mentioned in the introduction at 2.094, 2.176 and 2.881 eV [11] may not be involved in the anion formation, since the resonances appear at substantial higher energies.

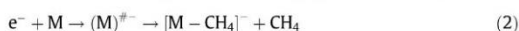
### 3.1.1. Fragment anions $CH_nS_2^-$ , $n = 1, 2, 3$

The resonance structures of these fragment anions are shown in Figure 1 ( $CH_3S_2^-$ , blue triangles) and Figure 3 ( $CH_2S_2^-$ , lower panel, and  $CHS_2^-$ , upper panel) with their energy positions listed in Table 3.  $CH_3S_2^-$  ion formation most probably proceeds via the following reaction:

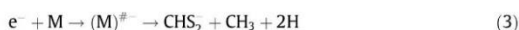


The  $CH_3S_2^-$  fragment anion (79 u) has been reported previously by Modelli et al. [8] with a single resonance feature peaking at 0.8 eV, in good agreement with the present experiment albeit the present modest electron energy resolution of  $\sim 1$  eV. The resonances observed at 9.2 and 10 eV for  $CH_3S_2^-$  and  $CHS_2^-$ , respectively, (Table 3) can be assigned likely to electronically excited TNI states (including Rydberg excitation), which may decompose via one fragment anion plus one or more neutrals. Taking W1BD energy values of the products and reactant, reaction (1) is endothermic by 0.72 eV, which corresponds to the experimental value, bearing in mind the current electron energy resolution. The intensities of the ion yields at 80 and 81 u are within the expected isotope ratio relative to 79 u.

The  $CH_2S_2^-$  fragment anion (78 u) has a calculated threshold formation of 4.46 eV. However if its formation proceeds through the formation of  $CH_4$ , the threshold is lowered by 4.48 eV (binding energy of H to  $CH_3$ ). Therefore the reaction will be slightly exothermic by 0.02 eV, obtained with a W1BD level of theory. This result matches with the experimental data obtained, where we find the peak at the electron energy of 0.3 eV. Hence, we propose that the formation of the fragment anion  $CH_2S_2^-$  proceeds through:



Concerning the fragment anion  $CHS_2^-$  (77 u), we ascribe the first peak close to 0 eV to form by electron attachment to thermal decomposition products of DMDS. The latter are likely generated in reactions of DMDS with the heated surfaces of the ion source or the hot filament. The calculated threshold indicates formation only above 7.43 eV, which is in agreement with the resonance observed at 10 eV. At this electron energy, the fragment anion is formed by cleavage of one S–C bond and the additional break of two H–C bonds in the fragment carrying the excess charge:



We note that another indication of thermal decomposition was the increase of the relative height of the 0 eV peak when the ion source temperature was raised. Analogous behavior was observed for the near 0 eV peak of  $S_2^-$ ,  $SH^-$  and  $S^-$ , i.e. we expect thermal decomposition of the neutral before electron capture to be involved in the formation of these resonances (see below).

### 3.1.2. Fragment anions $CH_nS^-$ , $n = 2, 3$

$CH_2S^-$  and  $CH_3S^-$  are by far the most dominant fragment anions in DEA to dimethyl sulphide. The resonances yielding  $CH_3S^-$  and  $CH_2S^-$  ions are listed in Table 3 and shown in Figure 1. The formation of these anions has been reported before but restricted to a low energy resonance peaking at 0.86 and 0.67 eV, respectively [8]. We observe reasonable agreement with this previous work concerning these low energy resonances, since we obtain a peak at 0.7 eV for  $CH_3S^-$  and 0.3 eV for  $CH_2S^-$ . In addition we observe

other resonance features at higher electron energies ( $>4$  eV). The formation of these anions requires the cleavage of the S–S bond and C–H bonds in the precursor ion, where such mechanism is remarkable at low incident electron energies. Interesting to note is that in  $CH_3S^-$  the excess electron is localized at the S atom (Figure 5C, left panel), whereas for  $CH_2S^-$  the MO 13 is mainly  $\pi^*(S=C)$  in character, which is delocalized over the whole fragment (Figure 5C, middle panel). This may explain the higher anionic yield for this fragment. For  $CH_2S^-$  the relative percentage of the isotope at 48 u to 46 u is 4.4% and the measured one is 4.4%, and for  $CH_3S^-$  the relative percentage of 49 u to 47 u is 4.4% and the measured one is 4.2%, i.e. both are in good agreement. The reaction yielding  $CH_3S^-$  formation is endothermic with a calculated threshold at 0.90 eV which is in reasonable good agreement with the experimental value. The threshold for  $CH_2S^-$  formation is 4.45 eV. Assuming that a neutral  $HSCH_3$  complex is formed, this reaction value is lowered by 3.72 eV (binding energy obtained at W1BD), which is in agreement with the present experimental results.

### 3.1.3. Fragment anions $S_2^-$ , $SH^-$ and $S^-$

The DEA anionic yields for  $S^-$  and  $S_2^-$  are shown in Figure 2; the observed resonance positions are listed in Table 3. Both fragment anions do not exhibit any abundant low energy resonance ( $<4$  eV), since the weak feature close to 0 eV (which is more evident for  $S_2^-$ ) is attributed to an artefact (thermal decomposition) as mentioned above. The relative percentages of 32 u:34 u and 64 u:66 u are approximately 4.3% and 10.6%, respectively, matching very well the natural abundance. The sulphur anion  $S^-$  is formed by cleavage of S–S and S–C bonds in the target molecule, whilst  $S_2^-$  results from the breaking of the two S–C bonds. The calculated threshold energies for the formation of  $S^-$  and  $S_2^-$  are 3.78 eV and 2.87 eV, respectively. The calculated threshold value for  $S_2^-$  fits with the presence of a resonance at 5.4 eV obtained in the present experiment. For the calculated value mentioned only simple bond cleavages are considered and no formation of any new neutral complexes. Instead, in the case of neutral  $CH_3SCH_3$  formation the binding energy of 3.13 eV is gained and thus the formation of  $S^-$  has an energy threshold of 0.65 eV (W1BD level of theory). This value agrees with the experimental results obtained for the first resonance of  $S^-$  (2.4 eV). The calculated threshold value at 3.78 eV may be assigned to the second resonance of  $S^-$  located at 5.5 eV.

The anion  $SH^-$  (33 u) shows a low energy resonance close to 0 eV (see Figure 2), which we ascribe to thermal decomposition, and three other less intense features at 1.9, 5.8 and 9.3 eV.  $SH^-$  results from the cleavage of several bonds (S–S, S–C and C–H) and intramolecular H atom transfer. The present calculations show that the singly occupied molecular orbital of the anion has a node in the S–H bond with the extra charge sitting at the sulphur atom (Figure 5C, right panel). The lowest calculated energetic threshold for  $SH^-$  formation is 0.76 eV assuming that a neutral  $H_2CSCH_3$  complex is formed. In case that neutral  $CH_3$  and  $SCH_2$  are formed the threshold value increases to 2.08 eV, which, though in fair agreement, may be assigned to the resonance obtained at 1.9 eV. The reaction involving neutral  $CH_2$  and  $SCH_3$  formation has the highest threshold of 4.64 eV, which can be ascribed to the presence of a measured resonance at 5.8 eV.

## 4. Conclusions

In the present DEA study with dimethyl disulphide anionic yields have been measured in the electron energy range of  $\sim 0$ –15 eV. In total, eight fragments were observed through the DEA process within the sensitivity limit of the apparatus. From all the fragments detected, five fragment anions have been detected

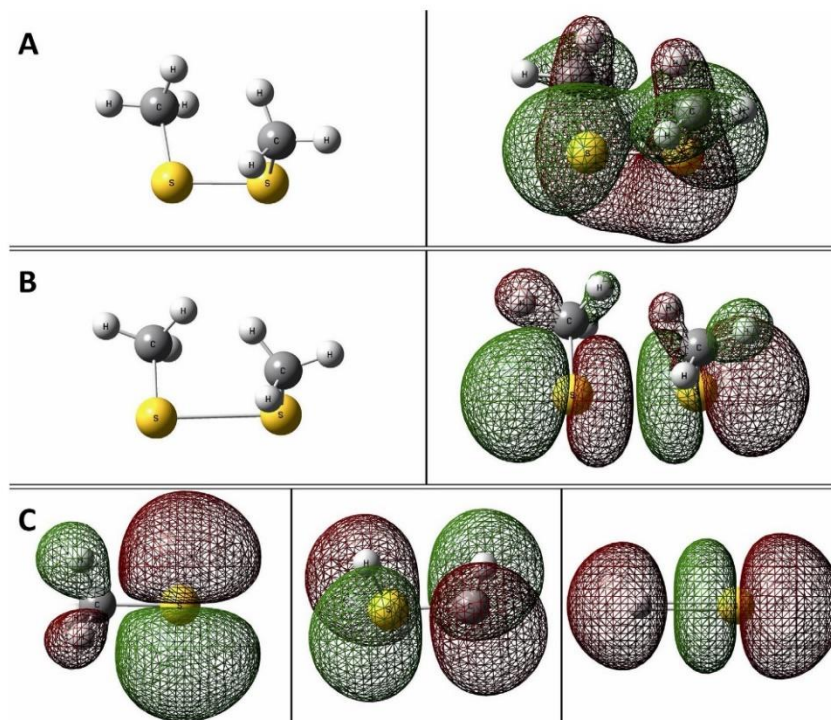


**Figure 5.** Optimized structures depicted for dimethyl disulphide as neutral (A left panel) and negatively charged (B left panel) molecule. Shown are also the highest occupied molecular orbital of the neutral molecule (A right panel, MO 25) and the singly occupied molecular orbital of the anion (B right panel, MO 26). The highest occupied molecular orbitals for  $\text{CH}_3\text{S}^-$  (C left panel, MO 13), for  $\text{CH}_2\text{S}^-$  (C middle panel, MO 13) and for  $\text{SH}^-$  (C right panel, MO 10) are shown as well. All results were obtained at MP2/aug-cc-pVTZ level of theory.

for the first time in comparison to previous DEA studies with  $\text{C}_2\text{H}_6\text{S}_2$ . For the three previously reported fragment anions ( $\text{CH}_2\text{S}^-$ ,  $\text{CH}_3\text{S}^-$ ,  $\text{CH}_3\text{S}_2^-$ ) we observe good agreement in the peak positions  $<1$  eV. Furthermore, we observe here that the DEA mechanism is also operative at higher electron energies leading to these anions. With the support of the quantum chemical calculations it was possible to assign the chemical composition of neutral and negatively charged fragments to the different resonances experimentally observed. We obtain a good agreement between the values derived upon WIBD and the experimental data.

#### Acknowledgements

This work has been supported by the Fonds zur Förderung der wissenschaftlichen Forschung (FWF Project No. P22665), Wien, the European Commission, Brussels, via COST Action MP1002 programme Nanoscale Insights into Ion Beam Cancer Therapy (Nano-IBCT), the Austrian Ministry of Science BMWF as part of the Konjunkturpaket II and as part of the UniInfrastrukturprogramm of the Focal Point Scientific Computing at the University of Innsbruck. A.M. acknowledges a Grant from the Nachwuchsförderung of the University of Innsbruck. PL-V acknowledges partial funding from the research Grants PEst-OE/FIS/UI0068/2014 and PTDC/FIS/ATO/1832/2012.

#### References

- [1] V. Aquilanti, M. Ragni, A.C.P. Bitencourt, G.S. Maciel, F.V. Prudente, *J. Phys. Chem. A* 113 (2009) 3804.
- [2] P. Limão-Vieira, S. Eden, P.A. Kendall, N.J. Mason, S.V. Hoffmann, *Chem. Phys. Lett.* 366 (2002) 343.
- [3] E.A. Drage, P. Cahillane, S.V. Hoffmann, N.J. Mason, P. Limão-Vieira, *Chem. Phys.* 331 (2007) 447.
- [4] S.D. Dai, C. Schwendtmayer, P. Schurmann, S. Ramaswamy, H. Eklund, *Science* 287 (2000) 655.
- [5] G.A. Rickard, J. Bergès, C. Houë-é-Levin, A. Rauk, *J. Phys. Chem. B* 112 (2008) 5774.
- [6] H. Nakamura, K. Nakamura, J. Yodoi, *Annu. Rev. Immunol.* 15 (1997) 351.
- [7] A. Baker, C.M. Payne, M.M. Briele, G. Powis, *Cancer Res.* 57 (1997) 5162.
- [8] A. Modelli, D. Jones, G. Distefano, M. Tronc, *Chem. Phys. Lett.* 181 (1991) 361.
- [9] C. Dezarnaud-Dandine, F. Bournel, M. Tronc, D. Jones, A. Modelli, *J. Phys. B* 31 (1998) L497.
- [10] S. Carles et al., *J. Phys. Chem. A* 105 (2001) 5622.
- [11] J.A. Gámez, L. Serrano-Andrés, M. Yáñez, *Int. J. Quantum Chem.* 111 (2011) 3316.
- [12] M. Fenzlaff, R. Gerhard, E. Illenberger, *J. Chem. Phys.* 88 (1) (1988) 149.
- [13] L.A. Curtiss, P.C. Redfern, K. Raghavachari, *J. Chem. Phys.* 127 (2007) 124105.
- [14] J.A. Montgomery Jr., M.J. Frisch, J.W. Ochterski, G.A. Petersson, *J. Chem. Phys.* 112 (2000) 6532.
- [15] J.M.L. Martín, G. de Oliveira, *J. Chem. Phys.* 111 (1999) 1843.
- [16] E.C. Barnes, G.A. Petersson, J.A. Montgomery Jr., M.J. Frisch, J.M.L. Martín, *J. Chem. Theory Comput.* 5 (2009) 2687.
- [17] Gaussian 09, Revision C.01, M. J. Frisch, G. W. Trucks, H. B. Schlegel, G. E. Scuseria, M. A. Robb, J. R. Cheeseman, G. Scalmani, V. Barone, B. Mennucci, G. A. Petersson, H. Nakatsuji, M. Caricato, X. Li, H. P. Hratchian, A. F. Izmaylov, J. Bloino, G. Zheng, J. L. Sonnenberg, M. Hada, M. Ehara, K. Toyota, R. Fukuda, J. Hasegawa, M. Ishida, T. Nakajima, Y. Honda, O. Kitao, H. Nakai, T. Vreven, J. A. Montgomery, Jr., J. E. Peralta, F. Ogliaro, M. Bearpark, J. J. Heyd, E. Brothers, K.

## Results and discussion

- N. Kudin, V. N. Staroverov, R. Kobayashi, J. Normand, K. Raghavachari, A. Rendell, J. C. Burant, S. S. Iyengar, J. Tomasi, M. Cossi, N. Rega, J. M. Millam, M. Klene, J. E. Knox, J. B. Cross, V. Bakken, C. Adamo, J. Jaramillo, R. Gomperts, R. E. Stratmann, O. Yazyev, A. J. Austin, R. Cammi, C. Pomelli, J. W. Ochterski, R. L. Martin, K. Morokuma, V. G. Zakrzewski, G. A. Voth, P. Salvador, J. J. Dannenberg, S. Dapprich, A. D. Daniels, Ö. Farkas, J. B. Foresman, J. V. Ortiz, J. Cioslowski, and D. J. Fox, Gaussian Inc, Wallingford CT, 2009.
- [18] E. Illenberger, in: C.-Y. Ng (Ed.), *Advanced Series in Physical Chemistry*, Vol. 10B, World Scientific, Singapore, 2000, pp. 1063–1160.

## **4.2. Technologically relevant molecules**

Nowadays, globalization has allowed an unprecedented interchange and access to information, in particular with people easily moving around the globe. Such has also led to an increase in narcotics, explosives, biological or chemical warfare, etc. [36] trading, with an enhancement threatening in terrorism attacks. Several governments have implemented already tightly security measures (in particular in airports) for explosives' detection and several devices have been proposed to perform such identifications: laser photon ionisation [37,38], chemical ionization mass spectrometry [39,40], proton transfer reaction mass spectrometry [36,41] and negative ion mass spectrometry based on free electron capture [42,43] technics. However, currently the equipment most commonly used in the detection of such threatening agents is based on Ion Mobility Spectrometry (IMS) [44,45]. Until today none of the proposed detection methods are able of satisfying the needed requirements: high speed, high sensitivity and high selectivity [46]. During the last years, the Innsbruck group has actively participated in identifying the fragmentation patterns of several explosive targets through low-energy electron impact experiments. As so, and in order to keep obtaining relevant data on such chemical compounds, this thesis also addresses this issue.

Almost 250 explosives have been listed by the United States Bureau of Alcohol, Tobacco, and Firearms [46]. Explosives are characterised by having both reducing and oxidizing constituents [47] which enable these chemical compounds to show high reaction velocities [46]. In a normal combustion of hydrocarbons the reaction velocity is dependent on the presence of oxygen from air, which is in contrast with the explosives. Usually, explosives are mainly comprised by high electronegative compounds (e.g. nitrogen and oxygen), which act as oxidizing constituents, whereas the presence of carbon and hydrogen will act as the reducing constituents. Thus, the C:H:N:O weight elemental ratios have been used to categorize nitrogen based explosives [46]. In Table 4.1 a list of common explosives and their composition is shown.

With the increase of regulation and control against explosives and narcotics, the ways of smuggling these agents are more and more creative, and detecting them in low concentrations is still a challenge. Other issue related to detection relies on the capability to distinguish the dangerous compounds among several other similar yet non-dangerous substances. So, despite the relative success of the techniques referred above, there are

### Results and discussion

technical aspects that still need to be improved and several chemical compounds that are yet to be fully explored.

<b>Explosives Based on Nitrogen</b>	<b>Formula</b>	<b>wt % C</b>	<b>wt % H</b>	<b>wt % N</b>	<b>wt % O</b>	<b>Sum N + O</b>
<b>Ammonium nitrate (AN)</b>	$\text{H}_4\text{N}_2\text{O}_3$	0	5.04	35.01	59.97	94.98
<b>Ammonium picrate (Expl D)</b>	$\text{C}_6\text{H}_6\text{N}_4\text{O}_7$	29.28	2.46	22.76	45.5	68.26
<b>Cyclonite (RDX)</b>	$\text{C}_3\text{H}_6\text{N}_6\text{O}_6$	16.22	2.72	37.84	43.22	81.06
<b>Hexamethylenetriperoxide diamine (HMTD)</b>	$\text{C}_6\text{H}_{12}\text{N}_2\text{O}_6$	34.62	5.81	13.46	46.11	59.57
<b>Hexanitrohexaazaisowurtzitane (HMIW)</b>	$\text{C}_6\text{H}_6\text{N}_{12}\text{O}_{12}$	16.45	1.38	38.36	43.82	82.18
<b>Nitroglycerin (NG)</b>	$\text{C}_3\text{H}_5\text{N}_3\text{O}_9$	15.87	2.22	18.5	63.41	81.91
<b>Nitroazolone (NTO)</b>	$\text{C}_2\text{H}_2\text{N}_4\text{O}_3$	18.47	1.55	43.08	36.9	79.98
<b>Octogen (HMX)</b>	$\text{C}_4\text{H}_8\text{N}_8\text{O}_8$	16.22	2.72	37.84	43.22	81.06
<b>Pentaerythritol tetranitrate (PETN)</b>	$\text{C}_5\text{H}_8\text{N}_4\text{O}_{12}$	19	2.55	17.72	60.73	78.45
<b>Picric acid</b>	$\text{C}_6\text{H}_3\text{N}_3\text{O}_7$	31.46	1.32	18.34	48.88	67.22
<b>Trinitrobenzene (TNB)</b>	$\text{C}_6\text{H}_3\text{N}_3\text{O}_6$	33.82	1.42	19.72	45.05	64.77
<b>Trinitrotoluene (TNT)</b>	$\text{C}_7\text{H}_5\text{N}_3\text{O}_6$	37.02	2.22	18.5	42.26	60.76
<b>1,3,3-Trinitroazetidine (TNAZ)</b>	$\text{C}_3\text{H}_4\text{N}_4\text{O}_6$	18.76	2.1	29.17	49.98	79.15
<b>Urea nitrate</b>	$\text{CH}_5\text{N}_3\text{O}_4$	9.76	4.09	34.14	52	86.14

**Table 4.1– List of representative common nitrogen explosives. Adapted from [47].**

#### 4.2.1. Dissociative electron attachment to enflurane, isoflurane and chlorinated ethanes (pentachloroethane and hexachloroethane)

The present study focuses on the evaluation of possible dopants for the detection of explosives by IMS. As mentioned before, IMS is the most ordinary instrument to deal with the detection of explosive substances. This is due to the fact that IMS instruments have low detection limit, short response time and operate at ambient pressure [48]. The principle of operation of this equipment is based on the ions velocities. The velocity of an ion is proportional to the mobility coefficient, which in turn depends on the mass, shape and dimensions of the ion in study [49,50]. Hence for different ion velocities, different compounds are discriminated.

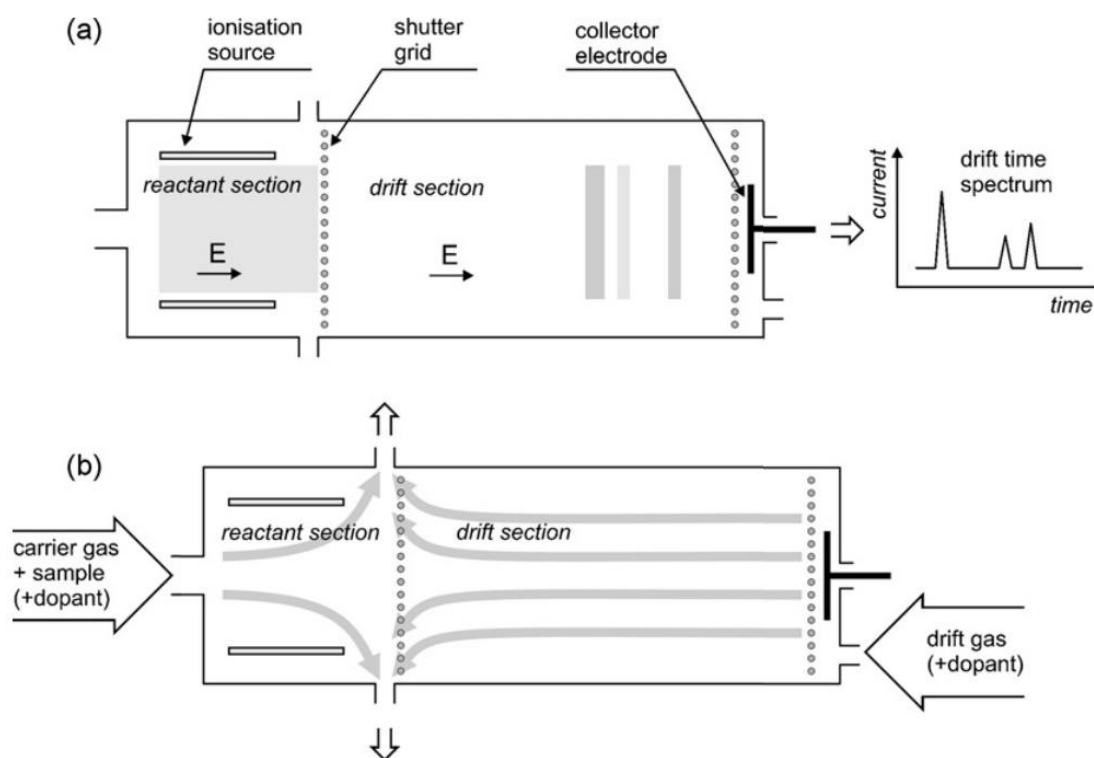
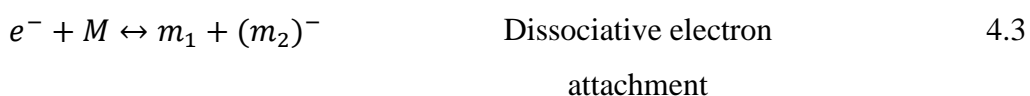


Figure 4.8 - Schematic drawing of an example of IMS. a) Principle of operation and b) the flow of gas inside an IMS apparatus. From [49].

In Figure 4.8, an example of an IMS apparatus is shown. Briefly, in order to introduce the sample into a IMS machine a carrier gas containing the neutral vapour of the sample is flown directly into the reactant region [51]. The ions are formed in the reactant section through complex and diverse cycles of ion-molecule reactions. The shutter grid allows the ions formed to be periodically introduced into the drift section [44]. Once in the

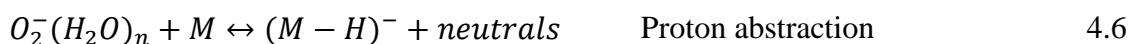
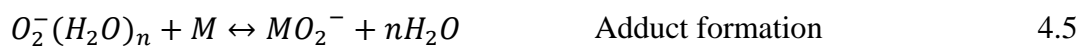
drift section the ionic products will be separated according to their mobility: heavier ions have low mobility reaching the collector electrode later than the lighter ions, which have higher mobility [49].

IMS is an instrument that allows the detection of positive and negative ions. Since explosives are usually composed by elements with high electronegativity, the usual polarity used in these studies is negative [44]. Depending on the carrier gas used, different reactions occur in the reactant section. If the carrier gas used is pure nitrogen, the following reactions are the main processes occurring:



$M$  represents the atom (or molecule), while  $m_1$  and  $m_2$  represent fragments of  $M$  in the case of a molecular target.

Another possibility is to use air as a carrier gas, where  $O_2^-(H_2O)_n$  are the dominant reagent anions produced:



Oxygen has a low electron affinity and so, depending on the differences in electron affinities, its reaction with a molecule frequently leads to low energy electron transfer processes [49]. One way of solving this problem is by adding a dopant to the carrier gas. A dopant is used with the aim of changing the ion-molecule chemistry occurring in the reactant section [49]. The dopant will preferentially ionise the sample, blocking possible signals from interfering substances (impurities) [49]. Thus, if the concentration of a dopant is high and the electron attachment rate coefficient is at, or close to, the maximum value, direct low-energy electron attachment can compete with that to  $O_2$ . This can allow to enhance the IMS selectivity and sensitivity [50,52].

In order to understand the role of dopants in the ion-molecule chemistry occurring in IMS systems, it is important to have a knowledge of the electron attachment properties.



Since the dopants used nowadays have been selected almost randomly, an understanding of the electron attachment properties of a dopant will probably be useful in the search of other compounds that can enhance the detection of a dangerous agent. A study resorting from DEA to possible dopants was performed, in order to obtain the knowledge of their electron attachment properties. This will provide evidence as to whether these molecules are good candidates as a dopant.

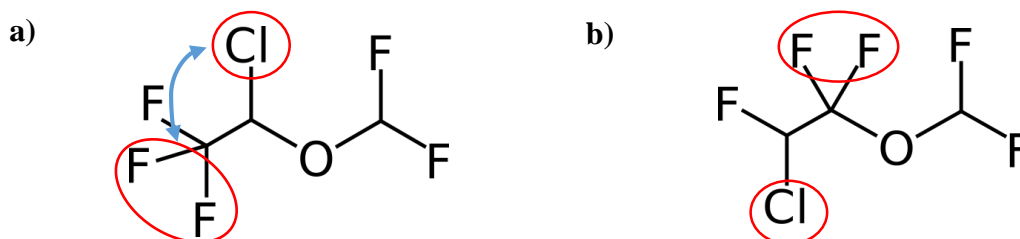


**Figure 4.9 - Schematic drawing of isoflurane a) and enflurane b). These two molecules are structural isomers. The position of two fluorine atoms are swapped with a chlorine and a hydrogen atoms, as pointed out in the figure. Adapted from [53,54].**

A typical explosive dopant will have a high electron detachment energy, which is the case of halogens. The halogen dopants (especially chloride) will enhance the detection of explosives [44] usually by creating monoatomic halide ions ( $MCl^-$ ) [49].  $Cl^-$  ions can be obtained by performing dissociative electron attachment to halogenated organic compounds [55]. In the paper presented below, results of a mass spectrometric study of DEA for electron energies between  $\sim 0 - 17$  eV to possible dopants in the gas phase under single collision conditions are discussed. Enflurane ( $CHFCl-CF_2-O-CF_2$ ), isoflurane ( $CF_3-CHCl-O-CHF_2$ ), pentachloroethane ( $C_2HCl_5$ ) and hexachloroethane ( $C_2Cl_6$ ) are the possible molecular dopants investigated (see Figure 4.9 and Figure 4.10). Enflurane and isoflurane belong to the group of halogenated ether compounds which have had extended use in medical applications, in particular inhalational anaesthesia. They are structural isomers (see Figure 4.9). Pentachloroethane ( $C_2HCl_5$ ) is a non-flammable but toxic chemical compound used as a solvent for oil and grease, in metal cleaning, and in the separation of coal from impurities, whilst hexachloroethane ( $C_2Cl_6$ ) is used in military activities for smoke-producing devices (e.g. grenades), in metal and alloy production, and as an ingredient in fungicides, insecticides, lubricants and plastics. To my knowledge there are no previous electron attachment data in the literature to these chlorinated ethanes.

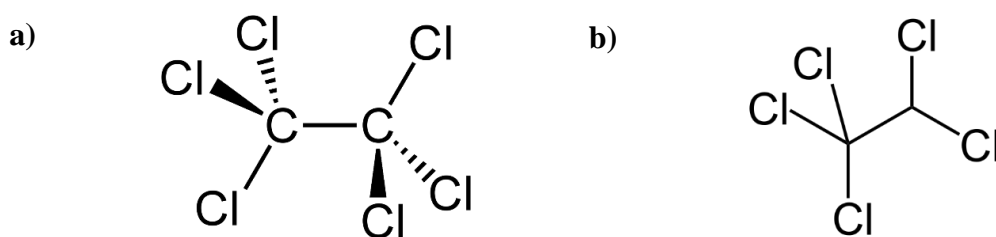


**Figure 4.10 – Schematic drawing of the chlorinated ethanes: hexachloroethane a) and pentachloroethane b) used to perform DEA experiments. From [56,57].**

In this contribution, the formation of negative ions formed upon DEA experiments were investigated using the experimental set-up briefly described in Chapter 3, section 3.1., and these results have been submitted to International Journal of Mass Spectrometry (see full manuscript below) which have just been accepted for publication.

## **Dissociative electron attachment to the volatile anaesthetics enflurane and isoflurane and the chlorinated ethanes pentachloroethane and hexachloroethane**

C. Matias,<sup>1</sup> A. Mauracher,<sup>1</sup> S. E. Huber,<sup>1</sup> S. Denifl,<sup>1</sup> P. Limão-Vieira,<sup>1,2,\*</sup> P. Scheier,<sup>1</sup> T. D. Märk,<sup>1</sup> R. González-Méndez,<sup>3</sup> C. A. Mayhew<sup>3,\*</sup>

<sup>1</sup> Institut für Ionenphysik und Angewandte Physik, Universität Innsbruck, Technikerstraße 25, A-6020 Innsbruck, Austria

<sup>2</sup> Laboratório de Colisões Atômicas e Moleculares, CEFITEC, Departamento de Física, Faculdade de Ciências e Tecnologia, Universidade Nova de Lisboa, 2829-516 Caparica, Portugal

<sup>3</sup> School of Physics and Astronomy, University of Birmingham, Edgbaston, Birmingham B15 2TT, UK

International Journal of Mass spectrometry (2015) accepted for publication.

### **Abstract**

Negative ion formation through dissociative electron attachment to the gas-phase volatile anaesthetics enflurane and isoflurane ( $C_3H_2ClF_5O$ ) and to two chlorinated ethanes, pentachloroethane ( $C_2HCl_5$ ) and hexachloroethane ( $C_2Cl_6$ ), have been studied in a crossed electron-molecular beam two sector field mass spectrometer experiment. Anion efficiency curves for the negatively charged fragments have been measured over an electron energy range of approximately 0 – 17 eV, with an energy resolution of ~1 eV. For the chlorinated ethanes, resonance features were generally found at ~ 0 eV and at 7.5 eV. For the volatile anaesthetics, no zero energy resonances were observed. Instead, product anions were detected mainly in the 2–3 eV and 9 eV energy regions, with the exception of  $Cl^-$ , whose dominant resonance occurs at approximately 0.6 eV and 0.9 eV for isoflurane and enflurane, respectively. To aid in the interpretation of the experimental results, quantum chemical calculations providing thermochemical thresholds of anion formation are also presented.

*Keywords:* Dissociative electron attachment; volatile anaesthetics; enflurane; isoflurane; chlorinated ethane; pentachloroethane; hexachloroethane

\* Corresponding authors:

Email address: [plimaovieira@fct.unl.pt](mailto:plimaovieira@fct.unl.pt) and [c.mayhew@bham.ac.uk](mailto:c.mayhew@bham.ac.uk)

## **1. Introduction**

Chlorinated molecules may be used in ion-mobility spectrometers as possible dopants to manipulate the ion-chemistry and hence to improve specificity of detection. A recent ion mobility spectrometric study by us investigating four chlorinated compounds showed that within the electron swarm environment of an ion mobility spectrometer (IMS) system, resulting in a mean electron energy of approximately 0.3 eV, electron attachment to pentachloroethane and hexachloroethane is very efficient, whereas that to the isoflurane and enflurane is not, despite their calculated electron affinities (DFT calculations using the B3LYP functional and the 6-31+G(d,p) basis set) being positive, 1.2 and 1.9 eV, respectively [1]. Chloride ion production following electron attachment was also calculated to be exothermic. We postulate that this unexpected behaviour may be due to the strongly positive Vertical Attachment Energies (VEA) calculated for isoflurane and enflurane to be 0.62 and 0.77 eV, respectively. To test this hypothesis we decided to investigate the electron attachment of the above molecules in more detail. The goal of this work is to determine the energy resonances and anion efficiencies of electron attachment, which to our knowledge have not previously been reported.

The present study represents a new experimental contribution for the measurement of negative ion yields for enflurane ( $\text{CHFCl-CF}_2\text{-O-CHF}_2$ ), isoflurane ( $\text{CF}_3\text{-CHCl-O-CHF}_2$ ), pentachloroethane ( $\text{C}_2\text{HCl}_5$ ) and hexachloroethane ( $\text{C}_2\text{Cl}_6$ ) molecules upon low-energy electron attachment. Although for an explanation of the IMS results energy resonances at less than 1 eV are of key importance, with the apparatus available we have taken the opportunity to investigate electron attachment to the above molecules over an electron energy range of 0 – 17 eV, which is of fundamental interest. To complement the experimental results, we have also carried out quantum chemical calculations on the electronic properties of all molecules studied in the present work. In the following sections we provide details on the experimental apparatus and the measurement technique that have been used. This will be followed by a brief discussion on the computational methods adopted and a presentation and discussion of the experimental results.

## **2. Experimental details**

Dissociative electron attachment (DEA) to the volatile anaesthetics and chlorinated ethanes was investigated by means of a crossed electron-molecular beam set-up utilizing a double focusing two-sector field mass spectrometer equipped with a standard Nier-type ion source [2]. The electron energy resolution close to 0 eV is about 1 eV full width at half maximum (FWHM). This low electron energy resolution is compensated by the high sensitivity that is available owing to the large electron current. The electron current is regulated to 10  $\mu\text{A}$ , which is achieved for electron energies higher than 2 eV. Below 2 eV the electron current decreases linearly down to a value of approximately 2  $\mu\text{A}$  at 0 eV. This reduction in current must be considered when comparing peak intensities below 2 eV to those above 2 eV for any particular energy scan for a given product anion. An effusive molecular beam emerges from an orifice of 3 mm diameter which is crossed with an electron beam to generate anions. A voltage drop of 6 kV accelerates product anions from the ion source towards the sector fields. Negative ion yields are obtained as a function of the electron beam energy. The electron energy scale and the electron energy resolution are calibrated to within  $\pm 0.2$  eV using the well-known  $\text{SF}_6^-/\text{SF}_6$  signal near 0 eV and the resonances of the  $\text{F}^-/\text{SF}_6$  and  $\text{F}_2^-/\text{SF}_6$  anions at higher electron energies.

Enflurane was purchased from Chempur. All other samples were purchased from Sigma-Aldrich with a minimum stated purity of 99%. Enflurane, isoflurane and pentachloroethane are liquid at room temperature and were degassed by a repeated freeze–pump–thaw cycle prior to experiments. Hexachloroethane is solid at room temperature but with a sufficient vapour pressure for it to be admitted into vacuum without the need for heating.

## **3. Computational details**

To aid in the interpretation of the experimental results, we have used several high-level extrapolation schemes for the determination of diverse quantum chemical properties, such as binding energies, (adiabatic) electron affinities and reaction thresholds. In particular we compare results from G3(MP2) [3], G4(MP2) [4] and CBS-4M [5, 6] which yield similar accuracy. CBS-4M yields a mean absolute deviation (MAD) of 2.0 kcal/mol for the G2 test set [7], G3(MP2) yields a MAD of 1.3 kcal/mol for the G2/97 test set [8, 9], whereas

G4(MP2) yields the lowest MAD of 1.04 kcal/mol for the G3/05 test set [10]. A comparison of different extrapolation schemes is often valuable as they might yield worse performance in individual cases than reflected by the average accuracy evaluated for selected systems in the respective test sets. For instance, it is well-known that G3(MP2) is (on average) more suitable for the hydrogen bonded complexes in the G3/05 test set. In general, it is found that G3(MP2) and G4(MP2) energies are very similar, whereas CBS-4M exhibits convergence problems for a few fragments under consideration. Therefore we shall restrict ourselves to reporting energies from G4(MP2) level of theory. In the case of isomers we take the one providing the lowest energy. Note, for comparison of the theoretically derived values with the experimental data, the former corresponds to the threshold of a resonance rather than the position of its maxima.

In addition to the above we employed the MP2/6-311++G(3df,2p) level of theory and its density to visualize the natural orbitals of the parent transient negative ions (TNIs). All calculations were performed using the Gaussian 09 suite of programs [11].

#### **4. Results and discussion**

Electron capture by a polyatomic molecule generates a TNI, which is seen as a quasi-bound state embedded in the auto-detachment continuum and unstable towards the loss of the extra electron. Therefore, the TNI may either be subject to auto-detachment or fragmentation (DEA). In the latter case, the TNI can decompose via single bond cleavages or undergo structural rearrangement. Symbolically these two processes can be written as:



where  $(ABC)^{* -}$  represents the TNI. In the case of isoflurane, enflurane and pentachloroethane, the computational work shows that optimization of the anionic state results in significant geometrical changes compared to the neutral molecule promoting the formation of a chloride ion and a neutral fragment rather than a single covalently bound anionic compound as can be seen in Figure 1A-C. In contrast, for the optimized anionic hexachloroethane the excess charge is distributed over two distant chlorine atoms in para position. The highest occupied natural orbitals (HONOs) plotted in Figures 1A-C

correspond nicely to the HONO of an isolated chloride ion. However, for hexachloroethane we observe a much delocalized HONO, see Figure 1D. The two previously mentioned distant chlorine atoms (left- and right-chlorine atoms in Figure 1D) show  $\sigma^*$  like bonding character, whereas the other chlorine atoms yield  $\pi^*$  bonding character overall weakening all C-Cl bonds. These calculations suggest that no parent anions will be observed in the experiment, because within the detection time of a few microseconds the parent anion would have dissociated. Table 1 and Table 2 provide the computational calculations of the threshold energies for formation of the experimentally observed product anions via single bond cleavages for the anaesthetics and chloroethanes, respectively. Results were obtained at G4(MP2) and CBS-4M level of theory.

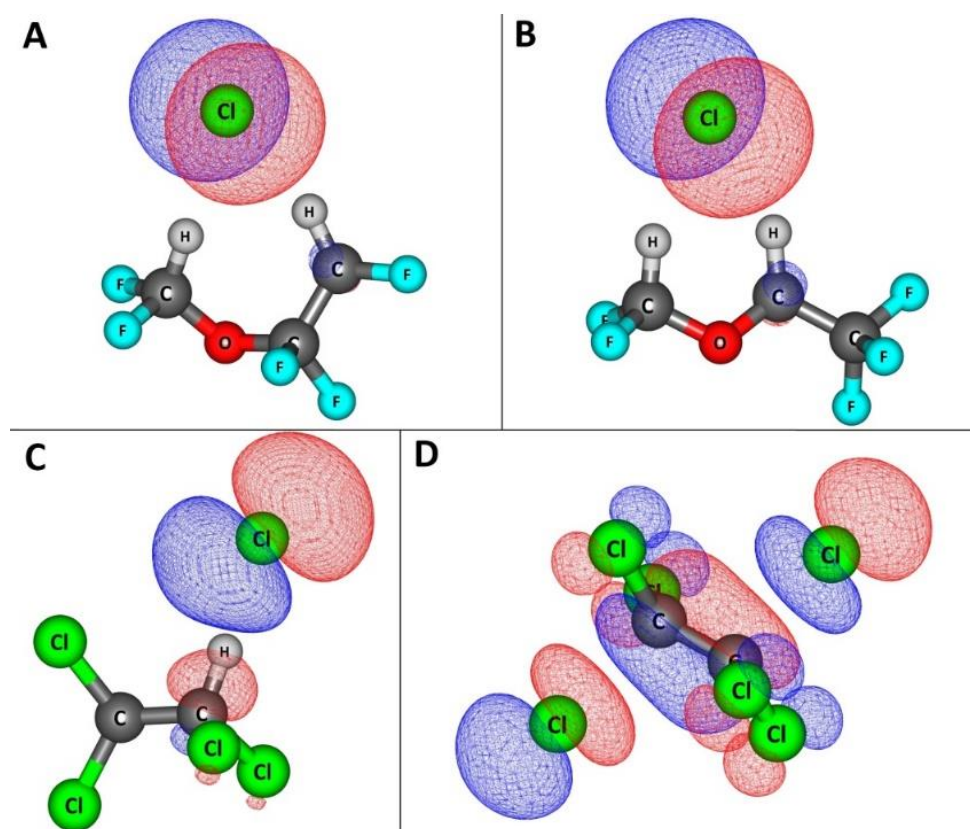


**Figure 1 - Highest occupied natural orbitals for the anionic states of (A) enflurane, (B) isoflurane, (C) pentachloroethane, and (D) hexachloroethane. Visualisation of the natural orbitals obtained using MP2/6-311++G(3df,2p) density.**

## Results and discussion

In agreement with the theoretical predictions and despite the high sensitivity of the instrument, we were not able to detect any parent anion, instead DEA dominates. This indicates that auto-detachment or fragmentation occurs in a time window shorter than the detection time, resulting in the absence of an observable parent negative ion. The  $m/z$  values of the most significant anion products resulting from DEA are listed in Table 3 and 4 for the anaesthetics and chlorinated ethanes, respectively, together with their possible assignments and the peak position of the corresponding resonances. The error in the peak positions is considered to be  $\pm 0.2$  eV, based on shifts of calibration peaks during the run of an experiment. For all compounds the dominant product anion is  $\text{Cl}^-$ . However, a surprising result is that although the elimination of  $\text{Cl}^-$  resulting from electron attachment to the anaesthetics is exothermic (Table 1), the resonance for  $\text{Cl}^-$  production peaks at relatively high electron energy (0.9 eV and 0.6 eV for enflurane and isoflurane, respectively). This experimental result therefore indicates that there must be an energetic barrier for zero energy electron attachment, explaining the results from the IMS study.

Anionic fragment	Enflurane	Isoflurane
	G4(MP2) (eV)	G4(MP2) (eV)
$(\text{M-H})^-$	2.11 / 2.37	1.69 / 2.28
$(\text{M-Cl})^-$	1.92	2.02
$\text{F}^-$	0.98 / 1.62 / 1.66	1.58 / 1.76
$\text{Cl}^-$	-0.23	-0.38
Adiabatic electron affinity		
M	1.25	1.52
M-H	2.00 / 1.96	2.29 / 1.96
M-Cl	1.49	1.84
F	3.50	3.50
Cl	3.64	3.64

**Table 1 - Calculated threshold energies for formation of anions via single bond cleavages for the anaesthetics. Results are obtained at G4(MP2) level of theory. Several numbers are given if more than one abstraction sites are possible. All energies are given in eV.**



Anionic fragment	Pentachloroethane	Hexachloroethane
	G4(MP2) (eV)	G4(MP2) (eV)
$(M-Cl)^-$	-0.29	-0.13
$Cl_2^-$	-0.89	-1.02
$Cl^-$	-0.64	-0.67
Adiabatic electron affinity		
M	1.44	1.22
M-Cl	3.11	3.29
$Cl_2$	2.37	2.37

Table 2 - Calculated threshold energies for formation of anions via single bond cleavages for the chloroethanes. Results are obtained at G4(MP2) level of theory. All energies are given in eV.

#### 4.1. Anion Mass Spectra

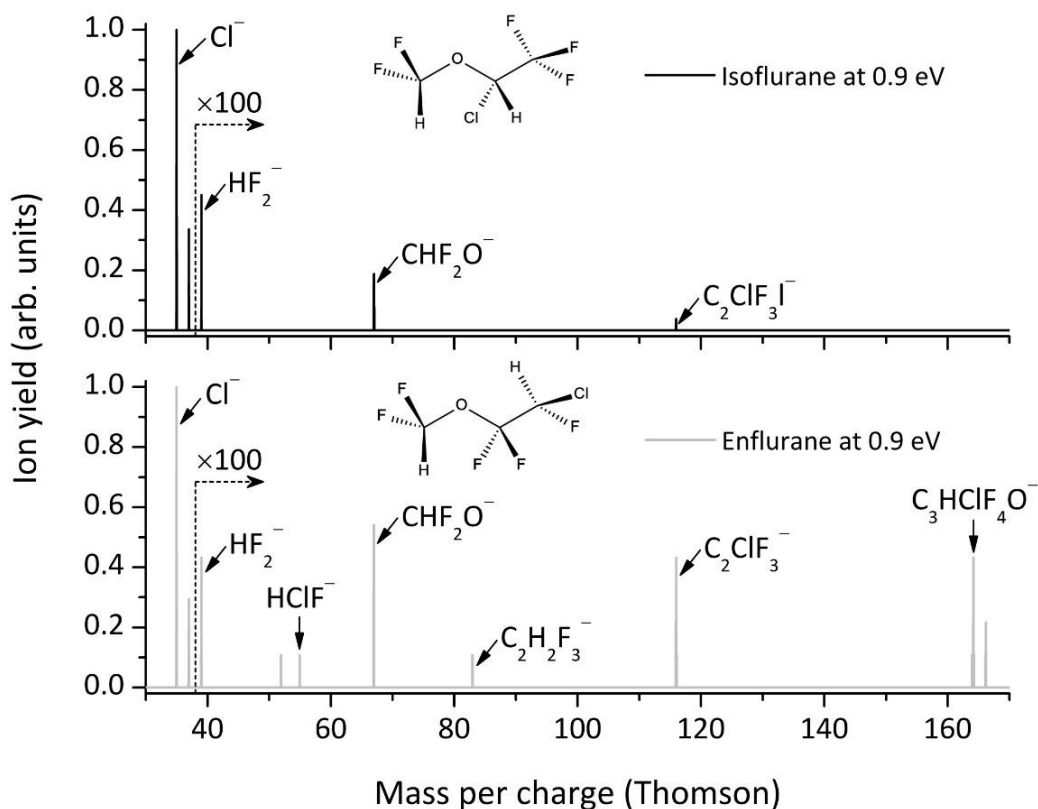
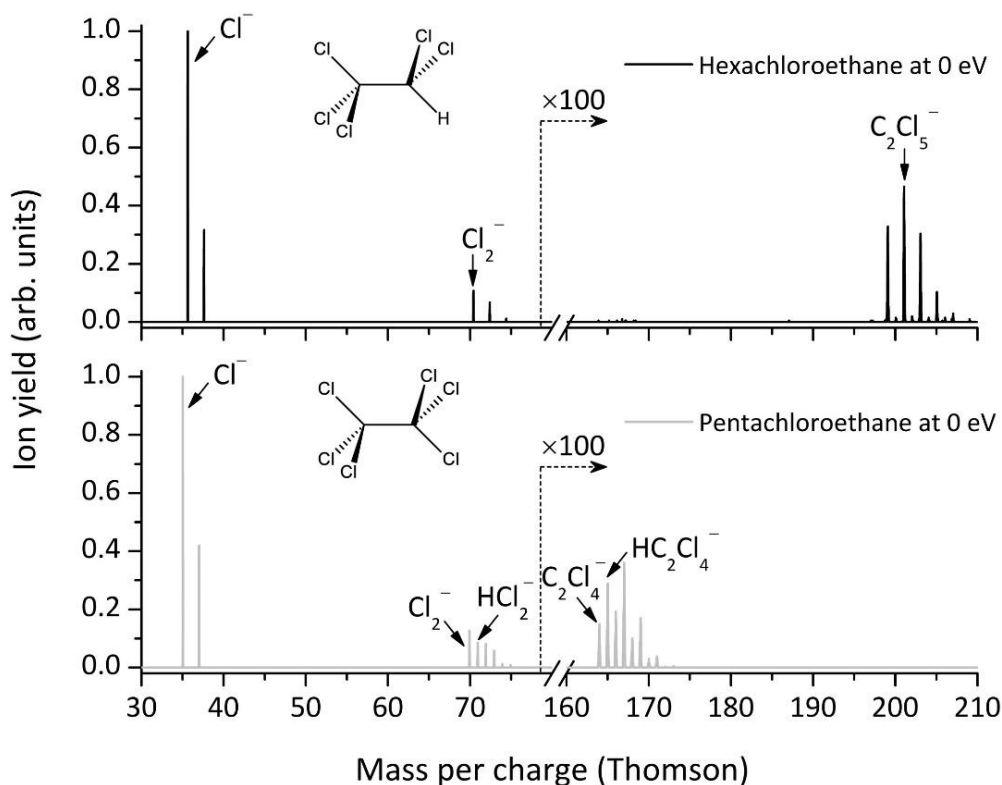


Figure 2 - Negative ion mass spectrum of isoflurane (upper panel) and enflurane (lower panel) measured at 0.9 eV electron energy. For ease of comparison both graphs were normalised to the highest signal intensity ( $Cl^-$ ), which is set at a value of 1.

## Results and discussion

Negative ion mass spectra are presented to provide an overview of the product anions at the electron energy corresponding to the peak resonance with the largest intensity. These spectra give an indication of the relative intensities of the product anions. For ease of comparison, intensities have been normalised relative to the dominant anion  $\text{Cl}^-$  which has been given an intensity of 1. Figure 2 shows the negative ion mass spectra of isoflurane and enflurane measured at 0.9 eV electron energy (corresponding to the lowest energy resonance peak observed for enflurane and close to that for isoflurane). In contrast to the anaesthetics, the chloroethanes have their dominant resonance closer to 0 eV. Therefore, Figure 3 shows the mass spectra for the anions formed by DEA to pentachloroethane and hexachloroethane at an electron energy of approximately 0 eV. Again for ease of comparison the intensities of all the anions have been normalised to that of  $\text{Cl}^-$  which has been set at a value of 1. As mentioned above,  $\text{Cl}^-$  is by far the most dominant anion product. However, for both the chloroethanes  $\text{Cl}_2^-$  and for pentachloroethane  $\text{HCl}_2^-$  are non-negligible product anions. The production of the anions is discussed in more detail in the following section.



**Figure 3 - Negative ion mass spectrum of hexachloroethane (upper panel) and pentachloroethane (lower panel) measured at ~ 0 eV electron energy. For ease of comparison both graphs were normalised to the highest signal intensity ( $\text{Cl}^-$ ), which is set at a value of 1.**

## **4.2 Electron Attachment Energy Resonances**

Figures 4-6 and figures 7-8 provide electron energy scans for all the observed product anions for the anaesthetics and the chloroethanes, respectively. Again to aid comparison, for these figures we have set the maximum peak intensity to one if an identical product anion was observed for the two molecules. Energy resolution plays a crucial role on the shape of the low energy resonances which are typically at electron energies of less than 4 eV, but it is not so relevant for the high-energy region owing to the broad nature of the observed features. The negative ion states at energies above 4 eV, can be considered to be formed via core excited resonances, which means, transient anions with the extra electron bound to an electronically excited state of the neutral. Moreover, the energy features in the range 9–11 eV can also be associated to Rydberg excitations [12].

### **4.2.1 Anion Yield Curves for Isoflurane and Enflurane (C<sub>3</sub>H<sub>2</sub>ClF<sub>5</sub>O)**

For ease of discussion, the anion yields of isoflurane and enflurane obtained in the DEA experiments have been placed into one of four groups (i) – (iv) according to their intensities. In order of relative intensities we have (i) Cl<sup>-</sup> (35 u) and HF<sub>2</sub><sup>-</sup> (39 u); (ii) F<sup>-</sup> (19 u), CFO<sup>-</sup> (47 u) and the species at *m/z* 67 and 116 where the former can be assigned to CHF<sub>2</sub>O<sup>-</sup> and the latter to C<sub>2</sub>ClF<sub>3</sub><sup>-</sup>; (iii) anions at *m/z* 55, 59, 79, 113 and 133, which are assigned as HClF<sup>-</sup>, C<sub>2</sub>FO<sup>-</sup>, C<sub>2</sub>HF<sub>2</sub>O<sup>-</sup>, C<sub>2</sub>ClF<sub>2</sub>O<sup>-</sup> and C<sub>2</sub>HClF<sub>3</sub>O<sup>-</sup>, respectively; (iv) anions at *m/z* 83, 85 and 164 are only observed to come from DEA of enflurane and are assigned to C<sub>2</sub>H<sub>2</sub>F<sub>3</sub><sup>-</sup>, CClF<sub>2</sub><sup>-</sup>, C<sub>3</sub>H<sub>2</sub>ClF<sub>5</sub><sup>-</sup>, respectively, whereas *m/z* 183 is only observed to result from DEA of isoflurane and is identified to be (M–H)<sup>-</sup>.

#### **4.2.1.1 Ion yields of Cl<sup>-</sup> (35 u) and HF<sub>2</sub><sup>-</sup> (39 u)**

Cl<sup>-</sup> is formed via rearrangement of the molecule upon electron attachment (see Figure 1) and subsequent expulsion of the chloride ion, whereas HF<sub>2</sub><sup>-</sup> formation requires breaking at least two of the five C–F bonds and one of the C–H bonds.

The maximum ion yield of Cl<sup>-</sup> is observed at electron energies of 0.9 and 0.6 eV for enflurane and isoflurane, respectively. The energy balance at G4(MP2) level of theory predicts in both cases an exothermic reaction. Optimized geometries are used in these

calculations, and therefore given that the neutral fragment (M-Cl) undergoes substantial geometrical changes in comparison to the structure shown Figure 1, there is a lowering the total energy of the products.

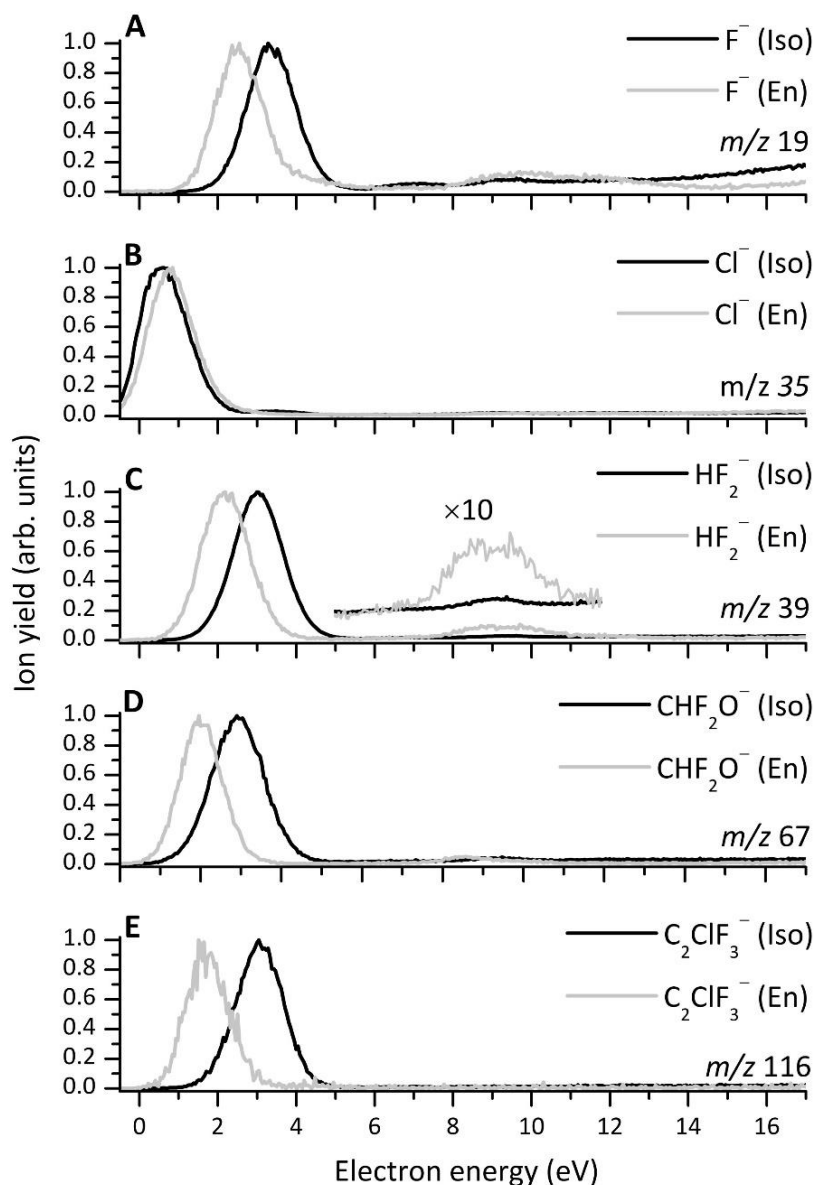


**Figure 4 - Anion efficiency curves of the isoflurane (black solid line) and enflurane (light-grey solid line) for the fragment ions (A)  $F^-$ , (B)  $Cl^-$ , (C)  $HF_2^-$ , (D)  $CHF_2O^-$ , and (E)  $C_2ClF_3^-$ . The width of the electron energy distribution is about 1 eV. For ease of comparison, the highest peak for each anion efficiency curve for both molecules have been normalised to a signal intensity of one.**

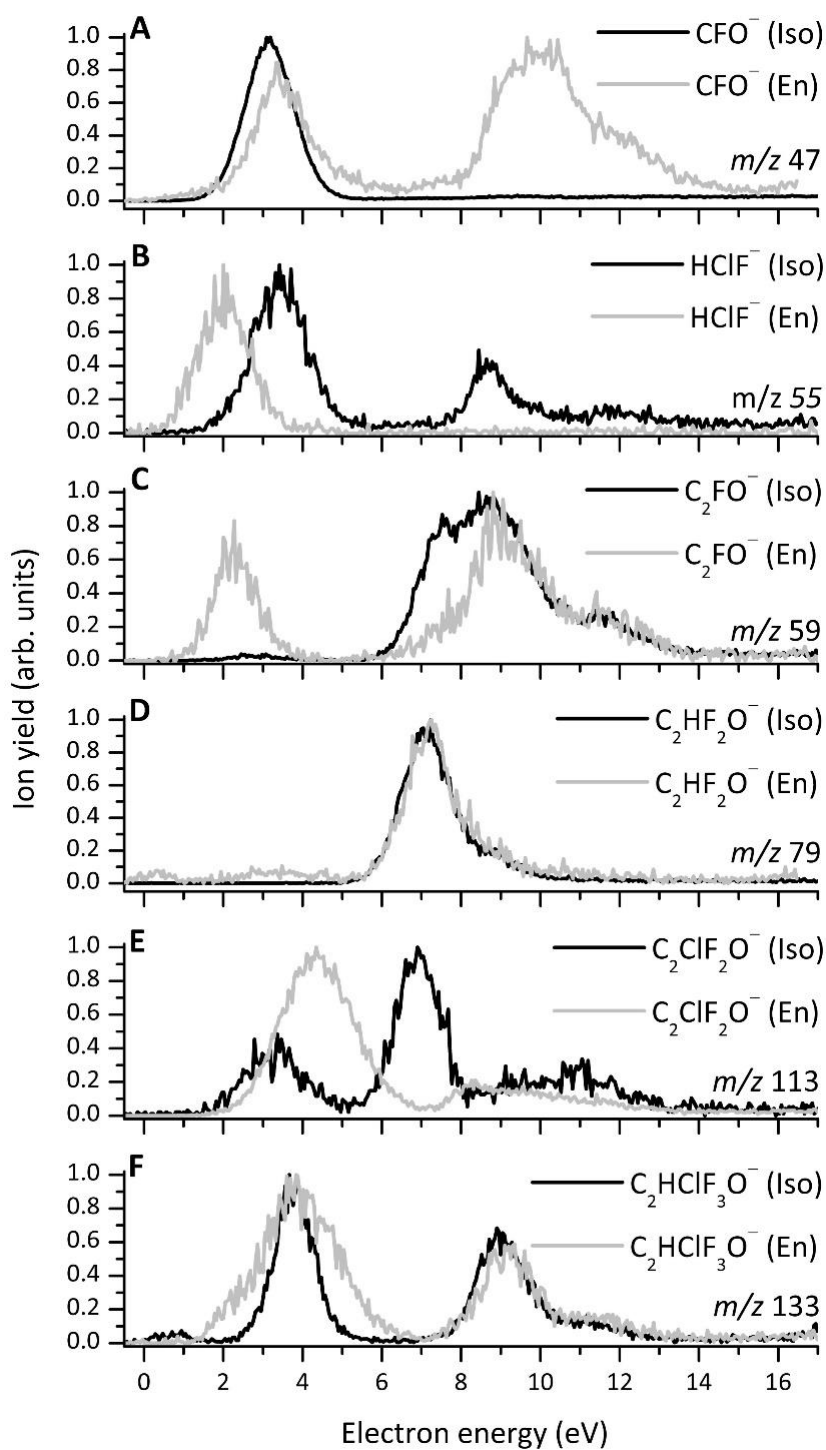


**Figure 5 - Anion efficiency curves of the isoflurane (black solid line) and enflurane (light-grey solid line) for the fragment ions (A)  $\text{CFO}^-$ , (B)  $\text{HClF}^-$ , (C)  $\text{C}_2\text{FO}^-$ , (D)  $\text{C}_2\text{HF}_2\text{O}^-$ , (E)  $\text{C}_2\text{ClF}_2\text{O}^-$ , and (F)  $\text{C}_2\text{HClF}_3\text{O}^-$ . The width of the electron energy distribution is about 1 eV. For ease of comparison, the highest peak for each anion efficiency curve for both molecules have been normalised to a signal intensity of one.**

## *Results and discussion*

The formation of  $\text{HF}_2^-$  is endothermic with a reaction threshold of 1.73 eV for enflurane. It is of note that the complementary exothermic DEA reactions, i.e. formation of the heavy anions  $(\text{C}_3\text{H}_2\text{ClF}_5\text{O}-\text{Cl})^-$  and  $(\text{C}_3\text{H}_2\text{ClF}_5\text{O}-\text{HF}_2)^-$  are absent meaning that the charge remains on the small fragments as the TNI dissociates.

The ionic yields of  $\text{Cl}^-$  and  $\text{HF}_2^-$  upon DEA to isoflurane and enflurane are shown in Figure 4B and 4C, respectively. It is to be noted that the anion efficiency curves measured show a full width at half maximum (FWHM) greater than the electron energy resolution ( $\sim 1$  eV). This can be related to high initial kinetic energy of these low-mass fragments. The strong extraction fields of the sector field instrument enhance substantially higher ion collection efficiency. The chloride ion provides a considerable contribution to the total anion formation, particularly via its low-energy resonance at  $\sim 0.9$  eV for enflurane and  $\sim 0.6$  eV for isoflurane.

Results and discussion

$m/z$ (u)	Anionic species	Peak positions in eV <sup>1</sup>													
		Enflurane							Isoflurane						
19	F <sup>-</sup>	-	2.6	-	-	-	9.5	11.7	-	-	3.3	7.1	9.3	-	-
35	Cl <sup>-</sup>	0.9	-	-	-	-	9.4	-	12.2	0.6	3.3	-	9.2	-	12.6
39	HF <sub>2</sub> <sup>-</sup>	-	2.2	-	-	-	9.3	-	-	-	3.0	6.9	9.5	-	-
47	CFO <sup>-</sup>	-	-	3.5	-	-	9.9	-	12.1	-	3.0	-	9.3	-	13.1
55	HClF <sup>-</sup>	-	2.0	-	-	-	-	-	-	-	3.4	-	8.7	11.9	-
59	C <sub>2</sub> FO <sup>-</sup>	-	2.3	-	-	7.1	9.0	11.3	-	-	2.8	7.3	8.8	11.5	-
67	CHF <sub>2</sub> O <sup>-</sup>	-	2.0	-	-	8.6	9.8	-	-	-	2.9	-	9.2	-	-
79	C <sub>2</sub> HF <sub>2</sub> O <sup>-</sup>	-	-	3.2	7.1	8.7	-	-	-	-	-	7.1	8.7	-	-
83	C <sub>2</sub> H <sub>2</sub> F <sub>3</sub> <sup>-</sup>	-	1.8	-	-	-	-	-	-	-	-	-	-	-	-
85	CClF <sub>2</sub> <sup>-</sup>	-	1.9	-	-	-	-	-	-	-	-	-	-	-	-
113	C <sub>2</sub> ClF <sub>2</sub> O <sup>-</sup>	-	-	4.4	-	8.3	9.6	-	-	-	3.3	6.9	-	10.9	-
116	C <sub>2</sub> ClF <sub>3</sub> <sup>-</sup>	-	1.7	-	-	-	-	-	-	-	3.1	-	-	-	-
133	C <sub>2</sub> HClF <sub>3</sub> O <sup>-</sup>	-	-	3.9	-	-	9.1	11.3	-	0.7	3.8	-	9.0	10.7	-
164	C <sub>3</sub> HClF <sub>4</sub> O <sup>-</sup>	-	1.4	-	-	-	-	-	-	-	-	-	-	-	-
183	C <sub>3</sub> HClF <sub>5</sub> O <sup>-</sup>	-	-	-	-	-	-	-	-	-	3.0	-	8.6	-	-

**Table 3 - Peak positions (eV) for the observed resonances corresponding to fragment anions of enflurane and isoflurane obtained in the DEA experiment.  
( $m/z$  of the monoisotopic fragments are only given.)**

<sup>1</sup> Estimated uncertainty in the peak value is  $\pm 0.2$  eV, based on shifts in calibration peaks during the run of an experiment.

#### **4.2.1.2 Ion yields of $F^-$ (19 u), $CFO^-$ (47 u), $CHF_2O^-$ (67 u) and $C_2ClF_3^-$ (116 u)**

Figures 4 and 5 present the yields of the fragment anions for  $F^-$ ,  $CFO^-$ ,  $CHF_2O^-$  and  $C_2ClF_3^-$ . DEA leading to  $CFO^-$ ,  $CHF_2O^-$  and  $C_2ClF_3^-$  formation, require considerable rearrangement. Comparisons between isoflurane and enflurane anion efficiency curves show clear distinctions in regard to the lowest resonance peak position maxima (see Table 3) whilst for the higher energy resonances ( $> 8$  eV) such differences are not present. Such behaviour can be due to the identical nature of the possible Rydberg states contributing to these resonances, i.e. in the two-particle one-hole mechanism, the delocalized electron may experience the same interaction of the cationic core in both isomeric volatile anaesthetics.

#### **4.2.1.3 Ion yields of $HClF^-$ (55 u), $C_2FO^-$ (59 u), $C_2HF_2O^-$ (79 u), $C_2ClF_2O^-$ (113 u) and $C_2HCIF_3O^-$ (133 u)**

These set of anions have the lowest intensities detected and constitute relative to  $Cl^-$  formation just 0.03–0.6% for isoflurane and 0.04–1.0% for enflurane of the total anion signal. The resonance peak positions are shown in figures 4-5 and are listed in Table 3. The fragment ion  $C_2HF_2O^-$  shows a weak resonance structure at 3.2 eV for enflurane which is absent for isoflurane.

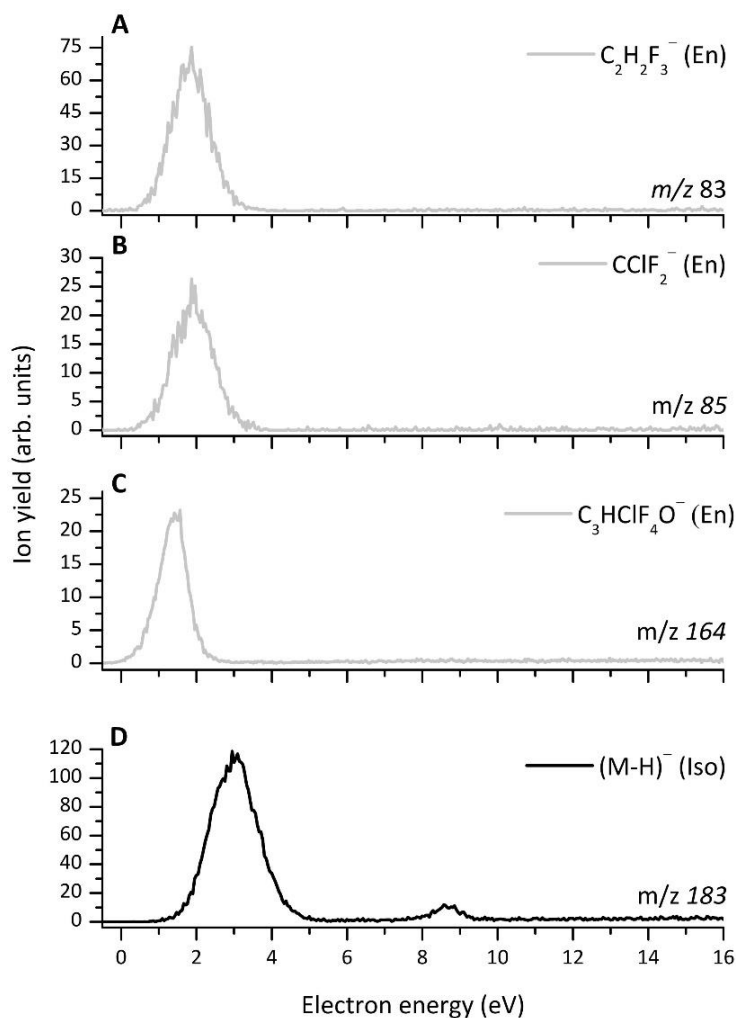
#### **4.2.1.4 Ion yields of $C_2H_2F_3^-$ (83 u), $CClF_2^-$ (85 u), $C_3HCIF_4O^-$ (164 u) and $C_3HCIF_5O^-$ (183 u)**

Figure 6 shows the yields of the fragment ions resulting only from enflurane at 83, 85, and 164 u and from isoflurane at 183 u. The 83 u anion is assigned to be  $CHF_2-CHF^-$ . 85 u is attributed to  $CClF_2^-$ . 164 u is assigned to be  $C_3HCIF_4O^-$ .

The dehydrogenated parent anion at 183 u is only observed for isoflurane. Our calculated values for the threshold energies are in a range of 1.69 – 2.38 eV depending on the site of hydrogen loss. A major difference between the two isomeric volatile anaesthetics becomes apparent. The lowest threshold energies for the dehydrogenated enflurane and isoflurane anions are at 2.11 and 1.69 eV, respectively. A possible explanation for the absence of the dehydrogenated enflurane anion is competing channels. In the case of enflurane, threshold energies for the formation of  $F^-$  and  $(M-Cl)^-$  via single bond cleavages



(see Table 3), are below the dehydrogenated enflurane anion threshold value, whereas in the case of isoflurane only the  $F^-$  channel is competitive according to our calculations within the estimated accuracy of 0.2 eV. Thus it is not possible to determine the most favourable channel solely from theory. However, from the experimental resonance energies we can determine that  $F^-$  is formed at higher electron energies than the calculation suggests (see Table 1). Also, we can rule out  $(M-Cl)^-$  since it is not experimentally observed. We note, that there are some fragments formed well below the range of the  $(M-H)^-$  thresholds, i.e.  $Cl^-$  and  $C_2HClF_3O^-$  (see Table 1 and 3). Owing to the resonant nature of DEA, these two channels do not compete in the formation of the dehydrogenated parent anion for both volatile anaesthetics under consideration.



**Figure 6 - Anion efficiency curves of the isoflurane (black solid line) and enflurane (light-grey solid line) for the fragment ions (A)  $C_2H_2F_3^-$ , (B)  $CClF_2^-$ , (C)  $C_3HClF_4O^-$ , and (D)  $(M-H)^-$ . The width of the electron energy distribution is about 1 eV.**

The results provided in Table 3 reveal a multitude of resonance energies close to the lowest calculated threshold energies for the formation of the dehydrogenated parent anions.  $\text{HF}_2^-$ ,  $\text{CFO}^-$ ,  $\text{HClF}^-$ ,  $\text{C}_2\text{FO}^-$ ,  $\text{C}_2\text{H}_2\text{F}_3^-$ ,  $\text{CF}_2\text{Cl}^-$  and  $\text{C}_2\text{ClF}_3^-$  are formed via multiple bond cleavages, and are thus less likely to occur than the simple  $(\text{M-H})^-$  channel. Although  $\text{CHF}_2\text{O}^-$  can be formed via a single bond cleavage, it will not be in competition with the formation of formation of the dehydrogenated parent anion. Owing to enhanced Coulomb and Pauli repulsion in the vicinity of the lone pair electrons of the oxygen atom, the attachment of a free electron in this region of the molecule is less likely. Hence, it appears that for enflurane the lack of an  $(\text{M-H})^-$  anion for enflurane is considered to the result of having a more favourable channel  $\text{F}^-$ . In contrast, in the case of isoflurane there are no other channels able to compete with  $(\text{M-H})^-$  formation at the resonance energy.

#### 4.2.2 Anion Yield Curves for the chlorinated ethanes, $\text{C}_2\text{HCl}_5^-$ and $\text{C}_2\text{Cl}_6^-$

$m/z$ (u)	Anionic species	Peak positions in eV <sup>2</sup>						
		Pentachloroethane			Hexachloroethane			
35	$\text{Cl}^-$	0.1	–	7.2	0.1	–	6.8	12.5
70	$\text{Cl}_2^-$	0.1	–	7.1	0.1	–	6.9	12.7
71	$\text{HCl}_2^-$	0.1	–	7.9	–	–	–	–
82	$\text{CCl}_2^-$	–	3.0	–	–	–	–	–
117	$\text{CCl}_3^-$	–	3.0	–	–	2.8	7.2	–
164	$\text{C}_2\text{Cl}_4^-$	0.0	–	8.0	–	–	–	–
165	$\text{HC}_2\text{Cl}_4^-$	0.0	–	–	–	–	–	–
199	$\text{C}_2\text{Cl}_5^-$	–	–	–	0	–	–	–

**Table 4 - Peak positions (eV) for the observed resonances corresponding to fragment anions of pentachloroethane and hexachloroethane obtained in the DEA experiment.**

( $m/z$  of the monoisotopic fragments are only given.)

The anion efficiency curves of the most intense fragment anions observed in the negative ion mass spectra of pentachloroethane and hexachloroethane are shown in Figures 7 and 8, where the most intense DEA signals can be found close to 0 eV. Several fragment

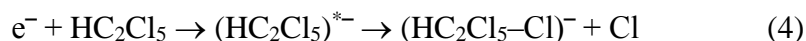
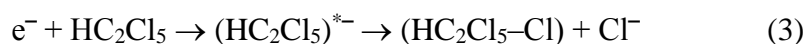
<sup>2</sup> Estimated uncertainty in the peak value is  $\pm 0.2$  eV, based on shifts in calibration peaks during the run of an experiment.

anions are also formed in an extended electron energy range showing resonance features at around 3 and 8 eV. However, the intensities of these high-energy resonances is for most of the fragment anions at least one order of magnitude lower than the feature close to 0 eV.

The fragment anions assigned in DEA experiments to pentachloroethane ( $\text{HC}_2\text{Cl}_5$ ) and hexachloroethane ( $\text{C}_2\text{Cl}_6$ ) are given in Table 4 and these will be discussed below. Given the larger number of product anions observed for pentachloroethane, for ease of discussion the anion yields has been separated into three different groups depending on intensities. The first group is  $\text{Cl}^-$  and  $\text{HC}_2\text{Cl}_4^-$ , the second contains  $\text{Cl}_2^-$ ,  $\text{HCl}_2^-$  and  $\text{C}_2\text{Cl}_4^-$ , and the third  $\text{CCl}_2^-$  and  $\text{CCl}_3^-$ .

#### **4.2.2.1 Ion yields of $\text{Cl}^-$ (35 u) and $\text{HC}_2\text{Cl}_4^-$ (165 u) from pentachloroethane**

The anions  $\text{Cl}^-$  and  $\text{HC}_2\text{Cl}_4^-$  are formed via complementary DEA processes:



Figures 7 and 8 show the ion yield curve for  $\text{Cl}^-$  and  $(\text{HC}_2\text{Cl}_5\text{-Cl})^-$ , respectively. G4(MP2) calculations show that for zero energy electrons reactions (3) and (4) are exothermic (see Table 2).

In contrast to its complementary fragment anion,  $\text{HC}_2\text{Cl}_4^-$ , which is restricted to the  $\sim 0$  eV resonance, the  $\text{Cl}^-$  signal extends to higher energies (see Figure 7). If we assume that the excess energy of the transient negative ion  $(\text{HC}_2\text{Cl}_5)^{* -}$  is statistically distributed over the vibrational degrees of freedom, the large fragment should take about 93% of the energy obtained from the electron attachment. In the case of  $\text{Cl}^-$  the neutral counterpart will become increasingly unstable towards dissociation which does not influence the anion efficiency curve of  $\text{Cl}^-$ . However, if the charge stays on the heavy fragment, the excess energy will drive further decomposition into lower mass fragments and thus the anion yield for 165 u at higher electron energies will be suppressed. Of relevance, is the fact that the heavier fragment anions (82 and 117 u) show a resonance at medium energies ( $\sim 3$  eV) with suppression of the high energy feature ( $\sim 7\text{--}8$  eV) while the lighter fragment anion (70 u) also exhibits the high energy resonance (see Figures 7 and 8). This indicates that the

subsequent decomposition of  $(\text{HC}_2\text{Cl}_5\text{-Cl})^{*-}$  may contribute to the formation of these anions.

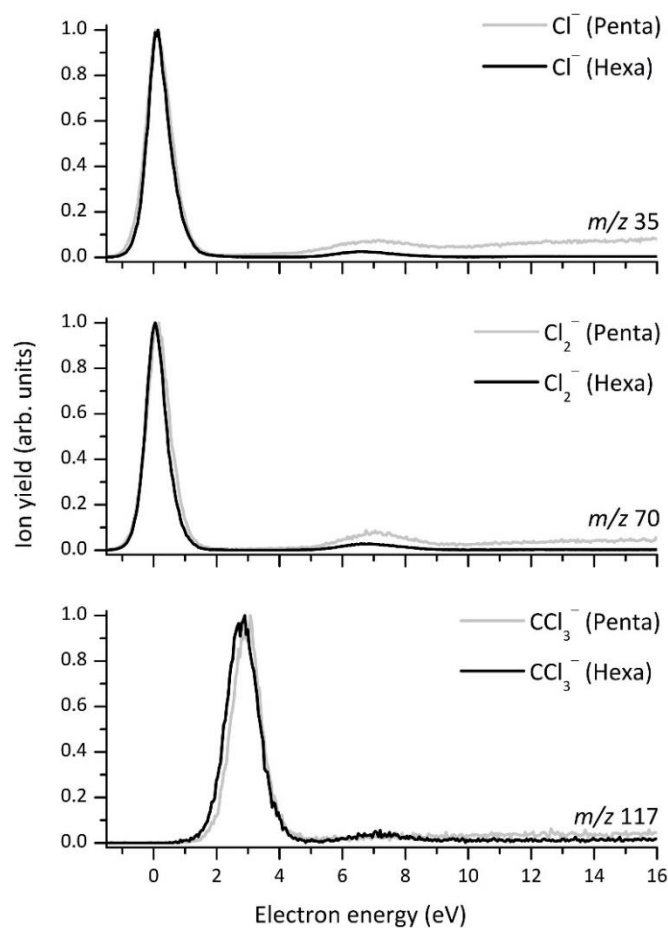


**Figure 7 - Anion efficiency curves of the pentachloroethane (light-grey solid line) and hexachloroethane (black solid line) for the fragment ions  $\text{Cl}^-$  (upper panel),  $\text{Cl}_2^-$  (middle panel), and  $\text{CCl}_3^-$  (lower panel). The width of the electron energy distribution is about 1 eV. For ease of comparison, the highest peak for each anion efficiency curve for both molecules have been normalised to a signal intensity of one.**

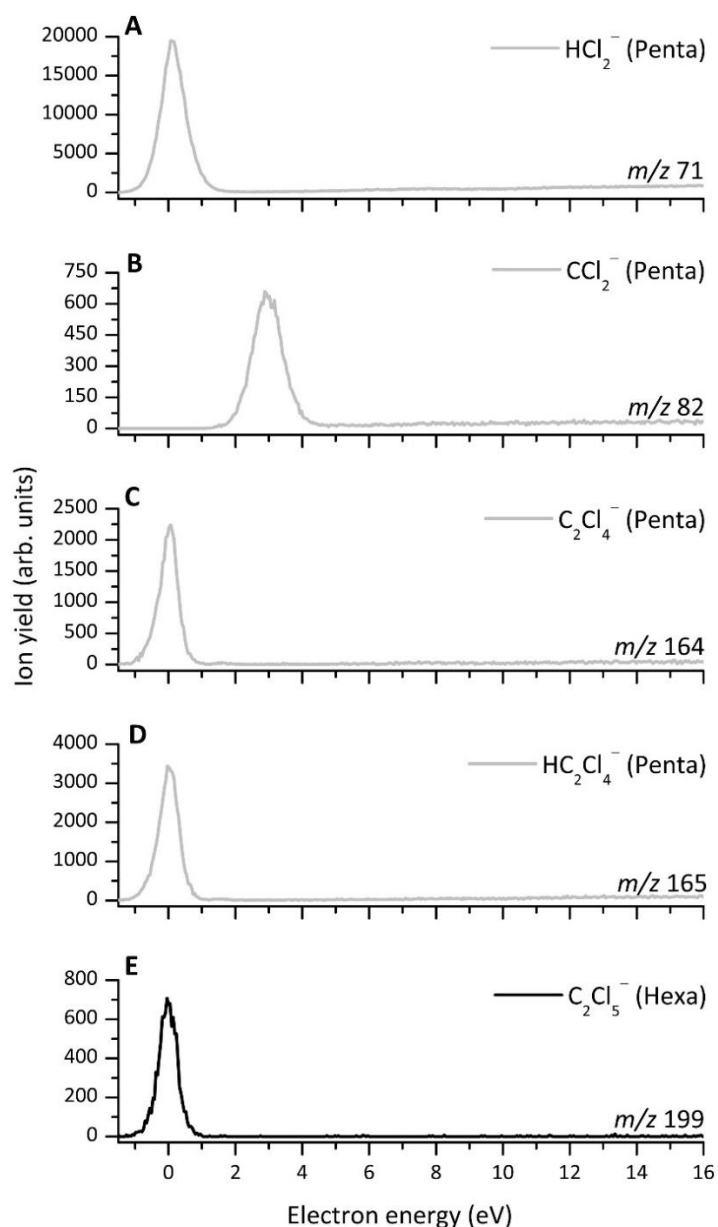


**Figure 8 - Anion efficiency curves of the pentachloroethane (light-grey solid line) and hexachloroethane (black solid line) for the fragment ions (A)  $\text{HCl}_2^-$ , (B)  $\text{CCl}_2^-$ , (C)  $\text{C}_2\text{Cl}_4^-$ , (D)  $\text{HC}_2\text{Cl}_4^-$ , and (E)  $\text{C}_2\text{Cl}_5^-$ . The width of the electron energy distribution is about 1 eV.**

#### 4.2.2.3 Ion yields of $\text{Cl}_2^-$ (70 u), $\text{HCl}_2^-$ (71 u) and $\text{C}_2\text{Cl}_4^-$ (164 u) from pentachloroethane

These product anions are mainly formed at virtually no electron kinetic energy ( $\sim 0$  eV), arising from surprisingly complex reactions associated with multiple bond cleavages and structural and electronic rearrangement. This is in line with our G4(MP2) calculations

yielding -0.89, -0.35 and -0.2 eV for the threshold energies for the formation of  $\text{Cl}_2^-$ ,  $\text{HCl}_2^-$  and  $\text{C}_2\text{Cl}_4^-$  from pentachloroethane, respectively. Fragment anions 71 u and 164 u assigned to  $\text{HCl}_2^-$  and  $\text{C}_2\text{Cl}_4^-$ , respectively, are formed at 0 eV resonance only, whereas  $\text{Cl}_2^-$  shows an extra resonance feature at  $\sim 7$  eV (see Table 4). Above an electron energy of 10 eV, the anionic signal intensity is observed to slightly increase which could be a result of ion-pair formation.

#### **4.2.2.4 Ion yields of $\text{CCl}_2^-$ (82 u) and $\text{CCl}_3^-$ (117 u) from pentachloroethane**

The shape and position of the only resonance feature at  $\sim 3$  eV for the fragment anion  $\text{CCl}_2^-$  (82 u) and  $\text{CCl}_3^-$  (117 u) are very similar, which may indicate that these anions have common precursor transient anion states.  $\text{CCl}_2^-$  and  $\text{CCl}_3^-$  formation are endothermic with a threshold of 1.36 and 1.16 eV, respectively. From Figures 7 and 8 we note that the experimental appearance energy is around 1.5 eV, a value which, within the current electron energy resolution of  $\sim 1$  eV, is in good agreement with the calculated threshold.

#### **4.2.2.5 Ion yields of $\text{Cl}^-$ (35 u), $\text{Cl}_2^-$ (70 u), $\text{CCl}_3^-$ (117 u) and $\text{C}_2\text{Cl}_5^-$ (199 u) from hexachloroethane**

DEA to  $\text{C}_2\text{Cl}_6$  is found to result in four fragment anions;  $\text{Cl}^-$ ,  $\text{Cl}_2^-$ ,  $\text{CCl}_3^-$  and  $\text{C}_2\text{Cl}_5^-$ , of which three ( $\text{Cl}^-$ ,  $\text{Cl}_2^-$  and  $\text{C}_2\text{Cl}_5^-$ ) have resonance features at 0 eV (see Table 4). This is in line with our computational calculations which yield -0.67, -1.02, 0.93 and -0.13 eV for the formation of  $\text{Cl}^-$ ,  $\text{Cl}_2^-$ ,  $\text{CCl}_3^-$  and  $\text{C}_2\text{Cl}_5^-$ , respectively. These anions are all formed via the cleavage of one of the six C–Cl bonds and the C–C bond, whereas  $\text{Cl}_2^-$  formation requires additional internal rearrangement. It is interesting to note that  $\text{CCl}_3^-$  formation from hexachloroethane, can proceed through two resonances at 2.8 and 7.2 eV, whereas in the case of pentachloroethane it proceeds via the lowest resonance only.

## 5. Conclusions

In this study of the dissociative electron attachment of two volatile anaesthetics (enflurane, isoflurane) and two chlorinated ethanes (pentachloroethane, hexachloroethane), we have obtained the anionic yields measured in the electron energy range of 0 – 17 eV with an energy resolution of  $\sim 1$  eV and a peak position accuracy of  $\pm 0.2$  eV. Such experiments have been performed in a crossed electron-molecular beam setup equipped with a double focusing two-sector field mass spectrometer with a standard Nier-type ion source.

The results show that the cross-section for the capture of an electron with virtually no kinetic energy by the volatile anaesthetics is very small. In fact the peak for electron attachment leading to the elimination of  $\text{Cl}^-$  occurs at just below 1 eV for both molecules. The opposite is true for pentachloroethane and hexachloroethane, for which there are zero electron attachment energy resonances with large cross-sections. These results explain our observations of the low and high electron attachment efficiencies of the anaesthetics and chlorinated ethanes, respectively, observed in the swarm (low mean electron energy) environment of an IMS system. We have proposed that the absence of zero energy electron attachment resonances for the anaesthetics results from an energy barrier. The onset of the low energy resonances for isoflurane and enflurane are in good agreement with the VEA values that we have calculated.

Although isoflurane and enflurane are isomers, interestingly they exhibit different DEA patterns. Only in the case of isoflurane it is possible to detect a dehydrogenated parent anion, whereas in the case of enflurane this fragmentation channel turns out to be entirely suppressed due to other dominant channels being available at the electron energy region for its formation, i.e. for  $(\text{M-Cl})^-$  and  $\text{F}^-$ . In the case of enflurane additional anions at mass 83 and 85 u have been detected. We propose that the high-energy attachment resonances in these isomers must originate from core-excited resonances, consisting of two electrons in normally unoccupied molecular orbitals moving in the field of the positive core.

The most dominant signal from DEA reactions to the chlorinated ethanes is the formation of  $\text{Cl}^-$  at electron energies  $\sim 0$  eV and  $\sim 7$  eV, the latter with a yield an order of magnitude lower than the former. The second most intense ion signal assigned to  $\text{Cl}_2^-$  shows also the same energy positions for these two resonances. Other reactions like the loss of several other neutral units with an onset of the resonant ionic yields at zero energy are observed as well.

## **Acknowledgments**

The funding of the Early Stage Researcher (RGM) was supported through the PIMMS Initial Training Network which in turn is supported by the European Commission's 7th Framework Programme under Grant Agreement Number 287382. This work was supported by the Austrian Ministry of Science BMWF as part of the UniInfrastrukturprogramm of the Focal Point Scientific Computing at the University of Innsbruck. AM acknowledges a grant from the Nachwuchsförderung of the University of Innsbruck. SEH gratefully acknowledges funding from the Austrian Science Fund (FWF) DK+ project Computational Interdisciplinary Modeling, W1227-N16. PLV acknowledges the Portuguese Foundation for Science and Technology (FCT-MEC) for partial funding from the research grants PTDC/FIS-ATO/1832/2012 and PEst-OE/FIS/UI0068/2014.

## **References**

1. R. González-Méndez, P. Watts, and C. A. Mayhew (in preparation).
2. D. Huber, M. Beikircher, S. Denifl, F. Zappa, S. Matejcik, A. Bacher, V. Grill, T. D. Mark and P. Scheier, *J. Chem. Phys.* 125 (8) (2006) 7.
3. L. A. Curtiss, P. C. Redfern, K. Raghavachari, V. Rassolov and J. A. Pople, *J. Chem. Phys.* 110 (10) (1999) 4703.
4. L. A. Curtiss, P. C. Redfern and K. Raghavachari, *J. Chem. Phys.* 127 (12) (2007) 8.
5. J. W. Ochterski, G. A. Petersson and J. A. Montgomery, *J. Chem. Phys.* 104 (7) (1996) 2598.
6. J. A. Montgomery, M. J. Frisch, J. W. Ochterski and G. A. Petersson, *J. Chem. Phys.* 112 (15) (2000) 6532.
7. L. A. Curtiss, K. Raghavachari, G. W. Trucks and J. A. Pople, *J. Chem. Phys.* 94 (11) (1991) 7221.
8. L. A. Curtiss, K. Raghavachari, P. C. Redfern and J. A. Pople, *J. Chem. Phys.* 106 (3) (1997) 1063.



9. L. A. Curtiss, P. C. Redfern, K. Raghavachari and J. A. Pople, *J. Chem. Phys.* 109 (1) (1998) 42.
10. L. A. Curtiss, P. C. Redfern and K. Raghavachari, *J. Chem. Phys.* 123 (12) (2005) 124107.
11. M. J. Frisch, G. W. Trucks, H. B. Schlegel, G. E. Scuseria, M. A. Robb, J. R. Cheeseman, G. Scalmani, V. Barone, B. Mennucci, G. A. Petersson, H. Nakatsuji, M. Caricato, X. Li, H. P. Hratchian, A. F. Izmaylov, J. Bloino, G. Zheng, J. L. Sonnenberg, M. Hada, M. Ehara, K. Toyota, R. Fukuda, J. Hasegawa, M. Ishida, T. Nakajima, Y. Honda, O. Kitao, H. Nakai, T. Vreven, J. A. Montgomery, J. E. Peralta, F. Ogliaro, M. Bearpark, J. J. Heyd, E. Brothers, K. N. Kudin, V. N. Staroverov, R. Kobayashi, J. Normand, K. Raghavachari, A. Rendell, J. C. Burant, S. S. Iyengar, J. Tomasi, M. Cossi, N. Rega, J. M. Millam, M. Klene, J. E. Knox, J. B. Cross, V. Bakken, C. Adamo, J. Jaramillo, R. Gomperts, R. E. Stratmann, O. Yazyev, A. J. Austin, R. Cammi, C. Pomelli, J. W. Ochterski, R. L. Martin, K. Morokuma, V. G. Zakrzewski, G. A. Voth, P. Salvador, J. J. Dannenberg, S. Dapprich, A. D. Daniels, Farkas, J. B. Foresman, J. V. Ortiz, J. Cioslowski and D. J. Fox, (Wallingford CT, 2009).
12. E. Illenberger and J. Momigny, *Gaseous Molecular Ions. An Introduction to Elementary Processes Induced by Ionization*. (Steinkopff/Springer, New York, 19

#### 4.2.2. Low-energy electron interaction with tungsten hexacarbonyl

Besides biomolecules and molecules that may enhance the detection of explosives, also molecular targets with a technological interest in the formation of metallic layers were studied. Metal carbonyl complexes are exciting compounds to study, since they have a huge potential in numerous fields such as chemistry and technology. This kind of molecules is widely used to prepare layers by using Electron Beam Induced Deposition (EBID) and Ion Beam Induced Deposition (IBID) techniques [58,59]. These molecules have especially been used in the field of plasma technology (to prepare metallic layers) [60] and in nanotechnology procedures (to prepare metallic structures) [61,62].

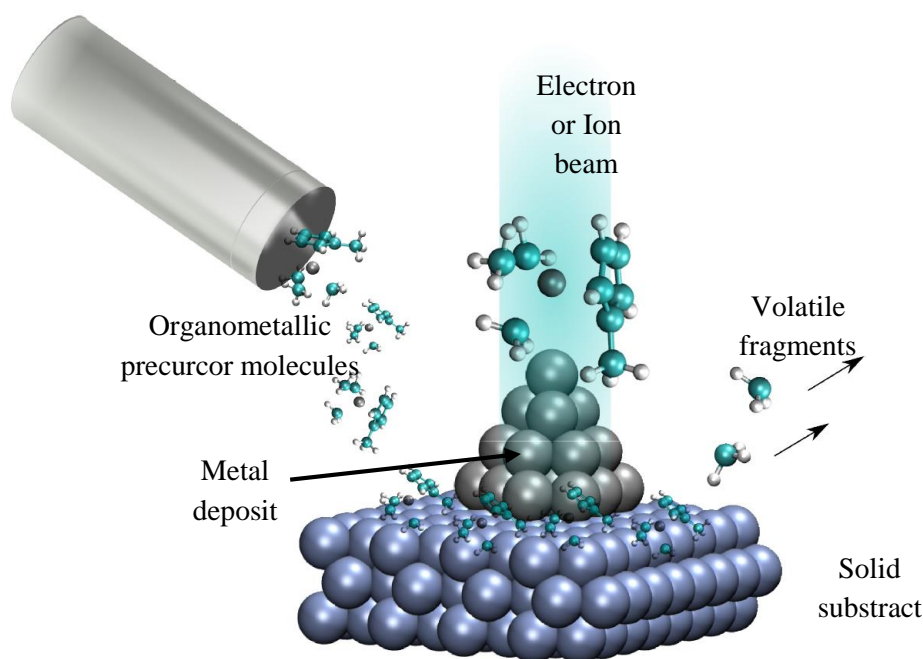


**Figure 4.11 - Schematic illustration of the EBID and IBID techniques. In EBID an electron beam used, while IBID uses an ion beam. Irradiation by high energy electrons and ions lead to metallic structures from adsorbed organometallic molecules on the surface of a solid substrate. Adapted from [63].**

Briefly, EBID is a technique that consists in dissociating adsorbed precursor molecules, forming a layer with the chosen molecules/atoms. A precursor molecule is a molecule that contains the material of interest to be deposited in a solid surface. The materials of interest are usually platinum, gold, copper or tungsten [64]. The sample in the gas phase is introduced in a vacuum environment (often a scanning or a transmission

electron microscope) close to the substrate for deposition. This proximity allows the sample to be adsorbed onto the solid substrate surface [64]. The precursor molecule is then dissociated by a high energy electron beam. This dissociation will give rise to a volatile and a non-volatile constituents. The volatile fragments will be pumped out by the vacuum system, while the non-volatile fragments, corresponding to the material of interest, will remain on the substrate [64]. The dissociated molecules will afterwards be replenished by a gas injection system (see Figure 4.11) [63]. EBID technique has high spatial resolution, low resistance and it is a direct-write synthesis method for multi-dimensional deposition of nanostructures [65]. IBID technique is basically identical to EBID with the difference that in IBID an ion beam is used instead of an electron beam. EBID has the advantage that the deposits tend to have higher purity. This characteristic is attributable to the combined effects of the larger cross section for dissociation by ions, the higher ions mass and possible beam-induced local heating [64]. However, as any other technique, EBID also has shown disadvantages because it presents a top surface damage and worse spatial resolution [66].

As it was pointed out before, one of the intents/uses of the techniques describe above is the formation of metallic structures by interacting high energy electrons or ions with organometallic molecules. However, the purity of the produced layers is still far from what it is desirable, with for instance carbon, oxygen and hydrogen having concentrations greater than the expected metal structure [64,65]. The origin of these impurities can be assigned to: i) the presence of precursor fragments, ii) incomplete precursor dissociation, iii) the hydrocarbons and water present in the vacuum residual gas, iv) substrate surface decomposition, or even due to v) the decomposition of the scanning or transmission electron microscope chamber walls [64]. These impurities will influence some of the properties (e.g. resistivity) and function (e.g. catalytic activity) of the created surface [67]. Since the majority of beam processing applications are improved by having a high material purity [65], such impurities are undesirable.

Secondary electrons with low energy (LEE) are formed from the interaction of the beam produced by the techniques referred above with the metallic surface. These secondary LEEs can have a considerable role in the deterioration of the spatial resolution of the techniques referred above [68]. It is known that these secondary electrons have a low impact energy distribution typically, up to 15 eV [59]. Thus, studies of the interaction of LEEs with such compounds are important to have a full understanding on the processes that are occurring during beam deposition. This can lead in the future to optimisation of the performance of these techniques.

The following publication is based on a straight collaboration between the Institute for Ion Physics and Applied Physics, Innsbruck, Austria and colleagues from the Department of Experimental Physics in Bratislava, Slovakia. The major contribution to this publication is related to the measurement of metastable decay products. The apparatus used in Bratislava does not allow metastable decay detection. However, the double focusing mass spectrometer presented in Chapter 3 allows the detection of these species in the  $\mu$ s-time scale.

The results presented (see below full publication) concern DEA studies to tungsten hexacarbonyl ( $\text{W}(\text{CO})_6$ ) in the gas phase for electron energies in the range  $\sim 0 - 14$  eV.  $\text{W}(\text{CO})_6$  is formed by a central tungsten atom surrounded by six carbon monoxide groups (CO) (see Figure 4.12) and it belongs to the group of organometallic molecules. It is often used as a precursor in EBID to obtain structurally well-defined metal containing nanostructures [67].

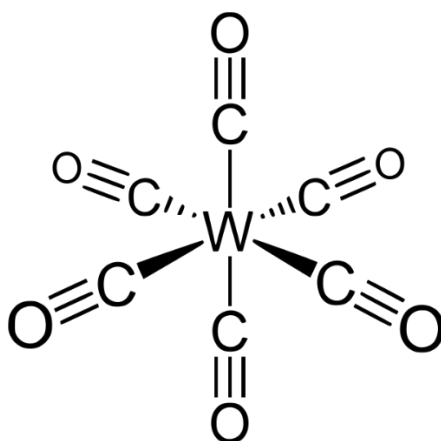


**Figure 4.12 - Schematic drawing of tungsten hexacarbonyl molecule. From [69]**

From the results obtained it was possible to observe an efficient cleavage of one or more of the CO groups and within the detection limit of the apparatus the following metastable fragments were assigned:  $\text{W}(\text{CO})_5^- \rightarrow \text{W}(\text{CO})_4^-$  and  $\text{W}(\text{CO})_4^- \rightarrow \text{W}(\text{CO})_3^-$ .

## Low-energy electron interactions with tungsten hexacarbonyl – $W(CO)_6$

K. Wnorowski<sup>2</sup>, M. Stano<sup>1</sup>, C. Matias<sup>3</sup>, S. Denifl<sup>3\*</sup>, W. Barszczewska<sup>2</sup> and Š. Matejčík<sup>1\*\*</sup>

<sup>1</sup>Department of the Experimental Physics, Comenius University, Mlynská dolina F2, 84248 Bratislava, Slovak Republic

<sup>2</sup>Department of Chemistry, Siedlce University, 3 Maja 54, 08-110 Siedlce, Poland

<sup>3</sup>Institute for Ion Physics and Applied Physics, University of Innsbruck, Technikerstrasse 25, A-6020 Innsbruck, Austria

**RATIONALE:** Low-energy secondary electrons are formed when energetic particles interact with matter. High-energy electrons or ions are used to form metallic structures from adsorbed organometallic molecules like  $W(CO)_6$  on surfaces. We investigated low-energy electron attachment to  $W(CO)_6$  in the gas phase to elucidate possible reactions during surface modification.

**METHODS:** Two crossed electron/molecular beam setups were utilised: (i) a high-resolution electron monochromator combined with a quadrupole mass spectrometer which was used for the measurement of relative cross sections as a function of the electron energy, and (ii) a double focusing mass spectrometer used for measurements of metastable decays of anions.

**RESULTS:** The study was performed in the electron energy range between ~0 and 14 eV.  $W(CO)_6$  efficiently decomposed upon attachment of a low-energy electron and no stable  $W(CO)_6^-$  anion was observed on mass spectrometric time scales. The transient negative ion formed lost instead sequentially CO ligands. The fragment anions  $W(CO)_5^-$ ,  $W(CO)_4^-$ ,  $W(CO)_3^-$ , and  $W(CO)_2^-$  were observed. However, no  $W^-$  was detectable.

**CONCLUSIONS:** Dissociative electron attachment (DEA) to  $W(CO)_6$  led to strong dissociation but a complete loss of all CO ligands was not observed in DEA. Deposit contaminations might be a direct result of DEA reactions close to the irradiation spot in beam deposition techniques. Copyright © 2012 John Wiley & Sons, Ltd.

Transition metal carbonyl complexes are substances with great potential for applications in various fields of chemistry and technology. In recent years metal carbonyl complexes have been used in the field of plasma technology for the preparation of metallic layers<sup>[1]</sup> and in nanotechnology to prepare metallic structures.<sup>[2,3]</sup> Tungsten hexacarbonyl is one of the most important molecules of this class, and due to its chemical properties is widely used to prepare tungsten layers and tungsten interconnection in the Electron Beam Induced Deposition (EBID), and Ion Beam Induced Deposition (IBID) techniques.<sup>[4,5]</sup> In these techniques high-energy electrons or ions are used to form metallic structures from adsorbed organometallic molecules on the surface of a solid substrate. However, low-energy secondary electrons are also produced by the interaction of the primary beam with the surface and thus low-energy electron scattering from surface and surface deposits may have a considerable effect, especially in causing deterioration of the spatial resolution of the techniques. As a result, only a few electron-scattering studies with surface deposits such as  $Pt(PF_3)_4$ <sup>[6,7]</sup> and  $Co(CO)_3NO$ <sup>[8]</sup> have been

carried out recently. Secondary electron distributions usually peak at low electron energies, <15 eV, where dissociative electron attachment (DEA) is an important decomposition pathway.<sup>[6]</sup> In order to understand and finally also optimise the performance of these techniques, simulations of the processes on the surface are necessary. This modelling requires low-energy electron-scattering data to take into account all processes occurring during beam deposition.

To the best of our knowledge there have been only two studies of low-energy electron interaction with tungsten hexacarbonyl. DEA to the  $W(CO)_6$  molecule was studied by George and Beauchamp,<sup>[9]</sup> who used an ion cyclotron resonance mass spectrometer to measure the rate coefficients for transition methyl carbonyls including  $W(CO)_6$  as a function of the pressure of  $CO_2$  added to relax epithermal electrons. The thermal rate coefficient for the formation of  $W(CO)_5^-$  from  $W(CO)_6$  was  $1.2 \times 10^{-7} \text{ cm}^3 \text{ molec.}^{-1} \text{ s}^{-1}$ .<sup>[9]</sup> This value indicates a very efficient process, which is comparable with electron capture by  $SF_6$ , where the thermal rate coefficient for the formation of  $SF_6^-$  is  $2.5 \times 10^{-7} \text{ cm}^3 \text{ molec.}^{-1} \text{ s}^{-1}$ .<sup>[10]</sup> Such a high rate coefficient is in good agreement with the observation of Compton and Stockdale,<sup>[11]</sup> who examined the dissociative products of  $Fe(CO)_5$  and  $Ni(CO)_4$  in gas-phase collision experiments using low-energy ( $\leq 10$  eV) electrons. They found that low-energy DEA to  $Fe(CO)_5$  and  $Ni(CO)_4$  occurs with a high probability to produce  $Fe(CO)_4^-$  and  $Ni(CO)_3^-$ .

Negative ion formation and the energies of the dissociative electron capture maxima for tungsten hexacarbonyl were studied by Winters and Kiser.<sup>[12]</sup> They investigated fragment

\* Correspondence to: S. Denifl, Institute for Ion Physics and Applied Physics, University of Innsbruck, Technikerstrasse 25, A-6020 Innsbruck, Austria.  
 E-mail: stephan.denifl@uibk.ac.at

\*\* Correspondence to: Š. Matejčík, Department of the Experimental Physics, Comenius University, Mlynská dolina F2, 84248 Bratislava, Slovak Republic.  
 E-mail: matejcik@fmph.uniba.sk

anions produced by dissociative electron capture and ion-pair formation, and reported five negative ions,  $W(CO)_6^-$ ,  $W(CO)_5^-$ ,  $W(CO)_4^-$ ,  $W(CO)_3^-$  and  $W(CO)_2^-$ , whose dissociative electron capture maxima were listed as 1.8, 2.6, 3.6, 7.5 and 10.8 eV, respectively. They also proposed a mechanism for the formation of tungsten hexacarbonyl fragments anions at 70 eV electron energy. The suggested mechanism was an ion-pair production process ( $W(CO)_5^- + CO^+$ ) followed by a series of consecutive unimolecular decomposition reactions involving the elimination of CO groups.

In this paper, we present a mass spectrometric study on free electron attachment to tungsten hexacarbonyl,  $W(CO)_6$ , in the gas phase. We have studied the energetics and reaction dynamics of the DEA reaction for this molecule. The DEA reaction is a resonant process, which proceeds via formation of a Transient Negative Ion (TNI) usually in a relatively narrow range of electron energy. The TNI may then dissociate so that fragment negative ions are finally detected:



where M represents the neutral molecule and  $M^{\#-}$  the TNI. The DEA reaction is a two-step process: in the first step an unstable transient negative ion  $M^{\#-}$  is formed, which in the second step either decays via autodetachment or decomposes into a fragment anion and neutral fragment(s).

We have studied DEA to  $W(CO)_6$  in the electron energy range from 0 to 14 eV, and have recorded the mass spectrometrically resolved ion yields as a function of electron energy for the ions with mass 324 u ( $W(CO)_6^-$ ), 296 u ( $W(CO)_5^-$ ), 268 u ( $W(CO)_4^-$ ), and 240 u ( $W(CO)_3^-$ ). It turns out that DEA leads to efficient dissociation of the molecule by cleavage of one or more CO groups. The cleavage of one CO group appears to be particularly efficient and proceeds even at thermal electron energies.

## EXPERIMENTAL

The present work was carried out using two different crossed electron/molecular beam apparatus, one at the Department of Experimental Physics in Bratislava (Slovak Republic) and the other one at the Institute for Ion Physics and Applied Physics in Innsbruck (Austria). The setup in Bratislava has already been described in detail previously<sup>13,14</sup> and therefore only a short description will be given. The electron beam is formed in a Trochoidal Electron Monochromator (TEM)<sup>15</sup> with an electron energy resolution in the present experiment of about 60 meV full width at half maximum (FWHM). A well-defined molecular beam with a narrow angular distribution function is formed by effusion of the molecules through a channel (4 mm long and 0.5 mm diameter). The molecular beam source is temperature controlled. The  $W(CO)_6$  sample (Strem Chemicals, France) was put inside the molecular beam source in the vacuum chamber; the vapor pressure of the sample was sufficient at room temperature to carry out the experiments. In the intersection zone, where the molecular beam crosses the monochromatic electron beam, negative ions were formed. The negative ions in the interaction region were extracted by a weak electric field towards the entrance of the quadrupole mass spectrometer. The mass-selected negative ions were detected, as a function of the electron energy, by a secondary electron multiplier and the

pulses were processed using a pulse-counting technique and computer. This technique allowed to observe resonance energies of DEA reactions and to estimate cross sections for the formation of the various fragment negative ions in the electron energy range from 0 to 14 eV.

The calibration of the electron energy scale and the estimation of the electron energy resolution were performed through measurement of the electron attachment (EA) process  $SF_6^-/SF_6$ . The  $W(CO)_6$  sample studied in the present experiment is a solid under normal conditions and the purity was 99%. No additional purification of the sample was carried out. All the measurements were carried out at room temperature ( $298 \pm 3$  K).

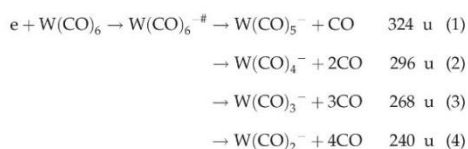
Studies of electron attachment to  $W(CO)_6$  were also carried out utilising a double focusing mass spectrometer in the Innsbruck laboratory. In brief, the setup consists of a neutral beam source, a Nier-type ion source and a double sector field mass spectrometer (for more details, see Mauracher *et al.*<sup>16</sup>). An effusive beam of  $W(CO)_6$  molecules was formed by expansion through a 2 mm capillary. This beam was crossed with an electron beam in the Nier-type ion source. The electron current used was about 10  $\mu A$  with a resolution of about 1 eV (FWHM). The anions formed were accelerated by 6 kV into the mass spectrometer. After passing a first field-free region (FF1) the anions were separated by their momentum in a magnetic sector and entered a second field-free region (FF2). Subsequently, the anions were separated by their kinetic energy in an electric sector. The mass- and energy-separated anions were detected finally by a channeltron-type secondary electron multiplier.

Two different scan techniques were used to monitor metastable decays in the FF1 and FF2.<sup>16</sup> The metastable decay of a negative ion with mass  $m_0$  in the FF1 was determined by variation of the acceleration voltage  $V$ . A metastable decay product in the FF1 (with mass  $m_1$ ) will keep its velocity; however, the kinetic energy is altered. Thus, a decay product with  $m_1$  will only pass the magnetic sector if the high voltage is increased to  $V_1 = Vm_1/m_0$ . Decays in FF2 were monitored by the mass-analyzed ion-kinetic energy (MIKE) scan technique. A negative ion with mass  $m_0$  is selected by the magnet and the electric sector field voltage is scanned. While a stable negative ion with mass  $m_0$  passes the electric sector at  $U_0$ , the anion (with mass  $m_1$ ) formed in the metastable decay of  $m_0$  passes through the electric sector at the reduced sector field voltage  $U_1 = U_0m_1/m_0$ . By these two scan techniques the metastable decay of a negative ion can be probed in different  $\mu s$ -time regimes. For example, for the  $W(CO)_5^-$  anion (324 u) the time windows between  $5 \mu s \leq t \leq 21.7 \mu s$  in FF1 and  $28.7 \mu s \leq t \leq 53.5 \mu s$  in FF2 are probed. The time regimes mentioned are proportional to the square root of the ion mass. We note that dissociation on time scales  $< 5 \mu s$  already occur in the ion source and they cannot be time-resolved in the present experiment. For comparison, the initial electron attachment process corresponds to a fast electronic transition occurring in  $\sim 10^{-16}$  s.

## RESULTS AND DISCUSSION

DEA to the  $W(CO)_6$  molecule proceeds through two steps: formation of the transient negative ion (TNI),  $W(CO)_6^{\#-}$  and dissociation of this TNI. In this study, we were not able to detect the TNI within the detection limit of the two

experiments utilised. The  $W(CO)_6^-$  anion may be observed if the autodetachment lifetime is longer than the transmission time of the ion from the reaction chamber to the detector, or if collisional or radiative stabilisation occurs prior to the detachment of the electron or dissociation of the ion. The experiment indicates that the lifetime of the  $W(CO)_6^-$  ion is shorter than the time scales of the present experiments (> tens of  $\mu$ s). To our knowledge, the observation of an intact molecular anion in the mass spectra of metal carbonyls has only been reported for  $V(CO)_6^-$ .<sup>[17]</sup> In the particular case, the  $V(CO)_6^-$  anion is stable due to attachment of the extra electron to a bonding  $t_{2g}$  orbital.<sup>[18]</sup> For other metal carbonyls including  $W(CO)_6^-$ , the TNI is not stable, because the extra electron must occupy an anti-bonding  $e_g$  orbital. The resulting states may actually be repulsive with respect to loss of a CO group and may be distorted sufficiently to inhibit electron autodetachment. A similar finding can be applied for other transition metal carbonyls, e.g.,  $Cr(CO)_6^-$ ,  $Fe(CO)_5^-$  or  $Ni(CO)_4^-$ .<sup>[19]</sup> In the present work we observed four dissociative channels:



The ion yields for the formation of the negative ions,  $W(CO)_5^-$ ,  $W(CO)_4^-$ ,  $W(CO)_3^-$  and  $W(CO)_2^-$  with masses 324, 296, 268 and 240 u, respectively, i.e., DEA associated with abstraction of one or more CO groups from the TNI, are shown in Fig. 1. These measurements represent relative cross-sections for the DEA channels (1)–(4). The cross-sections are given in arbitrary units; however, the values can be compared, i.e., they reflect the efficiencies of these reaction channels. One can see in Fig. 1 that the efficiency of the DEA process decreased with the number of carbonyl groups detached. The experimental appearance energies of the tungsten hexacarbonyl ions are summarised in Table 1. These values were derived from the relative cross-sections using a fitting routine, which also took into account the energy resolution of the electron beam (for more details, see Denifl *et al.*,<sup>[19]</sup>). The most favourable reaction channel (1) is related to the formation of  $W(CO)_5^-$  (324 u), by removal of one carbonyl group. The formation of this ion is most efficient in the thermal electron energy range. This is in accordance with the studies of George and Beauchamp,<sup>[9]</sup> who investigated thermal rate constants for the formation of  $W(CO)_5^-$  from  $W(CO)_6^-$ . The second fragment ion  $W(CO)_4^-$  (296 u) has a threshold at 0.9 eV, the third  $W(CO)_3^-$  (268 u) at  $\sim$ 2.9 eV and the fourth  $W(CO)_2^-$  (240 u) at  $\sim$ 6.5 eV.

The DEA reaction in  $W(CO)_6^-$  proceeds via several resonances. The resonance positions for all the fragment anions obtained are listed in Table 1. We note that the values obtained with the double focusing mass spectrometer agree within  $\pm 0.3$  eV for all the anions except  $W(CO)_5^-$  where the deviation is about 0.5 eV (see discussion below). The values presented by Winters and Kiser<sup>[12]</sup> are also listed for comparison in the table.

In our study the reaction channel (1) associated with cleavage of one CO group had a very high relative cross-section at energies close to 0 eV. In the ion yield curve we can

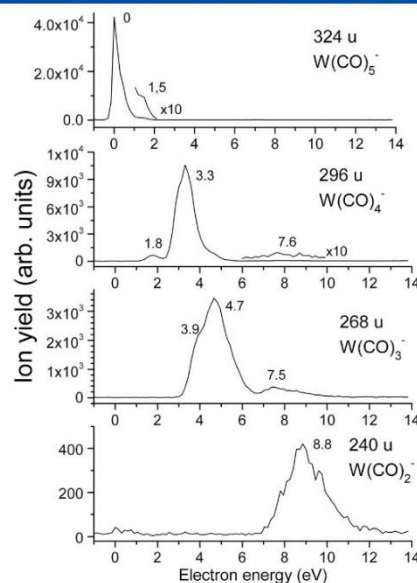


**Figure 1.** Ion efficiency curves of negatively charged fragments formed by dissociative electron attachment to tungsten hexacarbonyl measured with the electron monochromator.

recognise an additional structure at  $\sim$ 1.5 eV (see Table 1). The high reaction efficiency already occurring at thermal energies implicates possible exothermicity of this reaction channel, i.e., the W–CO bond energy is lower than the electron affinity of the  $W(CO)_5^-$  fragment. Moreover, it should be noted that the electron capture cross-section increases reciprocally with the electron energy, and cross-sections at energies close to 0 eV may be particularly high due to s-wave capture. In contrast to our study, Winters and Kiser<sup>[12]</sup> reported only one resonance, located at 1.8 eV.

The reaction channel (2) associated with cleavage of two CO groups has a threshold at 0.9 eV and three resonances are present in the ion yield curve at 1.8 and 3.3 eV, and a weak resonance at approximately 7.6 eV. The fragment ion  $W(CO)_4^-$  was also reported by Winters and Kiser.<sup>[12]</sup> However, only one resonance for the reaction channel (2) at 2.6 eV was mentioned by that group.

The abstraction of three CO groups is associated with reaction channel (3). The threshold for this channel is at 2.9 eV and three resonances at 3.9, 4.7 and 7.5 eV can be derived from the ion yield curve. Winters and Kiser<sup>[12]</sup> also listed for  $W(CO)_3^-$  only one resonance, located at 3.6 eV. The yield for the  $W(CO)_2^-$  ion exhibits two resonances, the first close to about 0 eV electron energy and the second at 8.8 eV. For energetic reasons the low-energy resonance is likely to be an artefact formed by electron attachment to impurities in the sample. Based on the isotope-resolved mass spectra measured with the double sector field instrument, this impurity can be identified as  $Mo(CO)_6^-$  which forms  $Mo(CO)_5^-$  at mass 240 u via DEA. The high-energy resonance is associated with

**Table 1.** Appearance energies (AE) and the resonance positions for all fragment anions observed in the present DEA study with  $W(CO)_6^-$ . The peak maximum of the most abundant resonance is underlined for the different fragment anions

Ion	m (u)	Neutral fragments	AE (eV)	Resonances (eV)					
				This work				Ref. [121]	
$W(CO)_5^-$	324	CO	0	<u>0</u>	1.5	-	-	-	1.8
$W(CO)_4^-$	296	2.CO	$0.9 \pm 0.1$	-	1.8	<u>3.3</u>	-	7.6	2.6
$W(CO)_3^-$	268	3.CO	$2.9 \pm 0.1$	-	-	<u>3.9</u>	<u>4.7</u>	7.5	3.6
$W(CO)_2^-$	240	4.CO	$6.5 \pm 0.1$	-	-	-	-	8.8	7.5
$W(CO)^-$	212	5.CO	-	-	-	-	-	-	10.8

cleavage of four CO groups from  $W(CO)_6^-$ , i.e., reaction (4). Again, in this case, the resonance position differs from that of Winters and Kiser,<sup>[121]</sup> who reported a resonance located at 7.5 eV.

Finally, we would like to point out that, in contrast to the previous study by Winters and Kiser,<sup>[121]</sup> we do not observe any production of an anion at mass 212 u, which can be ascribed to  $W(CO)^-$ . We do obtain an ion yield at this mass and nearby masses; however, this mass region is also contaminated by anions formed by DEA to the  $Mo(CO)_6^-$  impurity present in the sample ( $Mo(CO)_4^-$  at 212 u). In addition, no indication of the formation of the  $W^-$  ion is found. Comparing all the resonance positions found in this study with those published by Winters and Kiser,<sup>[121]</sup> it turns out that the peak positions of the strongest resonance for  $W(CO)_5^-$ ,  $W(CO)_3^-$  and  $W(CO)_4^-$  are systematically lower than the maxima reported in Winters and Kiser.<sup>[121]</sup> This deviation can probably be ascribed to the calibration of the electron energy scale in the previous study where the scale was calibrated using a DEA peak maximum of 5.98 eV for  $O^-/O_2^-$ . However, a more recent high-resolution study on DEA to oxygen reported a peak maximum of 6.5 eV for  $O^-$ .<sup>[20]</sup>

For  $W(CO)_5^-$  the opposite tendency can be observed (here maximum at about 0 eV, whereas a value of 1.8 eV was reported by Winters and Kiser<sup>[121]</sup>). We note in particular that the low-energy region close to 0 eV is difficult to access with standard ion sources as used by Winters and Kiser,<sup>[121]</sup> and here in the Innsbruck setup. For example, the electron beam is prone to space charge limitations which may lead to vanishing electron currents close to 0 eV and subsequently to blue-shifts of peaks. In the presently utilised setups magnetic guiding fields ensure the sustainment of electron currents close to 0 eV. This is particularly the case for the trochoidal electron monochromator where a pronounced 0 eV maximum can be obtained for  $W(CO)_5^-$ . Another remarkable difference from the results of Winters and Kiser<sup>[121]</sup> is the number of resonances reported for the various fragment anions. In the present study we can obtain up to three resonances in the respective ion yields while Winters and Kiser<sup>[121]</sup> reported only one resonance for each fragment anion. A possible explanation for this discrepancy (see Table 1) is the lower sensitivity of the experimental setup used by Winters and Kiser,<sup>[121]</sup> i.e., only the main resonances were observed and the other weak resonances were below the detection limit of the apparatus used.

The appearance energies of fragment anions obtained in this work may be used for estimation of the electron affinities of the  $W(CO)_x^-$  ( $x=2, 3, 4, 5$ ) fragments. Previously we have

measured the appearance energies (AEs) of positive ions formed via electron ionisation (EI) of  $W(CO)_6^-$ .<sup>[21]</sup> On the basis of the AE values for EI of  $W(CO)_6^-$ , thermochemical data were calculated by Wnorowski *et al.*<sup>[21]</sup> According to our EI studies, the average value of the W–CO bond dissociation energy is  $2.15 \pm 0.01$  eV in the molecule and  $2.07 \pm 0.02$  eV in  $W(CO)_6^-$ . We can expect that in the anion the average BDE is about 2 eV. On the basis of this value we have used the following formula to obtain a rough estimate for the electron affinities of the fragments formed:

$$EA(W(CO)_x^-) = AE(W(CO)_x^-) - (6-x) \cdot BDE(W-CO) \quad (I)$$

where EA denotes the electron affinity of the fragment, AE the appearance energy of the anion (see Table 1), and BDE is the bond dissociation energy of the W–CO bond (~2 eV).

Using equation (I) we have obtained the electron affinities of the  $W(CO)_x^-$  ( $x=2, 3, 4, 5$ ) fragments. The present values of EA are  $EA(W(CO)_5^-) \leq 2$  eV,  $EA(W(CO)_4^-) \leq 3.1$  eV,  $EA(W(CO)_3^-) \leq 3.1$  eV and  $EA(W(CO)_2^-) \leq 1.5$  eV. We note that these values give only rough estimates of the electron affinities due to the uncertainties of the BDE in the anions and represent the lower limit of the true values. To obtain more precise values it would be necessary to use more rigorous methods of EA estimation (see also Rayner *et al.*<sup>[22]</sup>).

As described in the Experimental section the Innsbruck setup allows the study of metastable decays in the  $\mu$ s-time regime. Within the detection limit of the apparatus we can observe two metastable decays:

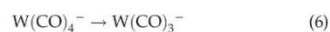
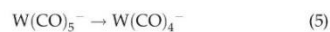
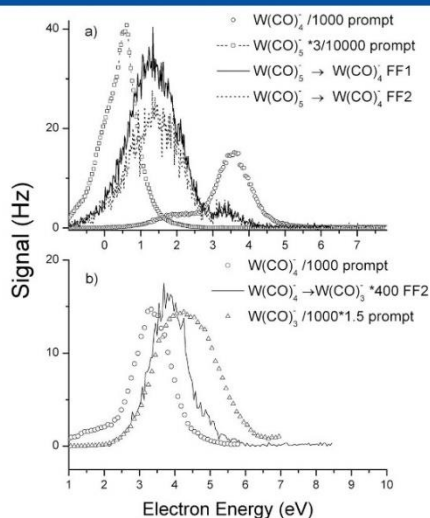


Figure 2(a) shows the electron energy dependence for the metastable reaction (5) in FF1 and FF2 (as mentioned in the Experimental section, this corresponds to a time window for the decay of  $W(CO)_5^-$  between  $5 \mu s \leq t \leq 21.7 \mu s$  (FF1) and  $28.7 \mu s \leq t \leq 53.5 \mu s$  (FF2)). Faster decays do occur in the ion source and these we call 'prompt fragment anions'; the corresponding yields for the formation of the prompt  $W(CO)_4^-$  and  $W(CO)_5^-$  anions are also included in Fig. 2. The metastable peaks are located between the maxima of the ion yields for prompt  $W(CO)_5^-$  and prompt  $W(CO)_4^-$ . Based on this result we conclude that the ion yield close to 0 eV for prompt  $W(CO)_5^-$  and the first resonance for prompt  $W(CO)_4^-$  at about 1.8 eV arise from the same resonance of the TNI. Such a conclusion can be drawn if we



Low-energy electron interactions with  $W(CO)_6$ 

**Figure 2.** Electron energy dependence for the metastable decay reaction (5) in FF1 and FF2 (a) and for the metastable decay reaction (6) in FF2 (b). For comparison, the prompt ion yields for the involved fragment anions are shown.

assume a unimolecular consecutive decomposition process of the TNI, where excess energy (deposited by the captured electron) is randomised in the vibrational degrees of freedom of the molecule before dissociation starts. At lower energies the excess energy is not sufficient for a prompt two-fold bond cleavage (occurring on a time scale  $< \sim 5 \mu\text{s}$ ), i.e., after one  $W-CO$  bond cleavage, the  $W(CO)_5^-$  anion formed remains stable. At higher electron energies close to 2 eV, the excess energy is now high enough for prompt formation of  $W(CO)_4^-$ . The second peak at 3.2 eV in the metastable anion yield is ascribed to a different electronic state which is correlated to the second resonance in the prompt ion yields for  $W(CO)_4^-$  and  $W(CO)_5^-$ . In this case also, the metastable peak is located energetically between the peaks of the prompt anions.

The electron energy dependence for metastable decay reaction (6),  $W(CO)_4^- \rightarrow W(CO)_3^-$ , is shown in Fig. 2(b). The metastable decay was measured with the MIKE scan technique, i.e., it corresponds to the decay in FF2 in the time window,  $27.4 \mu\text{s} \leq t \leq 51.1 \mu\text{s}$ . We observe one peak at about 3.8 eV in the metastable yield, which again lies between the main resonances of the involved prompt anions (3.5 eV for  $W(CO)_4^-$  and 4.7 eV for  $W(CO)_3^-$ ). This result indicates that the decomposition into either  $W(CO)_4^-$  or  $W(CO)_3^-$  also strongly depends on the excess energy deposited in the TNI. The occurrence of metastable reaction (6) moreover indicates that  $W(CO)_3^-$  is formed in a sequential decay process with subsequent loss of CO groups.

As mentioned in the Introduction,  $W(CO)_6$  is widely used in EBID and IBID applications to form metallic structures from adsorbed organometallic molecules on surfaces. It has been recently recognised that the low-energy secondary

electrons formed may play an important role in the dissociation of the organometallic molecules and the formation of metallic structures on the surfaces. For example, in EBID secondary electrons are formed in a considerable amount: of 0.1 secondary electrons per primary electron per eV.<sup>[23]</sup> The width of the deposits achievable is in the nm-region down to 0.7 nm, i.e., a few times larger than the typical spot size of  $\sim 0.2$  nm of a focused primary beam.<sup>[24]</sup> Reactions of low-energy electrons could be responsible for the deterioration of the resolution for these techniques as discussed recently in Engmann *et al.*<sup>[8]</sup> Another problem in EBID and IBID is contamination caused by metallic deposits. For example, it was suggested that  $WF_6$  should result in higher purity of the tungsten deposit than  $W(CO)_6$  due to the lack of carbon.<sup>[25]</sup> The former compound is, however, toxic and corrosive.<sup>[25]</sup> Considering the reactivity of low secondary electrons, the present results identify that DEA is a possible source of deposit contamination. Here we observe that (efficient) removal of only one or few CO groups occurs upon DEA, but the bare  $W^-$  anion cannot be observed within the detection limit of the setups utilised. In contrast, electron ionisation leads to efficient formation of bare  $W^+$  above the threshold of about 21 eV.<sup>[21]</sup> Thus, incomplete loss of CO ligands upon DEA may be responsible for the contaminations of deposits especially on the edge of the deposit.

Recent DEA studies on organometallic molecules like Pt( $PF_3$ )<sub>4</sub><sup>[7]</sup> and  $Co(CO)_3NO$ <sup>[8]</sup> showed no stable  $Pt(PF_3)_4^-$  and  $Co(CO)_3NO^-$  anions within the detection limit of the setups used. Moreover, the molecules studied in these works<sup>[7,8]</sup> also strongly dissociated upon electron capture as observed here in the case of  $W(CO)_6$ . However, for  $Pt(PF_3)_4$  and  $Co(CO)_3NO$  even complete ligand loss from the TNI occurred and the bare metallic fragment anion was observed weakly. We note that this is in particular contrast to the present results for  $W(CO)_6$ .

## CONCLUSIONS

We have measured DEA to tungsten hexacarbonyl in the electron energy range from thermal up to 14 eV. The DEA reaction proceeds via CO bond cleavages from the transient negative ion. A captured electron may lead to the dissociation of up to four CO groups from  $W(CO)_6$ . We have estimated the values of the electron affinities of  $W(CO)_x$  fragments based on experimentally obtained appearance energies of fragment anions and bond dissociation energies. The positions of the most abundant resonances differ from previously reported values which can be ascribed to a different calibration of the electron energy scale. The study of metastable decays allowed the assignment of resonances for prompt anions to common electronic states which decay by vibrational predissociation.

Considering the role of  $W(CO)_6$  for EBID and IBID applications we note that in contrast to positive ionisation, the complete loss of all CO ligands cannot be observed in DEA within the detection limit of the setups utilised. Hence the present study may identify DEA as a source for deposit contaminations. A study like the present one contributes to a better fundamental understanding of EBID and IBID processes on the molecular level with the long-term goal of optimising the deposition technique.

### Acknowledgements

This work was supported by the Slovak Research and Development Agency (Project No. APVV-0365-07), Slovak Grant Agency VEGA (Project No. 1/0379/11) and is also the result of the project implementation: 26240120012, 26240120026 and 2622020004 supported by the Research & Development Operational Programme funded by the ERDF. Work was partially supported by the COST Action CM0601 "Electron Controlled Chemical Lithography" (ECCL).

### REFERENCES

- [1] K. K. Lai, H. H. Lamb. Tungsten chemical vapor deposition using tungsten hexacarbonyl: microstructure of as-deposited and annealed films. *Thin Solid Films* **2000**, *370*, 114.
- [2] C. W. Hagen, W. F. van Dorp, P. A. Crozier, P. Kruit. Electronic pathways in nanostructure fabrication. *Surf. Sci.* **2008**, *602*, 3212.
- [3] K. E. Lewis, D. M. Golden, G. P. Smith. Organometallic bond dissociation energies: laser pyrolysis of iron pentacarbonyl, chromium hexacarbonyl, molybdenum hexacarbonyl, and tungsten hexacarbonyl. *J. Am. Chem. Soc.* **1984**, *106*, 3905.
- [4] I. J. Luxmoore, I. M. Ross, A. G. Cullis, P. W. Fry, J. Orr, P. D. Buckle, J. H. Jefferson. Low temperature electrical characterisation of tungsten nano-wires fabricated by electron and ion beam induced chemical vapour deposition. *Thin Solid Films* **2007**, *515*, 6791.
- [5] M. Song, K. Furuya. Fabrication and characterization of nanostructures on insulator substrates by electron-beam-induced deposition. *Sci. Technol. Adv. Mater.* **2008**, *9*, 023002.
- [6] M. Allan. Electron scattering in Pt(PF<sub>3</sub>)<sub>4</sub>: Elastic scattering, vibrational, and electronic excitation. *J. Chem. Phys.* **2011**, *134*, 204309.
- [7] O. May, D. Kubala, M. Allan. Dissociative electron attachment to Pt(PF<sub>3</sub>)<sub>4</sub> – a precursor for focused electron beam induced processing (FEBIP). *Phys. Chem. Chem. Phys.* **2012**, *14*, 2979.
- [8] S. Engmann, M. Stano, S. Matejčík, O. Ingolfsson. The role of dissociative electron attachment in focused electron beam induced processing: A case study on cobalt tricarbonyl nitrosyl. *Angew. Chem. Int. Ed. Engl.* **2011**, *50*, 9475.
- [9] P. M. George, J. L. Beauchamp. Dissociative electron attachment reactions of transition metal carbonyls and their apparent influence on the thermalization of electrons by CO<sub>2</sub>. *J. Chem. Phys.* **1982**, *76*, 2959.
- [10] I. Szamrej, M. Forys. The electron swarm method as a tool to investigate multi-body electron attachment processes. *Radiat. Phys. Chem.* **1989**, *33*, 393.
- [11] R. N. Compton, J. A. D. Stockdale. Formation of gas-phase negative ions in Fe(CO)<sub>5</sub> and Ni(CO)<sub>4</sub>. *Int. J. Mass Spectrom. Ion Phys.* **1976**, *22*, 51.
- [12] R. E. Winters, R. W. Kiser. Unimolecular decomposition of negative ions formed from the transition-metal carbonyls of Ni, Fe, Cr, Mo, and W. *J. Chem. Phys.* **1966**, *44*, 1964.
- [13] S. Matejčík, V. Foltin, M. Stano, J. D. Skalny. Temperature dependencies in dissociative electron attachment to CCl<sub>4</sub>, CCl<sub>2</sub>F<sub>2</sub>, CHCl<sub>3</sub> and CHBr<sub>3</sub>. *Int. J. Mass Spectrom.* **2003**, *223/224*, 9.
- [14] P. Papp, J. Urban, S. Matejčík, M. Stano, O. Ingolfsson. Dissociative electron attachment to gas phase valine: A combined experimental and theoretical study. *J. Chem. Phys.* **2006**, *125*, 204301.
- [15] A. Stamatovic, G. J. Schulz. Characteristics of trochoidal electron monochromator. *Rev. Sci. Instrum.* **1970**, *41*, 423.
- [16] A. Mauracher, S. Denifl, A. Edtbauer, M. Hager, M. Probst, O. Echt, T. D. Märk, P. Scheier, T. A. Field, K. Graupner. Metastable anions of dinitrobenzene: Resonances for electron attachment and kinetic energy release. *J. Chem. Phys.* **2010**, *133*, 244302.
- [17] R. L. Sullivan, M. S. Lupin, R. W. Kiser. Negative parent ion in mass spectrum of hexacarbonylvanadium. *J. Chem. Soc. D* **1969**, *12*, 655.
- [18] F. P. Pruchnik. *Organometallic Chemistry of the Transition Elements*, Plenum Press, New York, **1990**.
- [19] S. Denifl, S. Matejčík, J. D. Skalny, M. Stano, P. Mach, J. Urban, P. Scheier, T. D. Märk, W. Barszczewska. Electron impact ionization of C<sub>3</sub>H<sub>8</sub>: appearance energies and temperature effects. *Chem. Phys. Lett.* **2005**, *402*, 80.
- [20] S. Matejčík, A. Kiendler, P. Cicman, J. Skalny, P. Stampfli, E. Illenberger, Y. Chu, A. Stamatovic, T. D. Märk. Electron attachment to molecules and clusters of atmospheric relevance: Oxygen and ozone. *Plasma Sources Sci. Technol.* **1997**, *6*, 140.
- [21] K. Wnorowski, M. Stano, W. Barszczewska, A. Jówko, Š. Matejčík. Electron ionization of W(CO)<sub>6</sub>: Appearance energies. *Int. J. Mass Spectrom.* **2012**, *314*, 42.
- [22] D. M. Rayner, Y. Ishikawa, C. E. Brown, P. A. Hackett. Branching ratios and bond dissociation energies from the excimer laser photolysis of group 6 metal carbonyls. *J. Chem. Phys.* **1991**, *94*, 5471.
- [23] I. Utke, P. Hoffmann, J. Melngailis. Gas-assisted focused electron beam and ion beam processing and fabrication. *J. Vac. Sci. Technol. B* **2008**, *26*, 1197, and references cited therein.
- [24] W. F. van Dorp, I. Lazic, A. Beyer, A. Götzhäuser, J. B. Wagner, T. W. Hansen, C. W. Hagen. Ultrahigh resolution focused electron beam induced processing: the effect of substrate thickness. *Nanotechnology* **2011**, *22*, 115303.
- [25] S. J. Randolph, J. D. Fowlkes, P. D. Rack. Focused, nanoscale electron-beam-induced deposition and etching. *Crit. Rev. Solid State Mater. Sci.* **2006**, *31*, 55.

## **References**

- [1] Y. Yildirim, M. Balcan, A. Kinal, A.D. Bass, P. Cloutier, L. Sanche, *Eur. Phys. J. D* 66 (2012) 12.
- [2] B. Boudaïffa, P. Cloutier, D. Hunting, M.A. Huels, L. Sanche, *Science* 287 (2000) 1658.
- [3] S.M. Pimblott, J.A. LaVerne, *Radiation Physics and Chemistry* 76 (2007) 1244.
- [4] L. Sanche, *Mass Spectrom. Rev.* 21 (2002) 349.
- [5] S. Gohlke, E. Illenberger, *Europhysics News* 33 (2002) 207.
- [6] I. Baccarelli, I. Bald, F.A. Gianturco, E. Illenberger, J. Kopyra, *Phys. Rep.-Rev. Sec. Phys. Lett.* 508 (2011) 1.
- [7] M. Joiner, A.v.d. Kogel, *Basic Clinical Radiobiology*, Hodder Arnold, Great Britain, London, 2009.
- [8] K. Rothkamm, M. Kuhne, P.A. Jeggo, M. Lobrich, *Cancer Res.* 61 (2001) 3886.
- [9] P.L. Olive, *Radiat. Res.* 150 (1998) S42.
- [10] C.v. Sonntag, *The Chemical Basis for Radiation Biology*, Taylor and Francis, London, 1987.
- [11] L. Sanche, *Nature* 461 (2009) 358.
- [12] M.A. Huels, B. Boudaïffa, P. Cloutier, D. Hunting, L. Sanche, *Journal of the American Chemical Society* 125 (2003) 4467.
- [13] B.D. Michael, P. O'Neill, *Science* 287 (2000) 1603.
- [14] J.K. Wolken, E.A. Syrstad, S. Vivekananda, F. Turecek, *Journal of the American Chemical Society* 123 (2001) 5804.
- [15] S. Ptasinska, S. Denifl, V. Grill, T.D. Mark, E. Illenberger, P. Scheier, *Phys. Rev. Lett.* 95 (2005) 4.
- [16] L. Sanche, *Eur. Phys. J. D* 35 (2005) 367.

## *Results and discussion*

- [17] S. Denifl, S. Ptasinska, M. Probst, J. Hrusak, P. Scheier, T.D. Mark, *J. Phys. Chem. A* 108 (2004) 6562.
- [18] D. Almeida, D. Kinzel, F.F. da Silva, B. Puschnigg, D. Gschliesser, P. Scheier, S. Denifl, G. Garcia, L. Gonzalez, P. Limao-Vieira, *Phys. Chem. Chem. Phys.* 15 (2013) 11431.
- [19] S. Ptasinska, S. Denifl, B. Mroz, M. Probst, V. Grill, E. Illenberger, P. Scheier, T.D. Mark, *J. Chem. Phys.* 123 (2005) 8.
- [20] S. Denifl, S. Ptasinska, G. Hanel, B. Gstir, M. Probst, P. Scheier, T.D. Mark, *J. Chem. Phys.* 120 (2004) 6557.
- [21] D. Almeida, F.F. da Silva, G. Garcia, P. Limao-Vieira, *Phys. Rev. Lett.* 110 (2013) 5.
- [22] S. Denifl, F. Zappa, A. Mauracher, F.F. da Silva, A. Bacher, O. Echt, T.D. Mark, D.K. Bohme, P. Scheier, *ChemPhysChem* 9 (2008) 1387.
- [23] V. Aquillanti, M. Ragni, A.C.P. Bitencourt, G.S. Maciel, F.V. Prudente, *J. Phys. Chem. A* 113 (2009) 3804.
- [24] P. Limao-Vieira, S. Eden, P.A. Kendall, N.J. Mason, S.V. Hoffmann, *Chem. Phys. Lett.* 366 (2002) 343.
- [25] E.A. Drage, P. Cahillane, S.V. Hoffmann, N.J. Mason, P. Limao-Vieira, *Chem. Phys.* 331 (2007) 447.
- [26] R.B. Bernini, L.B.G. da Silva, F.N. Rodrigues, L.H. Coutinho, A.B. Rocha, G.G.B. de Souza, *J. Chem. Phys.* 136 (2012) 7.
- [27] H. Abdoul-Carime, L. Sanche, *J. Phys. Chem. B* 106 (2002) 12186.
- [28] <http://de.wikipedia.org/wiki/Dimethyldisulfid>, (Accessed August 2014).
- [29] <http://www.nobelprize.org>, (Accessed September 2014).
- [30] S.D. Dai, C. Schwendtmayer, P. Schurmann, S. Ramaswamy, H. Eklund, *Science* 287 (2000) 655.
- [31] H. Nakamura, K. Nakamura, J. Yodoi, *Annu. Rev. Immunol.* 15 (1997) 351.

- [32] A. Baker, C.M. Payne, M.M. Briehl, G. Powis, *Cancer Res.* 57 (1997) 5162.
- [33] G.A. Rickard, J. Bergès, C. Houèe-Levin, A. Rauk, *The Journal of Physical Chemistry B* 112 (2008) 5774.
- [34] A. Modelli, D. Jones, G. Distefano, M. Tronc, *Chem. Phys. Lett.* 181 (1991) 361.
- [35] C. Dezarnaud-Dandine, F. Bournel, M. Tronc, D. Jones, A. Modelli, *J. Phys. B-At. Mol. Opt. Phys.* 31 (1998) L497.
- [36] C.A. Mayhew, P. Sulzer, F. Petersson, S. Haidacher, A. Jordan, L. Mark, P. Watts, T.D. Mark, *Int. J. Mass Spectrom.* 289 (2010) 58.
- [37] C. Mullen, A. Irwin, B.V. Pond, D.L. Huestis, M.J. Coggiola, H. Oser, *Anal. Chem.* 78 (2006) 3807.
- [38] C. Mullen, M.J. Coggiola, H. Oser, *J. Am. Soc. Mass Spectrom.* 20 (2009) 419.
- [39] L.G. Song, A.D. Wellman, H.F. Yao, J.E. Bartmess, *J. Am. Soc. Mass Spectrom.* 18 (2007) 1789.
- [40] J. Florián, L. Gao, V. Zhukhovskyy, D.K. MacMillan, M.P. Chiarelli, *J. Am. Soc. Mass Spectrom.* 18 (2007) 835.
- [41] P. Sulzer, F. Petersson, B. Agarwal, K.H. Becker, S. Jurschik, T.D. Mark, D. Perry, P. Watts, C.A. Mayhew, *Anal. Chem.* 84 (2012) 4161.
- [42] J.A. Laramee, P. Mazurkiewicz, V. Berkout, M.L. Deinzer, *Mass Spectrom. Rev.* 15 (1996) 15.
- [43] S. Boumsellek, S.H. Alajajian, A. Chutjian, *J. Am. Soc. Mass Spectrom.* 3 (1992) 243.
- [44] R.G. Ewing, D.A. Atkinson, G.A. Eiceman, G.J. Ewing, *Talanta* 54 (2001) 515.
- [45] D.C. Collins, M.L. Lee, *Anal. Bioanal. Chem.* 372 (2002) 66.
- [46] D.S. Moore, *Rev. Sci. Instrum.* 75 (2004) 2499.
- [47] Existing and Potential Standoff Explosives Detection Techniques, The National Academies Press, 2004.

*Results and discussion*

- [48] E. Schramm, A. Kurten, J. Holzer, S. Mitschke, F. Muhlberger, M. Sklorz, J. Wieser, A. Ulrich, M. Putz, R. Schulte-Ladbeck, R. Schultze, J. Curtius, S. Borrmann, R. Zimmermann, *Anal. Chem.* 81 (2009) 4456.
- [49] J. Puton, M. Nousiainen, M. Sillanpaa, *Talanta* 76 (2008) 978.
- [50] G.A. Eiceman, Z. Karpas, *Ion Mobility Spectrometry*, Boca Raton, Fl, 2005.
- [51] G.A. Eiceman, Z. Karpas, H.H.H. Jr., *Ion Mobility Spectrometry*, CRC Press, Boca Raton, 2013.
- [52] C.J. Proctor, J.F.J. Todd, *Anal. Chem.* 56 (1984) 1794.
- [53] <http://en.wikipedia.org/wiki/Enflurane>, (Accessed August 2014).
- [54] <http://en.wikipedia.org/wiki/Isoflurane>, (Accessed August 2014).
- [55] F.W. Karasek, O.S. Tatone, D.W. Denney, *Journal of Chromatography* 87 (1973) 137.
- [56] <http://en.wikipedia.org/wiki/Hexachloroethane>, (Accessed August 2014).
- [57] <http://en.wikipedia.org/wiki/Pentachloroethane>, (Accessed August 2014).
- [58] I.J. Luxmoore, I.M. Ross, A.G. Cullis, P.W. Fry, J. Orr, P.D. Buckle, J.H. Jefferson, *Thin Solid Films* 515 (2007) 6791.
- [59] M.H. Song, K. Furuya, *Sci. Technol. Adv. Mater.* 9 (2008) 10.
- [60] K.K. Lai, H.H. Lamb, *Thin Solid Films* 370 (2000) 114.
- [61] C.W. Hagen, W.F. van Dorp, P.A. Crozier, P. Kruit, *Surf. Sci.* 602 (2008) 3212.
- [62] K.E. Lewis, D.M. Golden, G.P. Smith, *Journal of the American Chemical Society* 106 (1984) 3905.
- [63] S. Engmann, PhD thesis, University of Iceland, Iceland, 2013.
- [64] A. Botman, J.J.L. Mulders, C.W. Hagen, *Nanotechnology* 20 (2009) 17.
- [65] N.A. Roberts, C.M. Gonzalez, J.D. Fowlkes, P.D. Rack, *Nanotechnology* 24 (2013) 6.

*Results and discussion*

- [66] S. Matsui, T. Kaito, J. Fujita, M. Komuro, K. Kanda, Y. Haruyama, J. Vac. Sci. Technol. B 18 (2000) 3181.
- [67] S.G. Rosenberg, M. Barclay, D.H. Fairbrother, Phys. Chem. Chem. Phys. 15 (2013) 4002.
- [68] N. Silvis-Cividjian, C.W. Hagen, P. Kruit, Journal of Applied Physics 98 (2005).
- [69] <http://de.wikipedia.org/wiki/Wolframhexacarbonyl>, (Accessed August 2014).

# 5. Conclusions and further work

---

This thesis presents experimental gas-phase studies on dissociative electron attachment (DEA) and electron transfer processes in biological and technological relevant molecules. The main achievements in DEA experiments are related to several new anionic yields as a function of the electron impact energy, revealing therefore the nature of resonances involved in the temporary negative ion prior to fragmentation. Although electron transfer experiments are just a small fraction of this thesis since the main focus was on DEA processes, the unprecedented results on  $\text{NCO}^-$  formation in atom-molecule collision experiments in N1 and N3 methylated pyrimidines, has allowed to propose a concerted fragmentation mechanism within the pyrimidine ring. This chapter is divided into two sub-chapters, Biomolecules and Technologically relevant molecules, where the main achievements are briefly presented and to finish some perspectives for future work are presented.

## 5.1. Biomolecules

### 5.1.1. Comparative studies of potassium and electron collisions with biomolecules: site selectivity

A joint research study from Innsbruck, Lisbon and Reykjavik, using different but complementary methodologies, have been focused on DEA, electron transfer and matrix assisted laser desorption/ionisation experiments, respectively, to N-site methylated pyrimidine bases (thymine and uracil). Since the major focus of this thesis has been on DEA experiments and a minor contribution on electron transfer by atom-molecule collisions, the conclusions are restricted to these two experiments only. These novel studies have explored the intramolecular routes leading to site- and bond-selectivity in  $\text{NCO}^-$  formation. This is the dominant fragment anion formed upon DEA to gas phase thymine at electron energies of  $\sim 4$  eV, the only fragment observed in metastable decay of deprotonated thymine in MALDI and, in the case of potassium-N-site methylated pyrimidine collisions,  $\text{NCO}^-$  is the most abundant fragment anion for collision energies above 30 eV in the lab frame. The DEA results directly confirm that  $\text{NCO}^-$  is formed in a



sequential decay reaction with the dehydrogenated closed shell anion as the intermediate product. Of relevance, it was shown that the remarkable site selectivity in the  $H^-$  and  $[M - H]^-$  reaction channels in the pyrimidine bases is preserved for the subsequent decay reaction into  $NCO^-$ . Furthermore, this is true even if the decay takes place several tens of microseconds after the initial electron attachment process.

From the electron transfer experiments in potassium collisions with N-site methylated pyrimidines, the  $NCO^-$  branching ratios obtained show remarkable site- and bond-selectivity in this decay channel. In the case of N-site methylated uracil, the selectivity is verified for all collision energies. However for N-site methylated thymine the selectivity depends strongly on the collision energy. The dwell time of the potassium cation in the Coulomb complex will dictate the fragmentation pathways leading to the  $NCO^-$  formation. For longer collision times, some fragmentation channels are not accessible without cation stabilization, whereas for shorter collision times, they are blocked. In the latter situation, the selectivity of the  $NCO^-$  formation is clearly visible. This study has shown for the first time that site-selectivity in molecular fragmentation upon electron transfer can be conserved, even in complex, concerted reaction mechanisms that require multiple bond breaking.

When thymine and uracil are methylated at the N1 position, there are two fragmentation pathways involving ring break yielding  $NCO^-$  formation. However, in order to completely distinguish  $NCO^-$  formation from thymine and uracil, an alternative route is to explore the decomposition mechanisms of thiothymine and thiouracil, respectively. Thiothymine and thiouracil are molecules similar to thymine and uracil, respectively, where for the formers the oxygen (O) atom bonded to C2 is replaced by a sulphur (S) atom (see Figure 5.1).

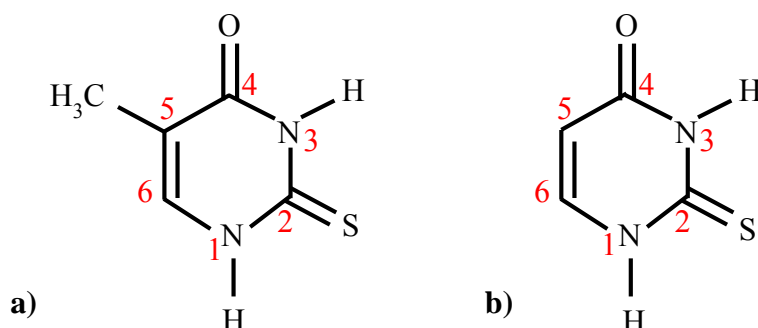


**Figure 5.1 – Schematic representation of a) thiothymine and b) thiouracil. These molecules are similar to thymine and uracil, respectively, with the difference that the oxygen in position C2 is replaced by a sulphur.**

### 5.1.2. Dissociative electron attachment to dimethyl disulphide

Concerning DEA experiments on dimethyl disulphide ( $C_2H_6S_2$ , DMDS), although the double focusing set up has a lower electron energy resolution than the set up used in previous DEA studies of Modelli *et al.* [1], its high sensitivity allowed the detection of new fragments. From the eight fragment anions detected in the electron energy range of  $\sim 0$ –15 eV, five were observed for the first time and assigned to:  $S^-$ ,  $SH^-$ ,  $S_2^-$ ,  $CHS_2^-$ ,  $CH_2S_2^-$ . No parent or dehydrogenated parent anion was observed. Taking into account the present resolution ( $\sim 1$  eV) all the three common fragments ( $CH_2S^-$ ,  $CH_3S^-$ ,  $CH_3S_2^-$ ) observed in both experiments show good agreement in respect to their peaks' positions. Furthermore, it was observed that the DEA mechanism is also operative at higher electron energies leading to these anions formation. With the support of the quantum chemical calculations it was possible to assign the chemical composition of neutral and negatively charged fragments to the different resonances experimentally observed. The by far dominant signal is assigned to the formation of  $CH_2S^-$ , whereas the second most dominant signal is assigned to  $CH_3S^-$ .

In the physiological environment cells are composed of  $\sim 70\%$  of water [2], so the presence of such solvent and how low-energy electron interacts with molecules in this environment would benefit from extensive and detailed investigations. However, it is not yet possible to perform liquid-phase DEA studies in high-vacuum conditions, so a reasonable approach would involve producing water clusters doped with the biological relevant molecules presented in this thesis. Another interesting molecule to investigate in water cluster is N-methylacetamide, since it is recognized to be relevant within the context of peptide bonding in proteins.

## 5.2. Technologically relevant molecules

### 5.2.1. Dissociative electron attachment to volatile anaesthetics (enflurane, isoflurane) and chlorinated ethanes (pentachloroethane and hexachloroethane)

DEA experiments on two volatile anaesthetics (enflurane, isoflurane) and two chlorinated ethanes (pentachloroethane, hexachloroethane), have been performed in the electron energy range of  $0$  –  $17$  eV with an energy resolution of  $\sim 1$  eV. The results showed that the ion yield for the capture of an electron with virtually no kinetic energy by the

volatile anaesthetics is very small. In fact the peak for electron attachment leading to the elimination of  $\text{Cl}^-$  occurs at just below 1 eV for both molecules. The opposite is true for pentachloroethane and hexachloroethane, for which there are zero electron attachment energy resonances with large yields (cross-sections). These results explain the observations of the low and high electron attachment efficiencies of the anaesthetics and chlorinated ethanes, respectively, observed in the swarm (low mean electron energy) environment of an IMS system. It is proposed that the absence of zero energy attachment resonances for the anaesthetics results from the rapid dissociation of the  $\text{Cl}^-$  from the TNI before geometry optimisation occurs.

Although isoflurane and enflurane are isomers, interestingly they exhibit different DEA patterns. Only in the case of isoflurane it is possible to detect a dehydrogenated parent anion, whereas in the case of enflurane this fragmentation channel turns out to be entirely suppressed due to other dominant channels being available. This leads to the formation of  $(\text{M-Cl})^-$  and  $\text{F}^-$ . The high-energy attachment resonances in these isomers must originate from core-excited resonances, consisting of two electrons in normally unoccupied molecular orbitals moving in the field of the positive core.

The most dominant signal from DEA reactions to the chlorinated ethanes is the formation of  $\text{Cl}^-$  at electron energies  $\sim 0$  eV and  $\sim 7$  eV, the latter with a yield an order of magnitude lower than the former. The second most intense ion signal assigned to  $\text{Cl}_2^-$  shows also the same energy positions for these two resonances. Other reactions like the loss of several other neutral units with an onset of the resonant ionic yields at zero energy were observed as well.

These studies allowed to conclude that enflurane and isoflurane are not as good dopants in ion mass spectrometry as the chlorinated ethanes.

Enflurane, isoflurane, pentachloroethane and hexachloroethane were just some of the possible dopants that could be used in the detection of explosives. Other compounds could be investigated for their use as dopants. Although it was observed that the present studied volatile anaesthetics are not suitable as dopants, it would be interesting to investigate what happens when DEA is performed with other volatile anaesthetics. The following molecular targets are proposed: halothane, desflurane and sevoflurane.

### **5.2.2. Low-energy electron interaction with tungsten hexacarbonyl**

From DEA studies to gas-phase tungsten hexacarbonyl ( $\text{W}(\text{CO})_6$ ) it was possible to assign resonances for prompt anions formation to common electronic states that decay by vibrational pre-dissociation. Low-energy electron interactions with  $\text{W}(\text{CO})_6$  can lead to a loss of up to four CO groups and from the metastable decay study of  $\text{W}(\text{CO})_6$  the following metastable fragments were assigned to:  $\text{W}(\text{CO})_5^- \rightarrow \text{W}(\text{CO})_4^-$  and  $\text{W}(\text{CO})_4^- \rightarrow \text{W}(\text{CO})_3^-$ . Since the loss of all CO ligands is not observed in DEA, which is in contrast with the electron ionisation results [3], it is possible to conclude that in the electron beam induced deposition technique, the deposits obtained on the surface are triggered by low-energy electron through dissociative electron attachment processes near to the electron irradiation spot. The information gained from these DEA studies to  $\text{W}(\text{CO})_6$  can be used in the future to help optimising the deposition technique, since the precursor molecule can be efficiently broken in a particular bond by setting a particular electron energy.

Further studies on  $\text{W}(\text{CO})_6$  can be performed beyond the context of this thesis and include embedding  $\text{W}(\text{CO})_6$  in helium clusters. DEA experiments on helium nanodroplets will allow to have a full stabilization of the molecule due to the cold environment (0.37 K), which may quench a particular dissociation channel or channels. This is particular relevant within the context of exploring direct fragmentation in detriment to concerted fragmentation mechanisms. As far as I am aware there are no studies in such cold environments in the literature.

Electron driven reactions are prevalent in many scientific research areas and technological applications, and so detailed knowledge of the underlying mechanisms in selected molecular targets appears to be extremely relevant. Finally, the work performed during this thesis also included collaborations with several colleagues from institutes and other universities in different countries.

## **References**

- [1] A. Modelli, D. Jones, G. Distefano, M. Tronc, *Chem. Phys. Lett.* 181 (1991) 361.
- [2] J. Koolman, K.-H. Roehm, *Color Atlas of Biochemistry*, Verlag, Stuttgart, 2005.
- [3] K. Wnorowski, M. Stano, W. Barszczewska, A. Jowko, S. Matejcik, *Int. J. Mass Spectrom.* 314 (2012) 42.

# Appendix I: List of other published papers

---

- 1. Dissociative electron attachment and dipolar dissociation in ethylene**  
Ewelina Szymańska, Nigel J. Mason, E. Krishnakumar, Carolina Matias, Andreas Mauracher, Paul Scheier, Stephan Denifl  
*Int. J. Mass Spectrom.* (2014) 365-366: 356-364
- 2. Dissociative Electron Attachment to the Nitroamine HMX (Octahydro-1,3,5,7-Tetranitro-1,3,4,7-Tetrazocine)**  
Johannes Postler, Marcelo M. Goulart, Carolina Matias, Andreas Mauracher, Filipe Ferreira da Silva, Paul Scheier, Paulo Limão-Vieira, Stephan Denifl  
*J. Am. Soc. Mass Spectrom.* (2013) 24:744Y752
- 3. Electron interaction with nitromethane embedded in helium droplets: Attachment and ionization measurements**  
F. Ferreira da Silva, S. Ptasińska, S. Denifl, D. Gschliesser, J. Postler, C. Matias, T. D. Märk, P. Limão-Vieira, P. Scheier  
*J. Chem. Phys.*, 135, 174504 (2011)

# Appendix II: Curriculum vitae

---

## 1. Personal Data

Name: Carolina Raquel Guedes Matias  
Birth Date: June 7<sup>th</sup> 1988  
Birth Place: Coruche, Santarém, Portugal  
Marital Status: Single  
ID Card: 13366257  
Address: Uferstraße 4 6020 Innsbruck - Austria  
Mobile phone: +43 0650 5330399  
e-mail: carolinaraquelmatias@hotmail.com

## 2. Education / qualifications

- 2.1 **October 2011 – (Present): PhD student**, under the supervision of Professor Doctor Stephan Denifl and Professor Doctor Paulo Limão-Vieira, co-tutored scheme between the Institut für Ionenphysik und Angewandte Physik, Leopold Franzens Universität, Innsbruck, Austria and Faculdade de Ciências e Tecnologia, Universidade Nova de Lisboa, Portugal;
- 2.2 September 2011: **M.Sc. in Physical Engineering (14 out of 20)**, Universidade Nova de Lisboa, Portugal, “*Decomposition of DNA bases by atom-molecule collisions: NCO<sup>-</sup> formation*”, (18 out of 20), under the supervision of Doctor Filipe Ferreira da Silva and Professor Doctor Paulo Limão-Vieira;
- 2.3 September 2009 – September 2010: Scholarship in Introduction to Research in Atomic and Molecular Physics, Unit of R&D Atomic Physics Center, Universidade de Lisboa, Portugal

## 3. Publications

### 3.1. Papers in international journals (peer-reviewed)

- P1. **Dissociative electron attachment to volatile anaesthetics (enflurane, isoflurane) and chlorinated ethanes (pentachloroethane and hexachloroethane)**  
**C. Matias**, A. Mauracher, S. E. Huber, S. Denifl, P. Limão-Vieira, P. Scheier, R. González-Méndez, C. A. Mayhew  
International Journal of Mass spectrometry (2015) accepted for publication.

- P2. Low-energy interactions with dimethyl disulphide**  
C. Matias, A. Mauracher, P. Scheier, P. Limão Vieira, S. Denifl  
*Chem. Phys. Lett.*, (2014) 605-606: 71-76
- P3. Dissociative electron attachment and dipolar dissociation in ethylene**  
Ewelina Szymańska, Nigel J. Mason, E. Krishnakumar, Carolina Matias, Andreas Mauracher, Paul Scheier, Stephan Denifl  
*Int. J. Mass Spectrom.* (2014) 365-366: 356-364
- P4. NCO<sup>-</sup>, a Key Fragment Upon Dissociative Electron Attachment and Electron Transfer to Pyrimidine Bases: Site Selectivity for a Slow Decay Process**  
Filipe Ferreira da Silva, Carolina Matias, Diogo Almeida, Gustavo García, Oddur Ingólfsson, Helga Dögg Flosadóttir, Benedikt Ómarsson, Sylwia Ptasinska, Benjamin Puschnigg, Paul Scheier, Paulo Limão-Vieira, Stephan Denifl  
*J. Am. Soc. Mass Spectrom.* (2013) 24:1787Y1797
- P5. Dissociative Electron Attachment to the Nitroamine HMX (Octahydro-1,3,5,7-Tetranitro-1,3,4,7-Tetrazocine)**  
Johannes Postler, Marcelo M. Goulart, Carolina Matias, Andreas Mauracher, Filipe Ferreira da Silva, Paul Scheier, Paulo Limão-Vieira, Stephan Denifl  
*J. Am. Soc. Mass Spectrom.* (2013) 24:744Y752
- P6. Low-energy electron interactions with tungsten hexacarbonyl – W(CO)<sub>6</sub>**  
K. Wnorowski, M. Stano1, C. Matias, S. Denifl, W. Barszczewska and Š. Matejčić  
*Rapid Communications Mass Spectrom.* (2012), 26, 2093–2098
- P7. Electron interaction with nitromethane embedded in helium droplets: Attachment and ionization measurements**  
F. Ferreira da Silva, S. Ptasinska, S. Denifl, D. Gschliesser, J. Postler, C. Matias, T. D. Märk, P. Limão-Vieira, P. Scheier  
*J. Chem. Phys.*, 135, 174504 (2011)

### 3.2. Thesis

- Th1. Decomposition of DNA bases by atom-molecule collisions: NCO<sup>-</sup> formation**, M. Sc. Thesis Universidade Nova de Lisboa, 2011

### 3.3. Oral Communications



**CA1. Comparative studies upon potassium and electron collisions with biomolecules: site selectivity**

C. Matias, F. Ferreira da Silva, D. Almeida, B. Puschnigg P. Scheier, P. Limão-Vieira, S. Denifl

1<sup>st</sup> Meeting of the DEA Club, 16<sup>th</sup>-19<sup>th</sup> September 2013, Trieste, Italy

**CA2. Laser Induced Acoustic Desorption of Biomolecules**

C. Matias, J. Postler, M. Goulart, D. Gschliesser, P. Scheier, S. Denifl

62<sup>nd</sup> Annual Meeting of the Austrian Physical Society, OePG 2012, September 18<sup>th</sup> to 21<sup>st</sup>, University of Graz, Austria

**3.4. Communications**

**CA1. Dissociative electron attachment to enflurane and isoflurane and the chlorinated ethanes pentachloroethane and hexachloroethane**

C. Matias, A. Mauracher, S.E. Huber, S. Denifl, P. Limão-Vieira, R. González-Méndez, P. Watts, and C. A. Mayhew

6<sup>th</sup> Conference on Elementary Processes in Atomic Systems 2014, July 9<sup>th</sup> to 12<sup>th</sup>, Bratislava, Slovakia

**CA2. Ionic Detection of TNT-diesel mixture by electron ionization and electron attachment**

Jusuf Khreis, Carolina Matias, Johannes Postler, Paul Scheier, Ralf Zimmermann, Stephan Denifl

19<sup>th</sup> Symposium on Atomic, Cluster and Surface Physics 2014, February 9<sup>th</sup> to 14<sup>th</sup>, Universitätszentrum Obergurgl, Austria

**CA3. Low-energy electron attachment to dimethyl disulphide**

Carolina Matias, Andreas Mauracher, Paul Scheier and Stephan Denifl

19<sup>th</sup> Symposium on Atomic, Cluster and Surface Physics 2014, February 9<sup>th</sup> to 14<sup>th</sup>, Universitätszentrum Obergurgl, Austria

**CA4. Using Dissociative Electron Attachment as a Fingerprinting Tool to Detect Explosives**

Postler, J.; Goulart, M. M.; Matias, C.; Mauracher, A.; Ferreira da Silva, F.; Scheier, P.; Limão-Vieira, P.; Denifl, S.

11<sup>th</sup> European Conference on Atoms Molecules and Photons 2013, June 24<sup>th</sup> to 28<sup>th</sup>, Aarhus, Denmark

**CA5. Electron driven chemistry close to 0 K**

Marcelo Goulart, Peter Bartl, Samuel Zöttl, Mathias Daxner, David Gschliesser, Johannes Postler, Carolina Matias, Benjamin Puschnigg, Violaine Vizcaino,

## Curriculum Vitae

Christian Leidlmair, Harald Schöbel, Lukas An der Lan, Stephan Deni, Andreas Mauracher, Michael Probst, Olof Echt, Andrew Ellis, Paul Scheier  
62<sup>nd</sup> Annual Meeting of the Austrian Physical Society, OePG 2012, September 18<sup>th</sup> to 21<sup>st</sup>, University of Graz, Austria

### **CA6. Electron induced reactions in acetamide clusters embedded in helium nanodroplets**

C. Matias, F. Ferreira da Silva, J. Postler, D. Gschliesser, P. Scheier, P. Limão-Vieira, S. Denifl

Isolated biomolecules and biomolecular, IBBI 2012, January 22<sup>nd</sup> to 27<sup>th</sup> 2012, Les Diablerets, Switzerland

### **CA7. New Approach to Laser Induced Acoustic Desorption: Increasing measurement times for sector-field mass spectrometry**, J. Postler, H. Schöbel, L. An der Lan, D. Gschliesser, C. Matias, C. Leidlmair, B. Puschnigg, P. Scheier and S. Denifl

Isolated biomolecules and biomolecular, IBBI 2012, January 22<sup>nd</sup> to 27<sup>th</sup> 2012, Les Diablerets, Switzerland

### **CA8. Low energy electron collisions with biomolecules and biomolecular clusters**

D. Gschliesser, J. Postler, L. AnderLan, C. Matias, V. Viczaino, Paul Scheier, S. Denifl

Isolated biomolecules and biomolecular, IBBI 2012, January 22<sup>nd</sup> to 27<sup>th</sup> 2012, Les Diablerets, Switzerland

### **CA9. Probing the intermolecular dynamics yielding CNO<sup>-</sup> formation in potassium uracil collisions**

C. Matias, D. Almeida, F. Ferreira da Silva, P. Limão-Vieira

11th Iberian joint meeting on atomic and molecular physics, IBER 2011, June 19<sup>th</sup> to 22<sup>nd</sup> 2011, Coimbra, Portugal

### **CA10. Construction of a UV He I/He II source vacuum system**

C. Matias, R. M. Pinto, A.A. Dias, M. L. Costa

17th National Conference of Physics, Física 2010, September 1<sup>st</sup> to 3<sup>th</sup> 2010, Vila Real, Portugal

## **4. Attended meetings**

**M1.** 6<sup>th</sup> Conference on Elementary Processes in Atomic Systems 2014, July 9<sup>th</sup> to 12<sup>th</sup>, Bratislava, Slovakia

**M2.** 19<sup>th</sup> Symposium on Atomic, Cluster and Surface Physics 2014, February 9<sup>th</sup> to 14<sup>th</sup>, Universitätszentrum Obergurgl, Austria

## *Curriculum Vitae*

- M3.** 1<sup>st</sup> Meeting of the DEA Club, 16<sup>th</sup> to 19<sup>th</sup> September 2013, Trieste, Italy
- M4.** 62<sup>nd</sup> Annual Meeting of the Austrian Physical Society, OePG 2012, September 18<sup>th</sup> to 21<sup>st</sup>, University of Graz, Austria
- M5.** Isolated biomolecules and biomolecular, IBBI 2012, January 22<sup>nd</sup> to 27<sup>th</sup> 2012, Les Diablerets, Switzerland
- M6.** 17th National Conference of Physics, Física 2010, 1st September to 3th September 2010, Vila Real, Portugal

### **5. Scientific Activity**

#### **5.1. Short Term Scientific Missions**

**STSM1.** August 28<sup>th</sup> to September 9<sup>th</sup> 2011, “Institut für Ionenphysik, Leopold Franzens Universität“, Innsbruck, Austria, Electron attachment to acetamide embedded in helium nanodroplets.

### **6. Other Activities**

- 6.1.** Member of “National Scouts Corps - Portuguese Catholic Scouting” at the group 1053, [1997 - 2005]
- 6.2.** Basketball player in Clube Náutico de Abrantes (CNA), Portugal [1999 - 2011]
- 6.3.** Basketball coach, level I, 2010
- 6.4.** Basketball player TSI Damen, Austria (2012 - present)

### **7. Languages**

Language <sup>3</sup>	speaking	reading	writing
Portuguese (mother tongue)	E	E	E
English	G	E	G
Spanish	P	G	-

---

<sup>3</sup> (E)xcellent, (G)ood, (P)oor